[redacted]

[redacted]

GPO PRICE $ _____

OTS PRICE(S) $ _____

Hard copy (HC) 4.00

Microfiche (MF) 1.00

FACILITY FORM 602

N65-22125
(ACCESSION NUMBER)

140
(PAGES)

CR62350
(NASA CR OR TMX OR AD NUMBER)

1
(THRU)

(CODE)

33
(CATEGORY)

Lockheed

MISSILES & SPACE COMPANY

A GROUP DIVISION OF LOCKHEED AIRCRAFT CORPORATION

SUNNYVALE, CALIFORNIA

N65-22125

Technical Report

M-52-65-2

THERMAL CONDUCTANCE OF POLYMER CHARS

by

G.R. Cunnington
W. Bradshaw
F.J. Smith

March 15, 1965

Prepared Under JPL Contract 950868

This work was performed for the Jet Propulsion Laboratory, California Institute of Technology, sponsored by the National Aeronautics and Space Administration under Contract NAS7-100.

LOCKHEED MISSILES & SPACE COMPANY
A Group Division of Lockheed Aircraft Corporation
Sunnyvale, California

FOREWORD

This report was prepared by the Thermophysics section of the Aerospace Sciences Laboratory and the Metallurgy and Ceramic section of the Materials Sciences Laboratory for the Jet Propulsion Laboratory, California Institute of Technology. The work was performed under Contract JPL No. 950868, "Study Program of Thermal Conductance of Polymer Chars." Mr. Robert Nagler of the Jet Propulsion Laboratory was the technical administrator for the program.

This report describes work conducted from 28 August 1964 to 28 February 1965.

The program was carried out under the direction of G. R. Cunnington as Project Engineer. The sample preparation, equipment fabrication and measurement phases were carried out by F. J. Smith, J. Bjeletich, G. Ledger, A. Lindahn, and K. Till. Metallographic and x-ray diffraction analyses were carried out by A. Gleason and J. Robinson, respectively.

CONTENTS

TABLES

ILLUSTRATIONS

Section 1
INTRODUCTION

Ablative composites have been proven successful at the moderate and high heat rates associated with the atmospheric entry of both ballistic and orbiting vehicles. As a result, attention has been given to these materials, particularly the organic reinforced charring compositions, for use in the construction of vehicles for entry into other planetary environments. Many investigations have formed physical models and mathematical descriptions of the complex ablation processes. However, in order to describe the energy transfer and absorption processes being carried out in the ablating material,the thermophysical properties of the composite must be known. One of the more important of the thermophysical properties required for the analysis of an ablating body is the thermal conductivity of the char zone, which is of particular significance in the determination of the extent of material consumption under highly transient conditions. The effects of parameters such as graphitization and pore spectra are of importance in the understanding of the thermal energy transport processes in a char structure.

This report presents the final results of the program to provide data on the thermal conductance of chars formed from nylon-phenolic composites as a function of degree of graphitization, density, and pore spectra. A variety of methods exist for measuring this property. However, factors such as long measurement time, sample size, and accurate temperature measurement difficulties at high temperature led to the choice of a transient method for measurement of the thermal diffusivity of the char specimens.

The flash technique, described in Ref. 1 , was selected for this program because it is applicable to rapid measurement and small sample size. Also, corrections for experimental losses can be calculated with reasonable accuracy.

Char specimens were prepared from six different nylon-phenolic composites. One virgin material was made from a powdered nylon, whereas, the remaining five were of woven nylon fabric composition. These materials varied both in the ratio of nylon to phenolic and in nylon fiber diameter. Samples were produced from each material at three char formation temperatures to achieve a variation in structure. In total, twenty specimens were evaluated for thermal diffusivity as a function of structure and pore spectra.

An analysis of the diffusivity, structure, and pore spectra data shows the chars undergo drastic changes when measurements are carried out at temperatures above the char formation temperature. Thermal conductance increased by as much as a factor of three upon exposure to temperatures above that of formation. Corresponding changes were observed in the extent of graphitization and ordering of the carbon structure. The experimental results have established a range of conductance values for nylon-phenolic chars as a function of porosity and crystal structure. However, no correlation of data has been established with any existing model for the thermal energy transport in a char structure.

Section 2

EXPERIMENTAL METHODS

2.1 CHAR PREPARATION

2.1.1 Experimental Development

As originally proposed, Ref. 2, chars were to be prepared as follows: (a) low-heat rate at 1500° F, (b) medium-heat rate at 2200° F, and (c) high-heat rate at 3300° F. It was proposed the low-heat rate chars be produced in a small muffle furnace, and that Types (b) and (c) be produced in a arc-image furnace facility. The purpose of variation in heat rate and temperature was to obtain maximum variation in the extent of graphitization of the char. Variation in pore spectra was to be obtained by varying the nylon content from 40 to 60% and by the use of three different fiber diameters. Also, additional variation in pore spectra was expected between the three different types of heating cycle.

During the course of the study, the proposed methods of char preparation were varied as follows to meet the suggestions of R. Nagler (Ref. 3). First, it was found that the chars produced in the arc-image furnace tended to warp and crack. This effect had not been noted in previous studies because thicker samples had been used, and they had less tendency to warp. However, to make thermal diffusivity measurements the char had to be prepared in wafer form. After some experimentation with sample holders, a relatively crack-free flat char could be produced. These samples were not uniform in thickness, which made data interpretation difficult. Consequently, the preparation procedure for Types (b) and (c) chars was modified so they were formed under condition of heating from all sides. This method employed a rapid-heat resistance furnace described in Sec. 2.1.2.

When formation of chars was attempted at 3600° F, problems were still encountered with buckling and cracking. The problems still remained even when the formation temperature was reduced to 2900° F with extremely rapid heat rates. Various ambiences

of char formation were attempted to determine which method would produce pore spectra deviating to the greatest extent from medium- and low-temperature chars, Table 1. It was found that at 2900° F gradual heating in vacuo, Method C, produced more large-pore chars than did any other method. Moreover, this was more effective for varying pore spectra, than rapid-heating in argon at higher temperatures, Method D. With the agreement of the contracting agency's technical administrator Method C was selected as one of the standard preparation procedures. The three types of char formation procedures selected for the remainder of the program were the following:

Type of Char	Maximum Char Preparation Temp. (° F)	Heat Rate	Ambient Pressure
A	1832	Very slow	Argon, 1 atm
B	2200	Moderate	Argon, 1 atm
C	2900	Moderate	Vacuo, 0.01 atm

2.1.2 Char Specimen Preparation Methods

For thermal diffusivity and heat capacity measurements, cylindrical samples were cut from each sheet of virgin material. For electrical resistance measurements flat rectangular specimens were cut from each sheet. The samples were then dimensioned and weighed.

Type A, 1832° F Laboratory Chars. Three to six samples of a specific sheet were prepared at a time in a flowing argon atmosphere. The samples were placed with their circumferential surface in a v-shaped piece of metallic sheet stock. The sample holder was then positioned in the hot zone of a conventional muffle tube furnace, and the system purged with flowing argon. Volatile hydrocarbon species were removed by the flowing argon atmosphere. Samples were brought to the maximum temperature under the heating schedule listed in Table 2. At completion of the charring cycle, the samples were permitted to cool in the furnace, then removed, dimensioned, weighed and set aside for their prescribed evaluation.

Table 1

EFFECT OF AMBIENCE OF CHAR FORMATION ON AMINCO POROSIMETRY DATA

Char*	Preparation Method	Fraction of Pores in Range 100 to 0.035 Microns						
		$< 80\ \mu$	$< 50\ \mu$	$< 30\ \mu$	$< 10\ \mu$	$< 5\ \mu$	$< 1\ \mu$	$< 0.1\ \mu$
D	Heated gradually in argon at 3800° F, P = 15 psi	18	58	67.5	86	90.5	94	100
C_1	Heated gradually in Vacuo at 2900° F, P = 0.15 psi	29	72	90	98	99.5	99.8	100
C_2	Heated rapidly in argon at 2900° F, P = 15 psi	20	58	82	95	97.8	99.8	100
C_3	Heated rapidly in Vacuo at 2900° F, P = 0.15 psi	10	36	62	92	96.8	99.8	100
C_4	Heated gradually in argon at 2900° F, P = 15 psi	18	49.5	50	67	80	99.8	100
B	Heated gradually in argon at 2200° F, P = 15 psi	14	18	52	76.5	84.5	92	99
A	Laboratory Char prepared slowly in argon, maximum temp. = 1832° F, P = 15 psi	4	21	42	69	78	88	97.5

*All tests carried out on material of type 9-15A, described in Table 1.

Table 2

SCHEDULE OF CHAR PREPARATION

Temperature (°F)		Time at Temperature (min)	
Type A – 1832° F, Laboratory Char Flowing Argon Atmosphere P = 15 psi			
Slowly heat to	932	Hold	45
Increase slowly to	1202	Hold	45
Increase slowly to	1472	Hold	45
Increase slowly to	1652	Hold	45
Increase slowly to	1832	Hold	60
		Total time at temp.	= 240 min.
		Total test time	= 300 min.
Type A', Zytel Only, 1832° F Laboratory Char, Argon Atmosphere P = 15 psi			
Increase to	212	Hold	20
Increase to	392	Hold	20
Increase to	572	Hold	20
Increase to	752	Hold	20
Increase to	932	Hold	30
Increase to	1012	Hold	15
Increase to	1292	Hold	15
Increase to	1472	Hold	15
Increase to	1652	Hold	15
Increase to	1832	Hold	15
		Total time at temp.	= 185 min.
		Total test time	= 185 min.
Type B – 2200° F, In Argon Atmosphere, P = 15 psi			
Rapidly bring to	1400	Hold	25
Increase to	1832	Hold	12
Increase to	2200	Hold	8
		Total time at temp.	= 45 min.
		Total test time	= 45 min.
Type C – 2900° F, In Vacuo, P < 0.15 psi			
Rapidly bring to	1400	Hold	15
Increase to	1832	Hold	10
Increase to	2200	Hold	6
Increase to	2900	Hold	4
		Total time at temp.	= 35 min.
		Total test time	= 35 min.

Type B, 2200° F Char, Argon Atmosphere. Three samples of a specific sheet type were prepared at a time in an argon atmosphere. The samples were placed on a graphite platform, Fig. 4. A graphite lid was placed on the specimens to prevent warping and maintain geometry, particularly flatness. The holder assembly was then positioned inside a graphite heater element in an electrical resistance furnace. The furnace chamber was evacuated and back-filled with argon at 15 psia. The heater was energized with a predetermined current flow corresponding to 1400° F, and the samples were rapidly introduced into the heater tube. Charring was accomplished in step increments to the final charring temperature, Table 2. Volatile hydrocarbon species remain within the chambers until termination of the test. At completion of the charring cycle, the samples were allowed to come to room temperature, removed, dimensioned, and weighed, and set aside for the prescribed analysis.

Type C, 2900° F Char, Prepared in Vacuo. Samples were prepared as described in the preceding section with the exception the chamber pressure was brought to 0.01 atm and maintained there till the completion of the charring cycle. Volatile hydrocarbon species were removed as they were formed. The heating cycle was carried out to reach the prescribed temperatures as indicated in Table 2.

2.2 CHAR CHARACTERIZATION

2.2.1 Pore Spectra Analysis

Two methods of pore spectra analysis were employed as described in the following sections.

Aminco Pore Spectra Analysis. As originally proposed, char pore spectra were to be determined using an Aminco porosimeter, capable of determining the volume of pores ranging in size from 0.035 to 100 μ.

In this method a small sample of weighed char is placed in a calibrated capillary filling device termed a penetrometer. The penetrometer and its contents housed in a

filling device, is evacuated to less than 100μ. Sufficient mercury is then introduced by differential pressure to fill the penetrometer completely minus the bulk volume of the sample. (Standard practice is to pressurize the system to 1.8 psia with mercury, which is supposed to surround the samples completely, but not fill the pores. However, subsequent evaluation showed that if a large proportion of the pores is greater than a 100μ, some penetration of pores can occur.) Mercury is then forced into the sample at increasing pressures in small increments to a maximum pressure of 5000 psi, and the corresponding volume displacement measured in the capillary stem of the penetrometer. In this way, the percentage of pores having a given diameter can be calculated from the equation:

$$Dp = -4s \cos \theta \qquad (1)$$

where

D = pore diameter (μ)
p = Hg-intrusion pressure (psi)
s = the surface tension of mercury, or 473 dynes/cm^2
θ = is the wetting angle, which is assumed to be 130 deg, (Ref. 4)

This wetting angle has been confirmed for nickel and is considered the most acceptable for a variety of materials as diverse as arc carbon, ceramics, sintered metal, and aspirin tablets (Ref. 4) The complete procedure is described in detail in Refs. 5, 6, and 7.

This method of pore spectra analysis has the following limitations:

- It can only be used for determining pore spectra within the range of the instrument, 100 to 0.035μ.
- It assumes a model of continuous interconnected circular voids. There is no way of distinguishing between 10 pores of length n and one pore of length 10n. The method cannot be used to distinguish between cylindrical, elliptical, or rectangular shaped voids, but assumes a cylindrical shape. If an ink-bottle shaped void occurred, that void would be detected as one having the diameter of the neck and a volume equivalent to that of the entire void. Consequently, the mercury porosimetry technique must be supplemented with an

analysis of microstructure including the methods of quantitative stereology. The porosimetry method has the advantage in that it can be used to obtain an estimate of bulk density and real density.

Quantitative Stereology for Determination of Pores Greater Than 100μ. In any microstructure in which one or more phases are distributed more or less randomly the volume fraction of Phase a, for example, can be determined from the relationships:

$$f_{V_a} = \frac{V_a}{V_T} = \frac{A_a}{A_T} = \frac{L_a}{L_T} = \frac{N_a}{N_t} \qquad (2)$$

where f_{V_a}, the volume fraction of Phase a, is defined as the volume ratio of Phase a to the volume of the total structure, V_a/V_t, and in turn equals the areal ratio A_a/A_T, the lineal ratios L_a/L_T, and the point ratios N_a/N_T. Using these relationships, a rapid point count method is used for determining the volume fraction of a constituent in a technique described in detail by Underwood (Ref. 8).

This approach was used to determine the volume fraction of pores greater than 100μ and obtain an estimate of their approximate diameter. The samples were mounted in cross section through the thickness of the char.* Two photomicrographs were made at random at 50 or 100X for each sample, Fig. 1. The dark regions are void and the light gray areas are char. The process of quantitative metallography was used to determine the volume of pores greater than 100μ. Phase a was taken as the void area greater than 100μ. Phase b was the area of voids less than 100μ in size, i.e., <5 mm in diameter at 50X. Phase c was the char area. (Pores smaller than 5mm in diameter,

*If they had been mounted in the direction normal to the surface of the char, erroneous estimates would be more likely as the void structure follows the configuration of the original fiber lay-up, and consequently is highly anisotropic.

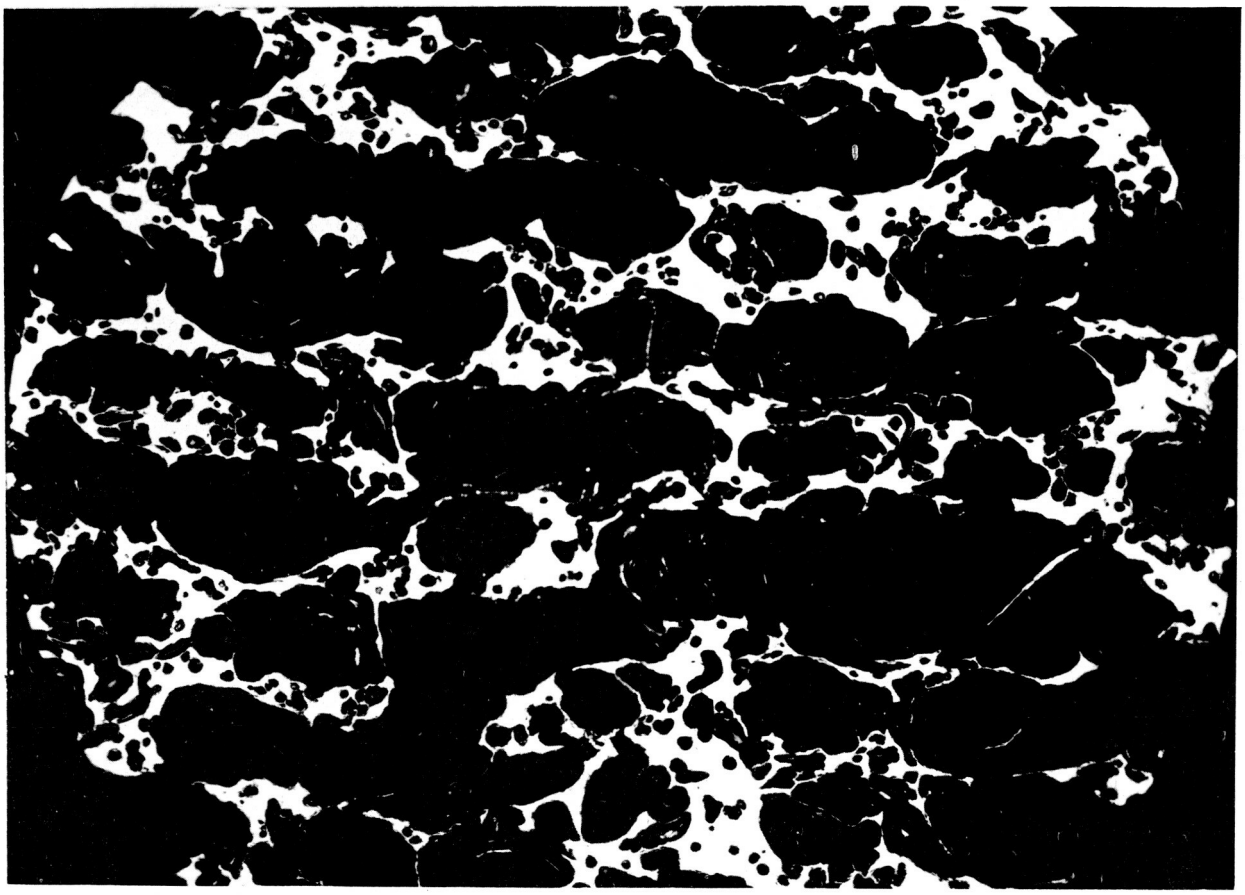

Figure 1

Typical Char Microstructure

at 50 X, were counted as a portion of Phase c). Then f_a, the volume fraction of voids greater that 100μ is given by the equation

$$f_a = \frac{N_a}{N_a + N_b + N_c} = \frac{N_a}{N_T} \qquad (3)$$

It should then be possible to compute the total volume of voids from combined Aminco spectra data and quantative stereology. However this was not possible since it was found that some of the pores greater than 100 μ were filled with mercury at the reference pressure of 1.8 psia. Consequently, total porosity was calculated from the differences between bulk and real volumes, Sec. 5.

2.2.2 Char Structure

Microstructure. Suitable char samples were selected from each test series for determination of large pores. The samples were mounted in a slow curing epoxy resin* selected for characteristics of viscosity and surface tension suitable for maximum penetration into the voids of the chars. The resultant mount is clear (has 90% light transmission), bubble free, and generally penetrates the open pore network.

To prepare a sample, it is vacuum impregnated and then cured in air at 160° F for 16 hr. The mount is then sectioned, so that a cross section is obtained through the thickness of the char. The specimens are polished by standard metallographic methods. After polishing, they are washed, dried, and photographed on a metallograph. For quantitative stereology two photomicrographs, 50 or 100X, were made at random of each sample.

*Maraset Epoxy Resin, TM, manufactured by Marblette Corporation, Long Island, N.Y.

Char Crystal Structure. Samples of char prepared in the manner described in Sec. 2.1.2 were analyzed for degree of ordering using conventional x-ray diffraction methods. In the 1832°F series, the front and side surfaces were analyzed to determine if fiber orientation caused any significant preferred crystal orientation. In the 2200° F series, both top and bottom were analyzed. In the 2900°F series, only the top face was analyzed, and in the samples evaluated after diffusivity tests the face which had been subjected to the laser beam was the one examined.

All x-ray measurements were made at room temperature with a GE XRD-5 Geiger counter diffractometer using nickel-filtered copper radiation from tubes operated at 40 kV and 20 mA. A 1-deg beam slit and 0.2-deg detector slit were used throughout. Using this geometry the depth of penetration of the detecting x-ray beam is approximately 90 mils. Peak position, width at half maximum and relative intensity were measured from 0002 lines corrected for background.

Corrections were made for instrumental line broadening using data obtained with the use of a quartz reference standard* Peak half widths, however, were not corrected for the effects of absorption or surface roughness and texture.

A previous study, Ref. 9 , using the techniques of Bragg and Packer (Ref. 10) had shown that the effect of absorption and incoherent scattering on the peak position and height in nylon phenolic chars is relatively small. Earlier studies (Refs. 11 and 12) had shown that the techniques employed with the Geiger counter diffractometer were adequate to obtain a comparative evaluation of the degree of ordering and the amount of crystallites. Debye-Scherrer photographs on the ground char and Laue photographs on the unground material confirmed diffractometer data.

2.2.3 Density

The bulk density of the as-received materials and the char samples was determined from the weight of the sample and its volume calculated from micrometer measurement of regularly shaped specimens.

*Total Correction for instrumental line broadening was 0.3-deg.

An apparent density was computed from the mass of the sample and its apparent volume when it was immersed in mercury within the penetrometer well of the Aminco porosimeter. The volume of displaced mercury was determined from the difference between the weight of the penetrometer completely filled with mercury and the weight of the penetrometer with the sample in it and filled with mercury at 1.8 psia. The apparent volume should approximate bulk volume less the volume of surface depressions. However, when a large number of voids greater than 100 μ were present, considerable difference between apparent and bulk density resulted from the partial filling of such pores.

The real density, the density of the solid material, was computed from the mass of the samples and the displacement volume of the char when the specimen had been completely filled with mercury to 5000 psi. This method includes in the real volume of the char all pores having an inlet diameter smaller than 0.035 μ and any closed pores. Study of the microstructure has shown that very few closed pores exist, although there are some of the order of 0.05 μ. Previous studies with ground chars (Ref. 13) had shown that the contribution of such microporosity to the real volume was negligible in comparison with the lack of complete homogeneity in the sample. Crystallite density was calculated from x-ray diffraction measurements by the method described in Sec. 5.

2.2.4 Electrical Resistivity

Special 1-in. long char specimens were prepared for determination of an effective electrical resistivity, uncorrected for pore distribution. The ends of the samples were painted with silver electrical contact paint. The resistance, R , was measured between the two conductive coatings using an appropriate ohmmeter. The effective resistivity was determined in the direction parallel to the original fiber axis.

2.3 THERMAL DIFFUSIVITY

The technique employed during this program for measuring thermal diffusivity is basically that originally described by Parker (Ref. 1). Essentially, the method consists of irradiating the front face of a disc-shaped specimen with a single pulse of energy. The specimen is located in a nearly isothermal environment, and the energy pulse is absorbed in a depth at the front face which is very small compared to its thickness. The time-temperature history of the rear face of the specimen is monitored by a suitable detector system. Thermal diffusivity is calculated on the basis of the thickness of the specimen and the time required for the rear face temperature rise signal to reach a specified percentage of its maximum value.

2.3.1 Theory

The theoretical considerations of the flash method have been presented by Parker (Ref. 14); Cape and Lehman (Ref. 15); and Cowan (Ref. 16). The equations are obtained from the solution of the heat transfer in a slab as discussed by Carslaw and Jaeger (Ref. 17).

The temperature distribution in a slab, assuming no heat transfer in a direction parallel to the faces, is given by the solution of the differential equation:

$$\frac{\partial T}{\partial \theta} = \alpha \frac{\partial^2 T}{\partial x^2} \tag{4}$$

where T is temperature, θ is time, α is thermal diffusivity, and x is the distance from the face receiving the energy pulse. This satisfies the boundary conditions

$$\begin{aligned} \frac{\partial T}{\partial x} &= \frac{h_o}{k} \quad , \; x = 0 \\ \frac{\partial T}{\partial x} &= -\frac{h_1}{k} \; , \; x = l \end{aligned} \tag{5}$$

where h is the energy loss rate from either surface. The general solution which accounts for losses from both faces of the sample (Ref. 16) is

$$\Phi = 2 \sum_{n=1}^{\infty} \frac{y_n^2}{D_n} e^{-y_n^2 \alpha \theta l^{-2}} \tag{6}$$

where

$$\Phi = T(l,\theta) \frac{\rho \cdot C_p \cdot l}{Q} = \frac{T(l,\theta)}{Tm} \tag{7}$$

T = temperature above steady state temperature
θ = time
ρ = density
C_p = heat capacity
l = sample thickness
Q = pulse energy per unit area
Tm = $Q/\rho \cdot C_p \cdot l$

and y_n is the solution in each $n\pi$ to $(n+1)\pi$ interval of

$$\cot y = \frac{y}{a} - \frac{b}{ay} \tag{8}$$

$$D_n = y_n \sin y_n \left[1 + a - \frac{2b}{a} + \frac{y_n^2}{a} + \frac{b}{y_n^2} + \frac{b^2}{ay_n^2} \right] \tag{9}$$

a and b are defined as:

$$a = l(C_o + C_l)$$

$$b = \frac{ra^2}{(1+r)^2} \tag{10}$$

$$r = \frac{C_o}{C_l}$$

and

$$C_1 = \left(\frac{\partial h}{\partial T}\right)\left(\frac{1}{k}\right)_{x=l}$$
$$C_o = \left(\frac{\partial h}{\partial T}\right)\left(\frac{1}{k}\right)_{x=0} \tag{11}$$

where h is the energy loss for each surface and is approximated by $h = \epsilon\sigma T^4$. Cowan (Ref. 18) has shown a and r may be evaluated by

$$r = \left(\frac{T_o}{T_1}\right)^3$$
$$a = 6.9\, l\epsilon \left(\frac{T}{1000}\right)^3 \left(\frac{1+r}{k}\right) \tag{12}$$

assuming k and ϵ are the same for both surfaces (T in °R, l in ft, and k in Btu/hr-ft-°F).

Thermal diffusivity may be calculated by measurement of the time, $\theta_{1/2}$, at which Φ reaches one-half of its maximum value. For the case of zero losses at both faces, Parker has shown that

$$\alpha = \frac{1.38}{\pi^2}\frac{l^2}{\theta_{1/2}} \tag{13}$$

The presence of losses changes the value of $\alpha\theta_{1/2}/l^2$ as shown by Fig. 2. This term may be determined by evaluation of the terms a and r from Eq. (12). However, the procedure requires a knowledge of k and ϵ. For this work, the method of determining the constant from the shape of the time-temperature curve (Ref. 18) was selected as the parameter, a, need not be calculated, and only an approximate value of r must be known. The ratio of Φ at five times the one-half

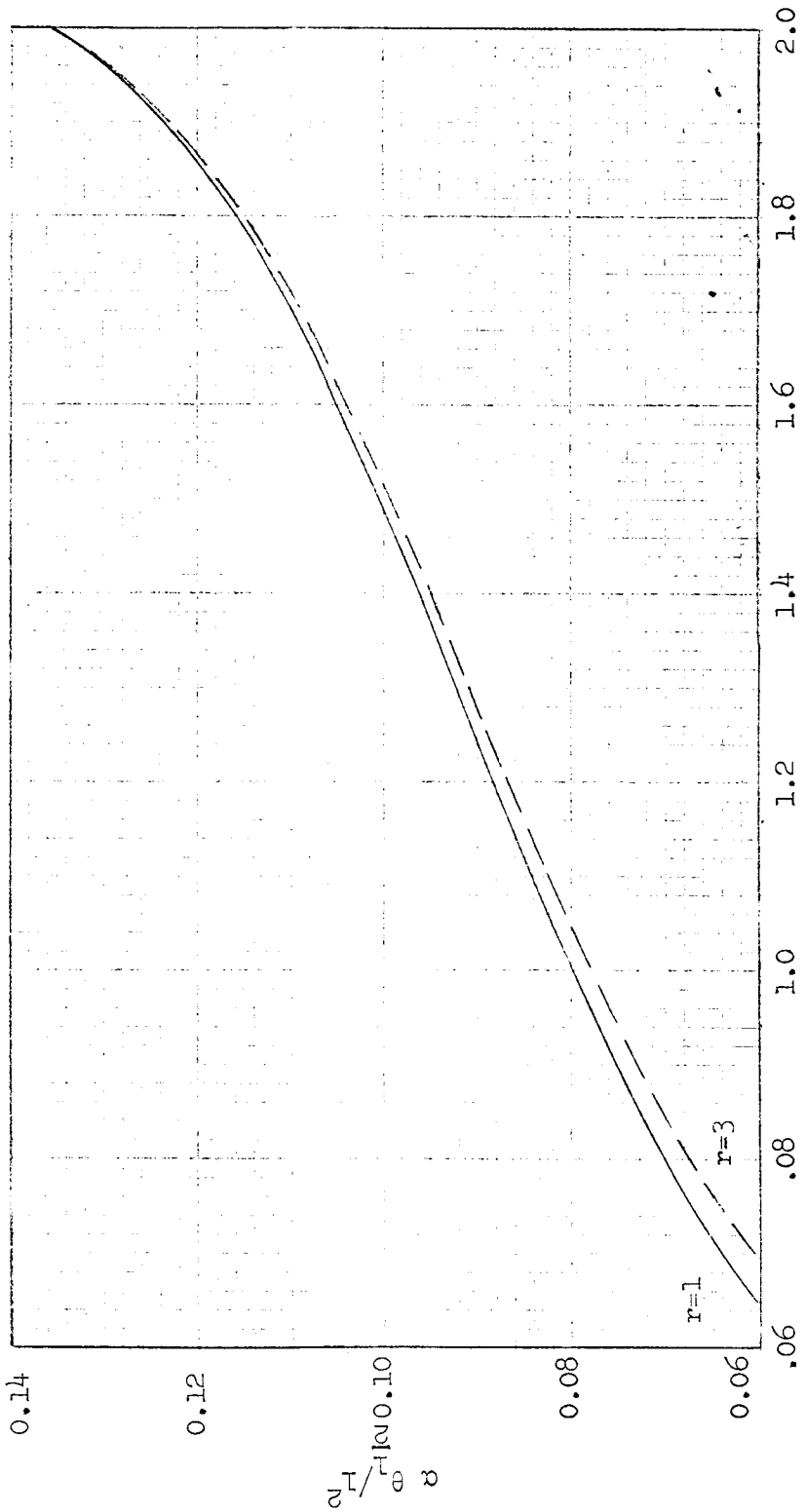

Figure 2. Loss Correction, $\alpha\ \theta_1/1^2$, Based on Sample Cooling Curve

rise time to the one-half rise time, $\Phi_{(5\theta_{1/2})}/\Phi_{(\theta_{1/2})}$, is determined from the data trace for each specimen temperature. Figure 2 graphically illustrates the value of the term $\alpha\theta_{1/2}/l^2$ as a function of $\Phi_{(5\theta_{1/2})}/\Phi_{(\theta_{1/2})}$ for value of $r = 1$ and $r = 3$.

2.3.2 Method of Operation

The diffusivity measurement sequence is initiated by determination of the weight and dimensions of the sample. Measurements are made using an analytical balance and a micrometer. The sample is then inserted in a 15/16-in. diam. by 1/2-in. thick ATJ graphite holder having a 3/8-in. diam. hole counterbored to a depth of 3/8 in. to receive the specimen. The sample is secured in the holder using two 1/16-in. diam. graphite tapered pins.

Prior to the installation of the sample in the furnace the alignment of the laser and detector are verified in the following manner. Detector alignment is checked by placing a disc having a 1/4-in. diam. aperture in the furnace. Illumination of the aperture with a diffuse light source permits visual observation of the resulting focus on the detector element. The disc is then removed and replaced by a sample holder having a 1-in. diam. disc of exposed photographic film attached to one face. The holder is positioned in the furnace so that the film surface corresponds to the position of the char sample front face. The laser is operated, and the film is removed from the furnace. The position of the burned spot resulting from the beam energy is noted, and the laser alignment is adjusted until the spot is in the center of the sample holder, thus insuring uniform irradiation of the sample front face. The laser beam diameter is approximately 3/4-in. at the specimen position. The holder containing the sample is now positioned in the center of the furnace and secured with a tapered wedge. The furnace is closed up and evacuated to a pressure of 10^{-5} Torr. Upon reaching this vacuum, furnace power is turned on for the initial measurement temperature. During this furnace warm-up period the detector system is adjusted for constant bias voltage and background level. At equilibrium furnace temperature the sample back face is

viewed by the detector and the resulting signal recorded to determine when the sample has reached thermal equilibrium. After steady-state conditions have been achieved the detector signal is measured for calculation of specimen temperature in the range of 500 to 1100°F. Optical filters are then used to prevent reflected energy from the laser from reaching the detector element. The ambient signal level from the heated specimen is reduced to zero by a bucking circuit before the signal is passed to a differential amplifier and the oscilloscope for recording the temperature history data. The oscilloscope is triggered and after a preset delay fires the laser. The laser firing circuit imposes a spike on the trace which is used for a time zero point. The detector signal versus time trace on the oscilloscope is recorded photographically. The temperature of the sample is again measured at the completion of the diffusivity data sequence, and furnace power is then increased to obtain the next temperature step.

The measurement procedures are modified when the specimen temperature exceeds 1300°F. The changes are the use of a micro-optical pyrometer for measuring sample temperature, and the use of cooled narrow bandpass filters to improve the detector response. Furnace operation above 4000°F requires pressurization of the system with argon to 20 psia.

2.4 HEAT CAPACITY

Heat capacity of nylon-phenolic chars has been determined from measurements of their enthalpy, as referenced to 32°F, as a function of temperature. A flooded ice-mantle calorimeter of the type described in Ref. 19 is used for these measurements. The enthalpy data are fitted by a least square method to an equation of the form:

$$\Delta H_{32} = a + bT^{-1} + cT + dT^{2} \qquad (14)$$

where ΔH_{32} is enthalpy and T is specimen temperature.

The heat capacity is obtained by taking the derivative of Eq. (14),

$$C_p = \frac{d(\Delta H_{32})}{dT} \tag{15}$$

and calculating C_p over the desired temperature range.

For this program the heat capacity data for nylon-phenolic chars from Ref. 20 were used for calculation of thermal conductance from thermal diffusivity data. The applicability of these heat capacity data was verified by measurement of the enthalpy of chars formed at 1800 and 2900°F. These measurements were made over the temperature range of 500 to 3000°F. As the enthalpy values measured on two of the specimens for the program agreed with values calculated from the data of Ref. 20 within 7% no measurements were made on the remaining specimens.

Section 3

EXPERIMENTAL APPARATUS

3.1 CHAR PREPARATION FURNACES

3.1.1 Laboratory Chars

A small muffle tube furnace was used to prepare 1832° F, Type A chars. This consists of a resistance – heated furnace with a 1 in. ID mullite tube in the central 6-in. long hot zone.

3.1.2 Rapid-Heat Furnace

This furnace consists of a tubular graphite resistance heating element housed in a heavy gage aluminum shell equipped with suitable ports for observing the sample and its temperature and designed for use in air or inert atmosphere at pressures ranging from 0.15 to 150 psia.

For preparing chars of Types B and C; 2200° F and 2900° F chars, respectively; three samples of a given sheet type are placed on a graphite platform which is an integral part of the specimen holder assembly, Fig. 4. A graphite lid is placed on the samples to assist in maintaining their geometry, particularly their flat surfaces. During test, the specimen holder assembly is inserted into the cylindrical graphite heater (Fig. 3). Power to the heater is supplied through water-cooled copper bus bars. Copper terminal clamps are used to provide contact between the heater and input leads. The graphite heater is aligned within the chamber so that the central axis of the tube heater and the central axis of the specimen holder are coincident. The specimen holder assembly is constructed to allow its fore and aft movement without affecting the enviroment within the chamber. Power for resistance heating is supplied by an 8000-A

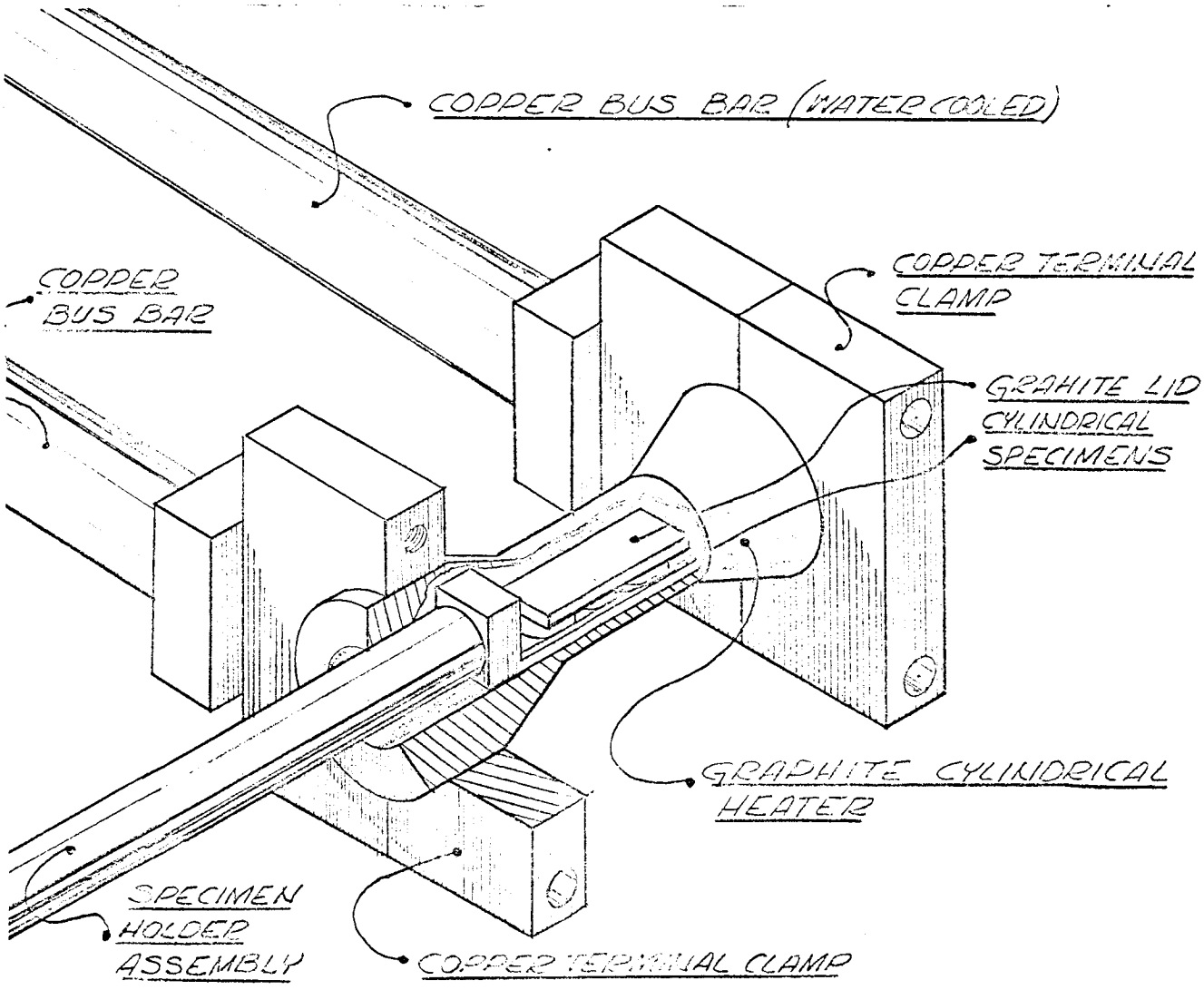

FIGURE 3

APPARATUS FOR CHAR FORMATION AT
2200 ^{o}F AND 2900 ^{o}F

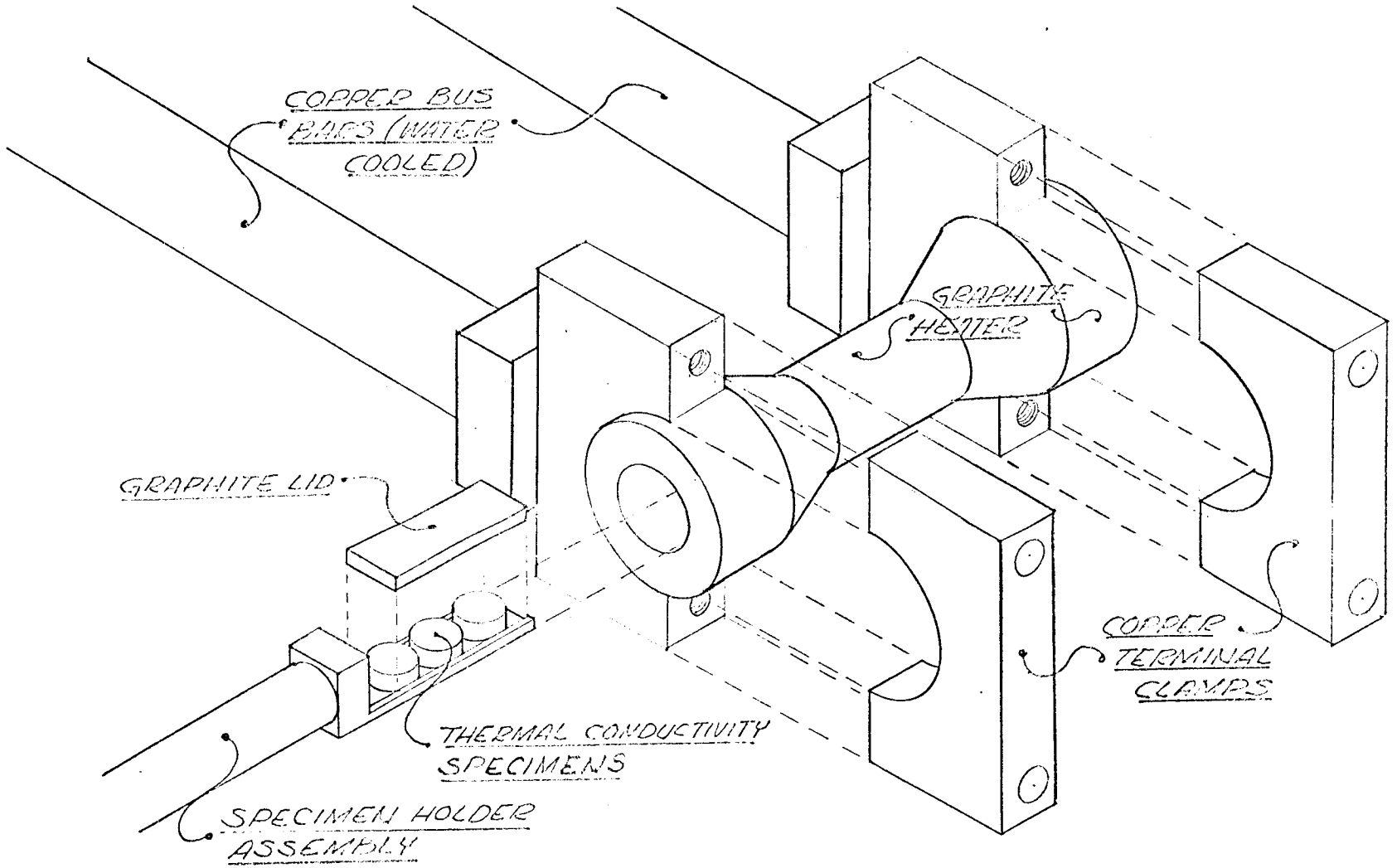

FIGURE 4

A SAMPLE HOLDER AND FURNACE DETAIL FOR CHAR FORMATIONS

JGB
3-2-65

power supply.* The furnace chamber is equipped with suitable gages for accurate pressure measurement, a heavy duty vacuum pump, and suitable gas inlets for pressuring the system.

3.2 CHAR CHARACTERIZATION

3.2.1 Pore Spectra

Mercury porosimetry to determine pore volume and distribution was carried out using an Aminco-Winslow porosimeter, Cat. No. 5-7107**, designed to analyze pore spectra in the range of 0.035 to 100μ. The instrument consists of:

- Penetrometer – a capillary tube with a well for housing the test sample.
- Penetrometer filling device – a glass housed chamber in which Hg is introduced under vacuum until the penetrometer is filled and then brought to atmospheric pressure.
- Hydraulic system in which the penetrometer and its contents can be brought to 5000 psia.
- Suitable pressure indicators.
- A vacuum pump for operating in the range 100μ to atmospheric pressure.

The instrument is described in greater detail in Refs. 5 and 6, and 7.

Pore spectra above 100 μ were determined by quantitative stereology as described in Sec. 2.

---

*Mfg. by L. H. Butcher Co., Los Angeles, Calif.
**Mfg. by American Instrument Co., Silver Spring, Md.

3.2.2 Density

Bulk density was determined from mass measurements obtained on an analytical balance sensitive to 0.0001 gm. Volume measurements were made with vernier calipers or micrometers. Apparent densities and real densities were obtained with the use of the porosimeter described in the previous section.

3.2.3 Structure

The microstructure of the chars was determined by using the methods described in Sec. 2. The metallographic laboratory includes complete sample preparation and examination equipment. Samples were prepared utilizing specialized automatic polishing and etching equipment developed by W. Coons and unique to LMSC. Samples were photographed using a Bausch and Lomb research model metallograph.

X-ray diffraction measurements were made using a General Electric XRD-5 diffraction unit.

3.3 THERMAL DIFFUSIVITY

3.3.1 Experimental Apparatus

The apparatus is composed of four major components: a pulsed laser source, a combination vacuum – inert gas furnace, a vacuum system, and instrumentation. The general layout of the apparatus is shown in Figs. 5 and 6. A schematic of the system is presented in Fig. 7. The detailed design of each subsystem is discussed below.

Laser Source. This system consists of a LMSC designed and fabricated ruby crystal laser. It includes a laser head and a combination power supply-triggering unit. The laser is capable of a 25-J output for a 7200-J input. The output pulse duration is approximately 1 msec.

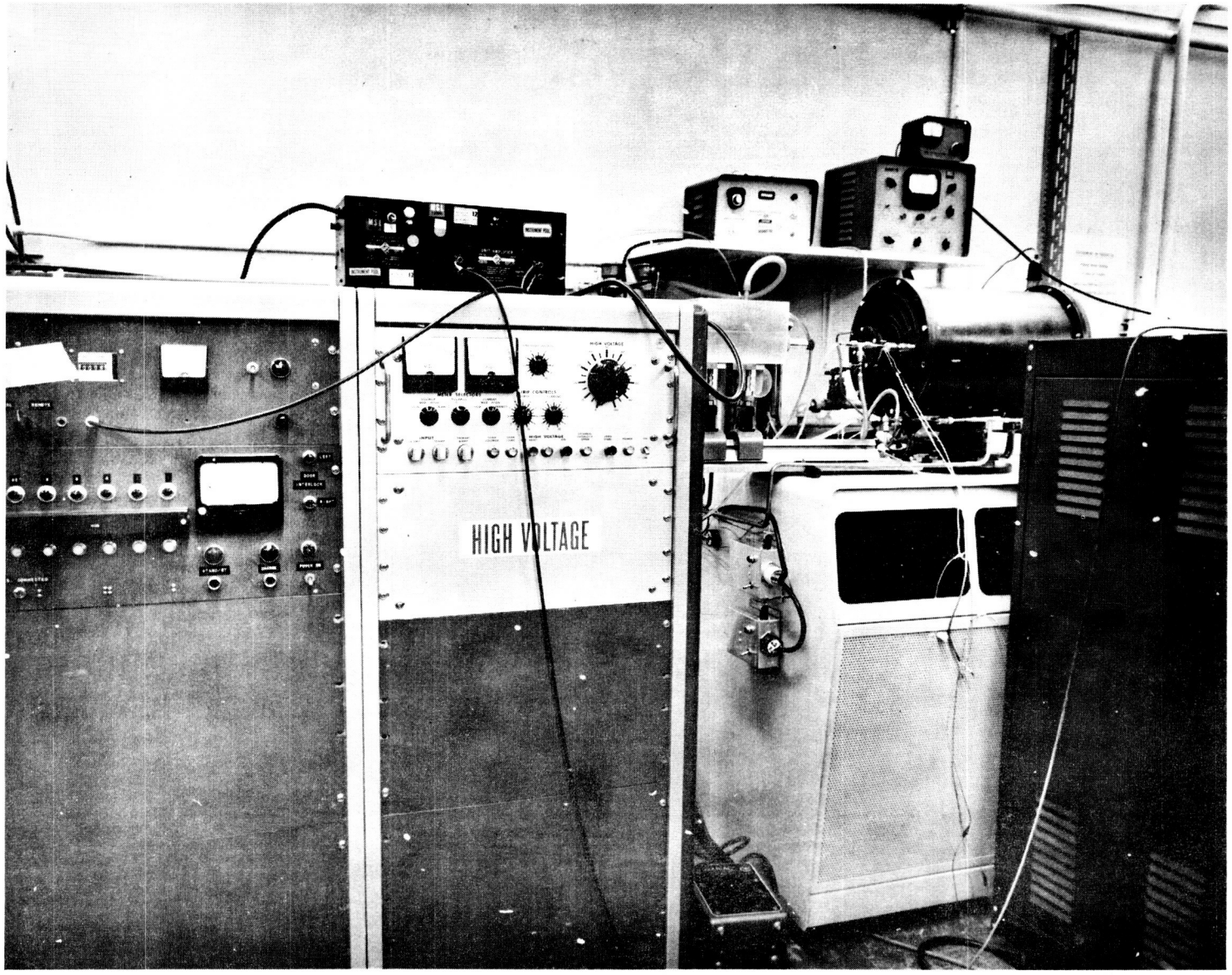

Figure 5 Thermal Diffusivity Apparatus

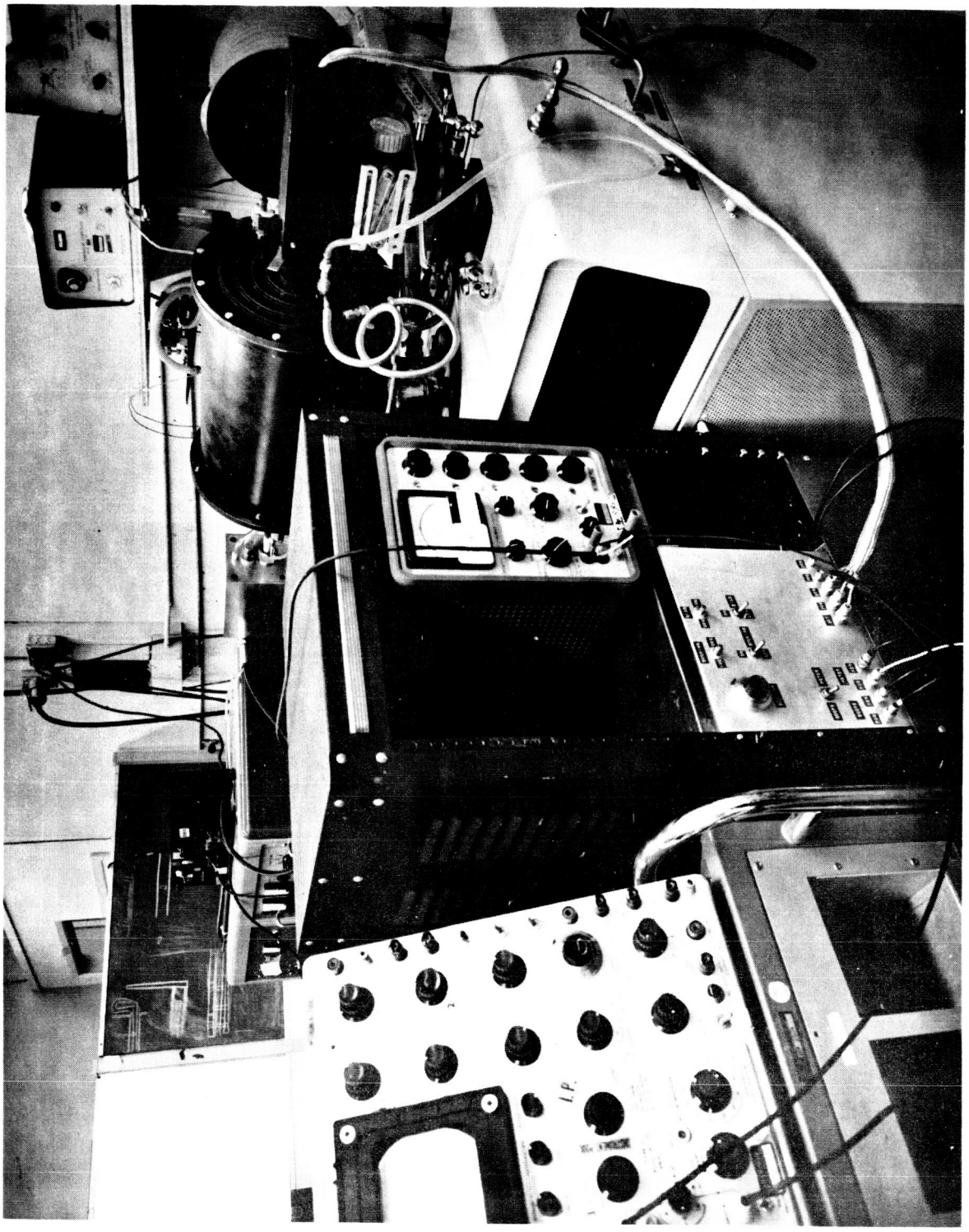

Figure 6 Thermal Diffusivity Apparatus

The head is composed of an elliptical pump cavity containing a 5/8-in diam. by 6-in. long ruby rod mounted at one focus. A linear xenon flash lamp is mounted at the second focus. The cavity and rod are cooled with cold nitrogen gas. An optical rail is used for mounting the head to allow accurate positioning with respect to the furnace.

The power supply-triggering unit contains the capacitors for storage of lamp input energy, circuits and controls for charging the capacitors, triggering circuits, and a pulse shaping circuit. The oscilloscope delay trigger source is employed to supply a trigger pulse to the laser trigger circuit.

Furnace. Figure 8 illustrates the combination vacuum-inert gas furnace. The furnace is basically a water- cooled pressure-vacuum shell housing a graphite tube heating element and the necessary radiation shields and thermal insulation. Power is provided by a 25-kVA low voltage supply.

The shell is a 16-in. diam. stainless steel water-cooled cylinder mounted with its axis in a horizontal plane. The cylinder is provided with a 4-in. diam. vacuum pumping port that also serves as a mounting for the furnace. Ends of the shell are removable to allow access to the heater element and shields. The end plates contain windows, water-cooled shutters to protect the windows, and inert gas pressuration ports. The Vycor window on the laser end of the furnace is 2 5/8-in. diam. by 1/2-in. thick. Samples may be removed and replaced through this window. A 1 1/2 by 1/8-in. thick sapphire window is provided for the detector.

The heater element is an ATJ graphite tube 12-in. long by 1-in. ID. A hot zone is formed by three 2 1/2 turn helical slots machined in the central 6 in. of the tube. The tube is supported concentrically in the shell by two water-cooled clamps that also serve as electrical power connections. Thermal insulation in the furnace is provided in the form of concentric radiation shields and an outer wrapping of fibrous insulation. The radiation shielding consists of three concentric graphite cylinders adjacent to the heater plus four concentric tantalum outer shields. The shields are supported in two grooved end plates.

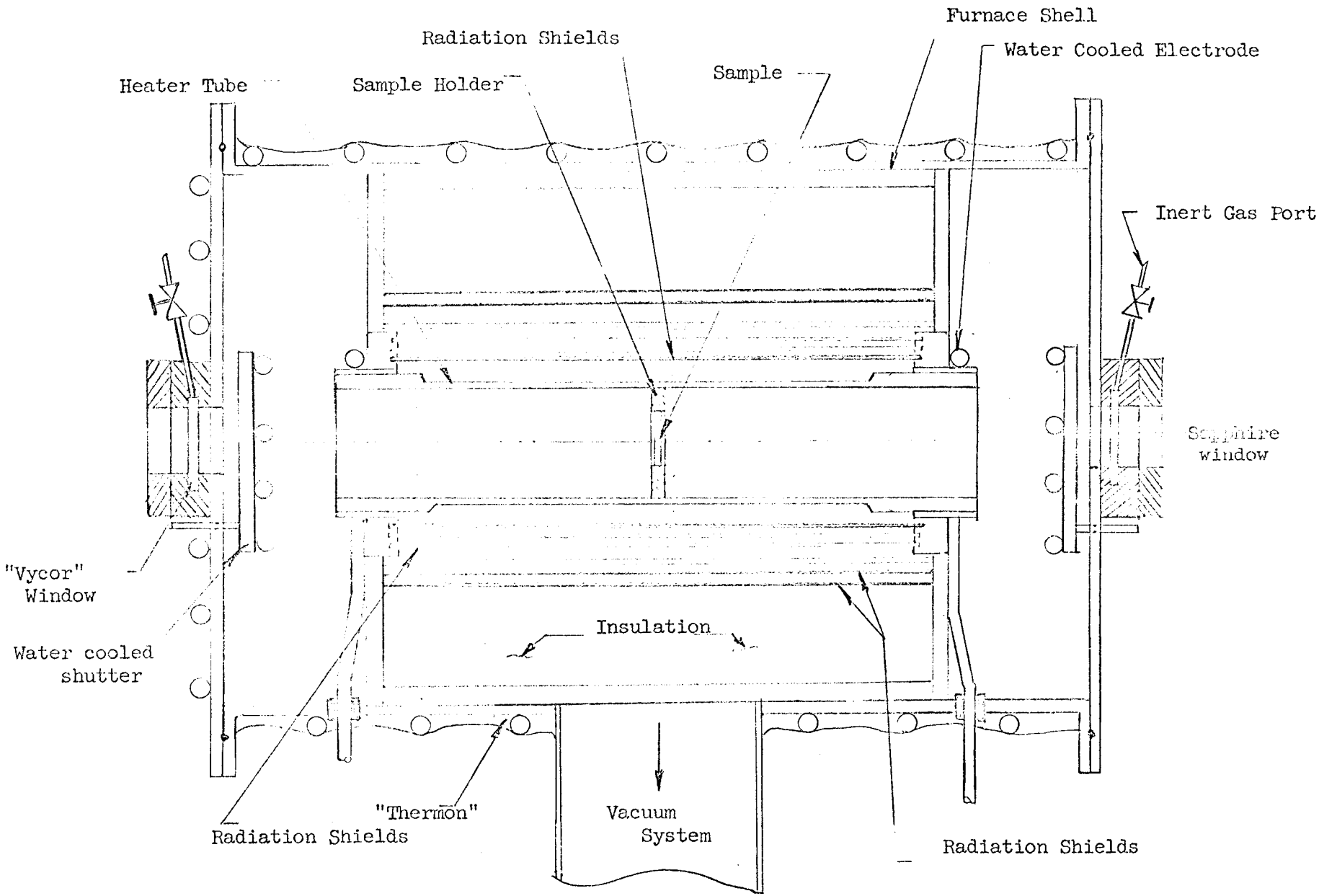

Figure 8 Furnace Assembly for Thermal Diffusivity Apparatus

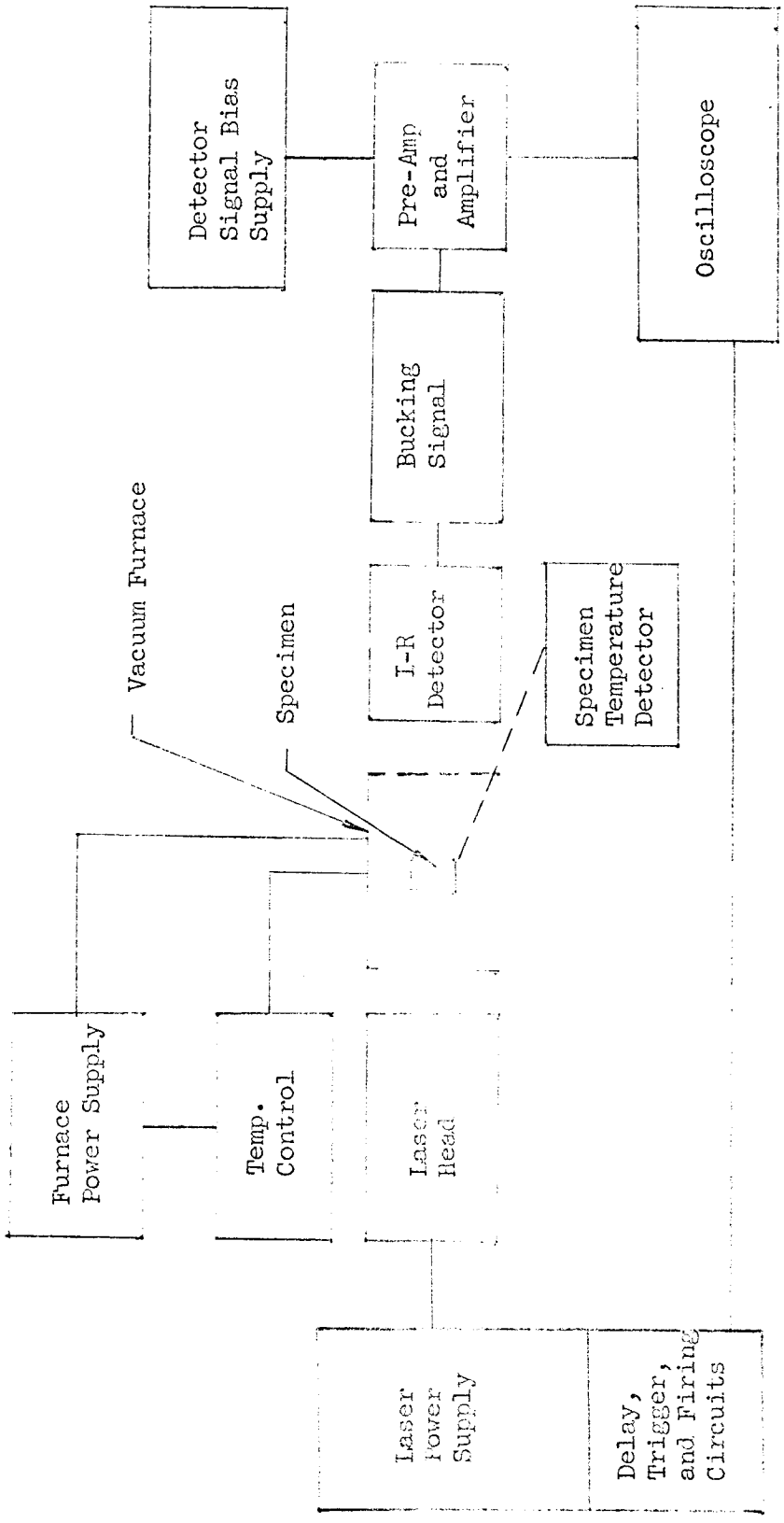

FIGURE 7

Instrumentation Schematic for Thermal Diffusivity Apparatus

Vacuum System. The vacuum pumping system consists of a 4-in. oil diffusion pump and a 5-cfm mechanical pump. The system is provided with a LN_2 cold trap. Both thermocouple and an ionization vacuum gage are provided in the furnace.

Instrumentation. The detector system consists of two matched PbS elements (1-mn square) mounted in a copper cavity on a single copper plate. One detector is mounted so it receives no energy from the furnace or specimen, and it is used as a load resistor. A fused silica lens focuses the energy from a central 3-mm diameter area at the rear of the sample into the active element. The image is approximately 2 mm in diameter so the element is completely flooded with energy from the specimen back face. Detector and optics are mounted in a light-tight enclosure which includes filter holders and movable front surface mirror for sighting a pyrometer on the specimen and transferring energy from a reference blackbody source on the detector. This enclosure is mounted on compound feeds for alignment of the entire assembly.

A differential d-c to 2-kc band pass low noise amplifier having a gain of approximately 10^3 is employed to amplify the detector signal before it is passed to the oscilloscope preamplifier. A bucking circuit is connected between the detector and amplifier so the ambient signal of the detector may be nulled for measurement of rear face temperature rise. The amplified detector signal is fed into an oscilloscope which is fitted with a camera for recording the display. Detector signal level for specimen temperature determination to 1100° F is measured with a differential d-c voltmeter sensitive to 10^{-5} V when used as in the null meter mode.

An optical pyrometer system is used for specimen temperature measurement from 1400 to 5000° F. The pyrometer is sighted on the rear face of the specimen through a sapphire window off of a front surface mirror. A micro-optical pyrometer having an object size of 0.010-in. was used for this program.

3.3.2 Apparatus Calibration

Calibration of the experimental apparatus for measurement of the thermal diffusivity of the char specimens consisted of calibration of the PbS detector system for measuring sample temperatures in the range of 500 to 1100° F, calibration of the optical pyrometer system for temperature measurement from 1400 to 5000° F , and measurement of thermal diffusivity of Armco Iron and CS grade graphite for verification of overall equipment performance.

Detector and Temperature Measuring Instrumentation. Calibration of the PbS radiometer for measurement of specimen temperature in the range of 500 to 1100° F was accomplished by focusing the detector through a sapphire window in the furnace enclosure on a char specimen located at the diffusivity sample position in the furnace. The specimen was instrumented with platinum- platinum 13% rhodium thermocouples, and the temperatures measured by these were assumed to be true specimen temperature. The results of four runs are plotted in Fig. 9 as a signal versus sample temperature calibration curve. The maximum deviation of any point from the curve was 2% and this occurred for only a single point. All other points were within 1% of the smoothed curve through all points.

This calibration does not account for variations in sample emittance from that of the calibration specimen. Measurement of emittance could not be achieved by optical pyrometer data as energy from the furnace was reflected from the sample surface in addition to that emitted by the specimen. Therefore, specimen temperature was not corrected for the variation in emittance from sample to sample. Accuracy of temperature measurement is estimated to be 4% based on an emittance variation of 0.20 between the calibration char and the individual diffusivity specimen. No instability of the detector system was noted during the entire measurement program.

Calibration of the optical pyrometer system was accomplished through the use of an Infrared Industries blackbody source. The system consisted of a micro-optical pyrometer, sapphire window, and front surface mirror. Window transmission and

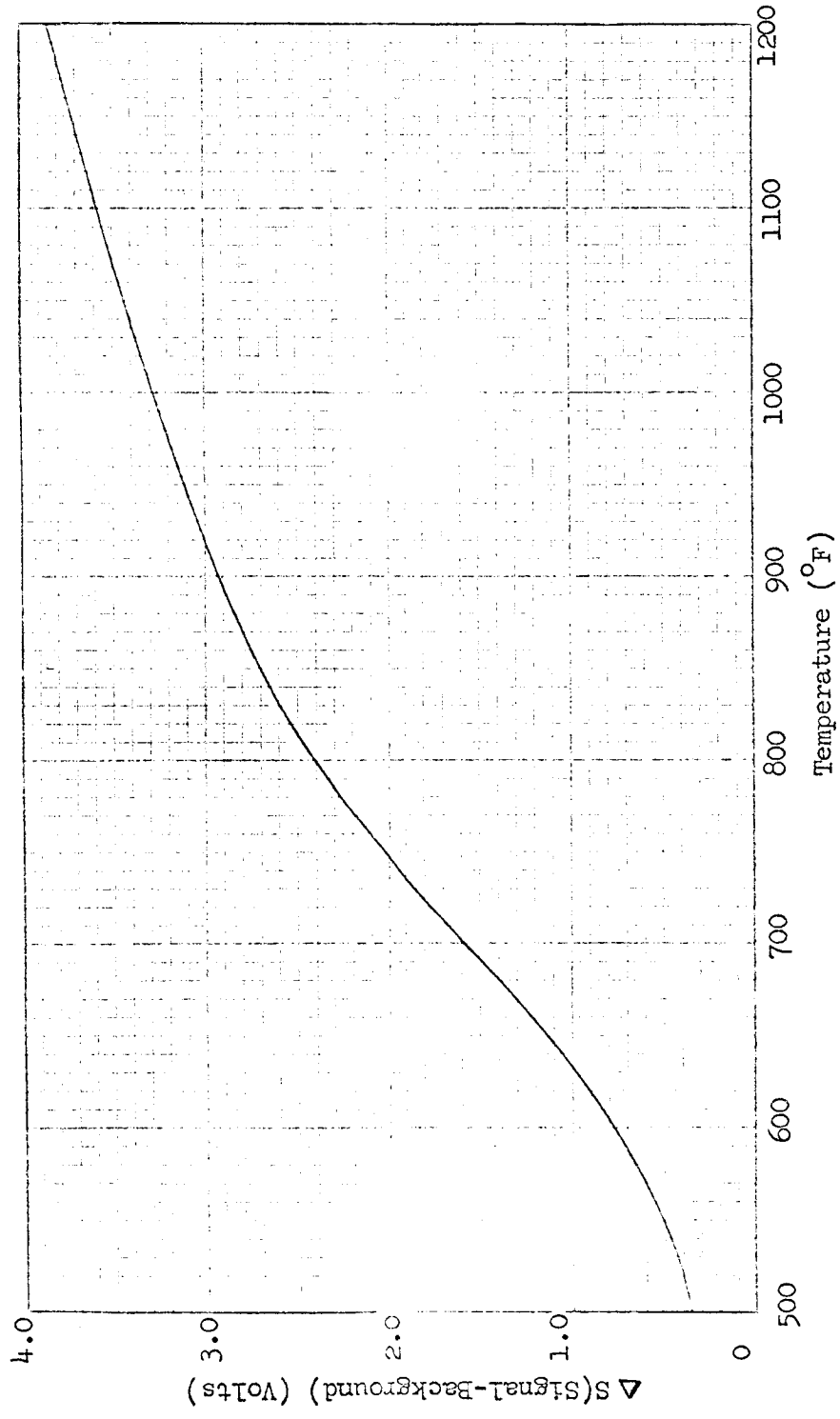

Figure 9. Radiometer Calibration; Signal as a Function of Char Temperature

mirror reflectance were measured by using the blackbody source. Pyrometer calibration was periodically checked against this source. Temperature corrections were made for pyrometer temperature as a function of the product of window transmittance and mirror reflectance. Specimen temperature was determined by measuring the temperature of the holder by sighting into a small cavity opening located adjacent to the specimen. The temperature of the specimen was assumed to be the same as that of the holder as pyrometer measurements showed no difference in apparent temperature between furnace tube, sample holder and specimen. Thus it was felt the assumption of specimen temperature being equal to holder temperature introduced a negligible error in specification of a sample temperature.

Thermal Diffusivity Measurements. To verify the overall operation of the experimental apparatus, it was decided to measure the thermal diffusivity of two materials having well-documented thermal properties. Armco Iron was selected for the temperature range of 500 to 1800° F as its thermal diffusivity has been measured by a number of investigators and its thermal conductivity is accurate to within 5%. For the higher temperature range a graphite material was selected so there would be no reaction between the furnace holder and test specimen. No conductivity data of the accuracy of Armco Iron were found for any of the graphites. However, it was felt the thermal conductivity and heat capacity data available in the literature were sufficiently accurate to verify the temperature dependence of thermal diffusivity and consequently bring out any gross errors which might occur in the experimental apparatus at high temperatures.

Armco Iron. The test specimen was cut from a 3/8-in. diam. bar of Armco Iron. Specimen dimensions were 3/8-in. diam. by 0.094-in. thick. Both faces were polished with No. 600 paper. Temperature of the specimen was measured with a platinum-platinum 13% rhodium thermocouple spot-welded to its edge. Prior to testing the sample was annealed in the furnace at 1700° F for 2 hr.

Thermal diffusivity was calculated from the sample back face time-temperature response, as sensed by the PbS detector, in the manner discussed in Sec. 2.3.1.

The front face temperature, T_o, was estimated from a solution of Eq. 5 of Ref. 2 by plotting temperature at location x as a function of time for x equals 1/8, 1/4, 1/2, 3/4 and 1 times the thickness. Front face temperature was obtained by extrapolation to x = 0. T_o was calculated by graphically integrating the front face temperature over the time interval to the one-half rise time. The values of r were calculated using this value for T_o and the specimen steady-state temperature for T_ℓ as the maximum back face temperature rise was less than 10° F. The values of r were calculated using the thermal conductivity of Armco iron and an emittance of 0.55 for oxided iron, the data being from Refs. 21 and 22 respectively.

The measured thermal diffusivity data for the Armco iron specimen, as a function of temperature, are shown by Fig. 10. The solid line represents diffusivity calculated from ORNL data on thermal conductivity and heat capacity of Armco iron (Ref. 20).

CS Grade Graphite. A 3/8-in. diam. by 0.094-in. thick specimen was machined from a bar of CS stock. Both faces were finished with No. 600 paper. A platinum-platinum 13% rhodium thermocouple was inserted in a hole in the edge of the specimen and secured with a graphite pin driven into the hole. This thermocouple was used for sample temperature measurement to approximately 2800° F. It was then removed and a micro-optical pyrometer used for temperature measurement above this level.

The data for CS graphite are shown graphically by Fig. 11. Loss corrections were calculated from a cooling curve as discussed in Sec. 2.3.1. This method does not require the estimation of ϵ as k for the specimen. These data are compared with diffusivity calculated from thermal conductivity and heat capacity data from two sources (Refs. 22 and 23). Density of the diffusivity specimen calculated from weight and micrometer measurements was 102 lb/ft^3. The significance feature of these data is the slope or temperature dependency of the diffusivity curve is the same as that calculated from conductivity and heat capacity data. Thus, it is shown the corrections for losses are applicable for this material over the temperature range of interest.

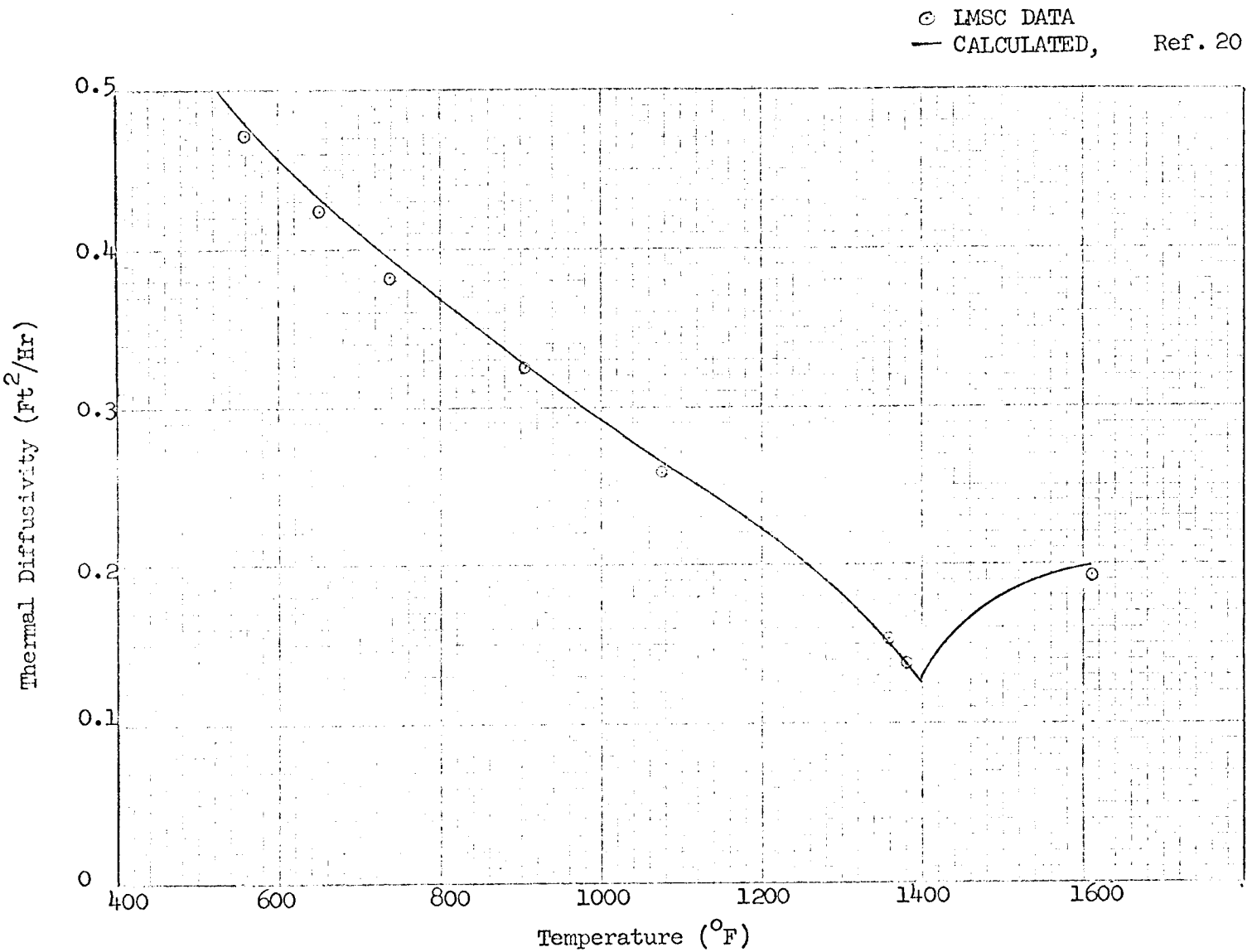

Figure 10 Thermal Diffusivity of Armco Iron(Compared with Diffusivity Calculated from the Conductivity and Heat Capacity Data)

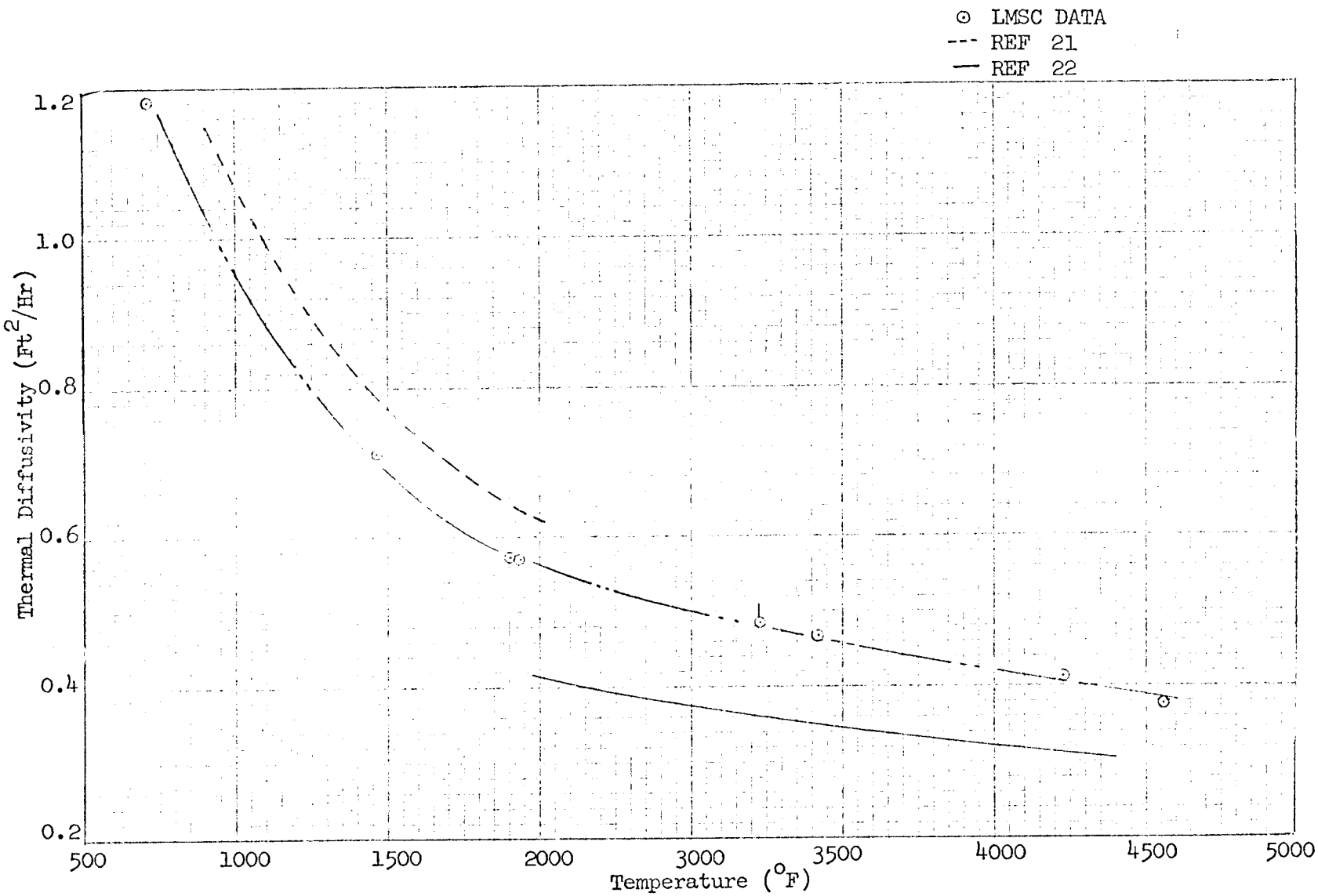

Figure 11 Thermal Diffusivity of Grade CS Graphite (Compared with Diffusivity Calculated from Thermal Conductivity and Heat Capacity Data)

3.4 ENTHALPY

The apparatus used for the enthalpy measurements was a flooded ice-mantle calorimeter similar in construction to that described in Ref. 19. A resistance wire-wound alumina tube furnace was used to heat specimens to 1900° F, and a vertical graphite tube furnace was used for heating to 5000° F. Both furnaces were argon purged at atmospheric pressure. A drop mechanism which consisted of two L-shaped rotatable legs was used to support the capsule containing the sample at the midpoint of the furnace. For measurements to 1700° F a chromel-alumel thermocouple was located in a sheath in the center of the drop capsule. A hole was drilled in the center of the specimen to receive this temperature probe. Above 1700° F, an optical pyrometer was used to measure capsule temperature, assumed to be the same as the specimen temperature.

An ATJ graphite capsule was used for these char measurements. The capsule heat content was first measured over the temperature range of interest. This capsule calibration accounted for capsule heat content as well as heat losses which occur during the finite drop interval. Enthalpy of the specimen is measured with reference to 32° F by subtracting the heat content of the capsule from the total heat content measured by the calorimeter.

Calibration of the calorimeter was verified by using α alumina to 1900° F. Agreement with NBS data is within 1% for enthalpy over this temperature range.

Section 4
DESCRIPTION OF SAMPLES

Six types of nylon phenolic panels, Table 3, were procured for the program. The first five samples consisted of panels (12 in. by 12 in. by 1/2 in.) purchased from a vendor. The samples were produced so that the direction of fiber layup was parallel to the surface of the sheet. This was done to obtain a char of homogeneous surface. It has been found that the char penetration front does not move in evenly on chars formed from material with a chopped fiber or 45-deg angle orientation.

Nominal resin contents of 50 and 60% were specified, as well as the four types of fiber diameter. The vendor (Ref. 24) reported resin solids somewhat different from the nominal. The vendor's reported specific gravity is that calculated for the entire sheet. LMSC data are those obtained on individual samples cut from the sheet. It was found that the sheet stock was quite nonhomogeneous. This was shown by the density variations and by variation in color of the sheet. Color in a sheet would vary from yellow to brown which indicated an uneven distribution of resin content.

A sixth type of material, 9-15-F, had also been purchased from the same source. Nominal resin content was 40%; reported resin content was 37.1%. This material formed puff shaped chars under laboratory conditions, Type A, which were entirely unsuitable for making thermal diffusivity measurements.

In place of the 9-15F material, Zytel S/N 1, furnished by R. Nagler of JPL was used as the sixth type. In this material the nylon is introduced as a powder, rather than as a fiber. The result is a product with randomly distributed nylon particles in a phenolic material. The particular product tested was produced from nylon having a 40/50 mesh size.

TABLE 3

DESCRIPTION OF NYLON PHENOLIC TEST MATERIAL

Material Designation	Nylon Description				Resin Description			Specific Gravity	
	Code	Fiber Dia. (mils)	Polymer Type	Count	Solids, % Nominal	Solids, % Reported*	Resin Type	Westech*	LMSC
9-15A	A-2571**	13	6-6	42x42	50	48.5	EC-201+	1.190	1.186 ± .004
9-15B	A-2951**	9.5	6-6	74x70	50	50.8	EC-201	1.202	1.170 ± .003
9-15C	A-2553**	4.5	6-6	52x52	50	53.4	EC-201	1.198	1.188 ± .015
9-15D	13080***	8.5	6-6	39x37	60	59.8	EC-201	1.212	1.168 ± .026
9-15E	13080***	8.5	6-6	39x37	50	46.5	EC-201	1.210	1.198 ± .032
Zytel S/N 1++	--	--		40/50 Mesh++	50	--	--	--	--

+Product of Evercoat Co., Cincinnati, Ohio

++ Furnished by R. Nagler, Jet Propulsion Laboratory, Pasadena, Calif. (DuPont Nylon "Zytel 103", Bakelite "BPR-5549" resin)

*Furnished by Westech Plastic and Chemical Co., Menlo Park

Data furnished with shipping memo and subsequent communication, Ref. 23

** Product of Stern & Stern, Hornell, N.Y.

*** Product of Burlington Industries, Greensboro, N.Y.

To prepare representative char samples, multiple specimens were removed from each of the five sheets and Zytel block with a circular saw and machined to a final cylindrical configuration. After removal of machining burrs each sample was dimensioned and weighed.

At least six small samples, original dimensions 0.375-in. thick by 0.4-in. diam. were prepared from each sheet. On material 9-15-A, two extra samples were prepared to permit a test of reproducibility of pore spectra determinations. Three were for thermal diffusivity, and one each for pore spectra, x-ray diffraction analysis, and microstructure examination. Samples of each test type, A, B, and C; i.e., 1832, 2200, and 2900°F were prepared.

Six larger samples, original dimensions 0.5-in.-thick by 0.4 in., were prepared for each sheet type and test type for measurement of heat capacity. The total number of such samples was 108.

Larger rectangular specimens, 1 in. by 3/8 in. by 3/16 in., were prepared for measurement of electrical resistivity of chars of two formation types. A total of thirteen samples was prepared.

Section 5

DATA REDUCTION METHODS

5.1 PORE SPECTRA

5.1.1 Mercury Porosimetry

Data from the porosimeter readings are furnished in the form of a penetrometer stem reading (cm^3) as a function of total absolute pressure (psia). A representative table of raw data is given below:

Pressure (psia)	Penetrometer Stem Reading	Pore Diam. (μ)	Volume Percent Porosity
1.8	0	97.5	0
3.6	0.062	48.7	73.8
4.7	0.072	37.2	85.7
6.8	0.077	25.8	91.7
5011.4	0.084	0.035	100

The pore diameter in μ is given by

$$D = \frac{175}{P} \tag{16}$$

which is merely Eq. (1) reduced to its simplest form; D is the pore diameter and P is the absolute pressure. Volume percent porosity is the fraction of a given penetrometer stem reading divided by the total stem reading at completion of the test, multiplied by one hundred. These data can be used to obtain a typical pore spectra curve of pore distribution. A given volume percent porosity, i.e. 73.8%, merely indicates that the

fraction of the total volume of pores determined have a pore diameter of 48.7 or greater. Since this method does not include pores greater than 100 μ or smaller than 0.035 μ, these data do not include those fractions of voids not in the 100- to 0.035-μ diam. range.

$$\% \text{ Total porosity}^* = 100 \times \frac{13.55\, v_1}{(w_1 + w_2 - w_3)} \tag{17}$$

where

v_1 = pore volume of the sample, i.e., the penetrometer stem reading (cm^3)

13.55 = density of Hg (gm/cc)

w_1 = weight of the penetrometer filled with Hg at 1.8 psia (gm)

w_2 = weight of the sample (gm)

w_3 = weight of the penetrometer with sample and filled with Hg at 1.8 psia (gm)

This total porosity neglects the voids greater than 100 μ and smaller than 0.035 μ. The fractions outside of this range can be calculated if the true density of the material is known. However in carbonaceous materials, true specific gravity can vary from 1.2 to 2.2. Consequently the fraction of voids larger than 100 μ must be determined by other means such as quantitative stereology.

5.1.2 Quantatitive Stereology

Determination of the volume fraction of pores greater than 100 μ by quantitative stereology was described in Sec. 2. For the series at hand a rectangular grid, marked 10 by 10, was used for a point count. The number of points along each line which fell on solid material, or closed pores were counted for each line. The grid was allowed to fall randomly on each sample four times on each of two photomicrographs making

*This is the volume percent of material which is in the range 100- to 0.035-μ. Values calculated in this manner are listed as Type B total porosity in Table 7.

a total of 80 counts per sample. When a point fell directly on a solid-void boundary, it was counted as half a unit. Each count is directly proportional to the solids fraction. Then total volume percent porosity of pores greater than 100 μ is given by the following:

$$\text{Total volume percent pores}^* > 100\,\mu = 100\,(1 - f_s) \tag{18}$$

where f_s is the solids fraction as determined by the above method.

A typical analysis is given below for sample of Zytel prepared at 1832° F:

Analysis of Solid Volume of Sample Z-1-10-8-1832

Points per line falling on solid material or on a closed pore smaller than 100 μ	2.5	2	0	2	1	2	0	5
	0	2	2	3	1	2	4	4
	2	1.5	0	2	5	1	2	3
	2	3	1	1	3	1	5	3
	1.5	4	2	1	4	2	3	1
	0	2	4	1	2	2	1	5
	2	0	2	1	5	5	2	1
	2	0.5	1	5	4	3	5	1
	4	4	1	2	1	2	1	2
	1	2	1	1	1	0	4	2
Average solid fraction (%)	17.0	21.0	14.0	19.0	27.0	20.0	27.0	27.0

The average solid fraction, f_s, in percent is given by

$$f_s = \frac{\Sigma x}{n} \tag{19}$$

$$f_s = 21.5$$

where x is the sum of each column and n is the number of such columns.

*This is listed as total porosity Type A in Table 7.

The total volume percent of pores greater than 100 μ is 78.2 as calculated by Eq. (18). The standard deviation is calculated from

$$\sigma = \frac{\Sigma(x - f_s)^2}{n - 1} \tag{20}$$

The average void diameter was obtained in a rather simple manner. Ten diameters were selected at random, measured, and corrected for magnification. The average diameter was calculated from these measurements, and sigma, the standard deviation, was calculated in the usual manner.

For a more precise analysis the statistical approach to measurement of particles and spacing described by Underwood (Ref. 8), could have been adapted for use. In this method lineal analysis is used to compute a mean free distance (MFD) between particles or phases. The MFD is given by:

$$\text{MFD} = \frac{1 - f_v}{P_L} \tag{21}$$

where P_L represents the number of particles per unit length and f_v stands for the volume fraction of the particles. This equation possesses generality as it is independent of the size, shape, or disposition of the second phase. P_L is obtained by random straight-line traverses across the microstructure. However, in our case random sampling could only be obtained by traverses normal to the fiber orientation.

MFD is the mean edge-to-edge distance between particles, i.e., void diameter, assuming a cylindrically shaped rod. S_p, the reciprocal of MFD, is the mean center-to-center distance between particles, or in this case between char fragments. The time available for this study did not permit this more precise analysis of average void diameters.

5.1.3 Total Porosity

Total porosity, Type A (TP_A), is the total volume percent of pores greater than 100 μ is given by Eq. (17). The total porosity of Type B (TP_B) is the total volume percent of pores 100 to 0.035 μ calculated from Eq. (16).

The two functions are not directly additive since TP_B represents the fraction of voids in the 100- to 0.035-μ region, divided by the apparent volume. Moreover, some of the voids greater than a 100 μ may be partially filled when the apparent volume is measured.

To get an estimate of total porosity, of all pores greater than 0.035 μ, the following calculation was made

$$TP_C^* = 100\left(\frac{d_2 - d_1}{d_2}\right) \tag{22}$$

where d_2 is the real density as determined by mercury porosimetry and d_1 is the bulk density as determined from the ratio of mass to volume as calculated from micrometer measurements.

5.2 DENSITY

5.2.1 Bulk Density

The bulk density is calculated from the following:

$$\text{Bulk density} = \frac{w}{\pi r^2 h} \tag{23}$$

where w is the weight of the sample, r is the average radius, and h is the thickness of the specimen.

---

*These data are listed as total porosity, C, in Table 7.

5.2.2 Apparent Density

The apparent density in cgs units, or specific gravity, was determined from mercury porosimetry data, and it is calculated as follows:

$$\text{Apparent density} = \frac{13.55\, w_2}{w_1 + w_2 - w_3} \tag{24}$$

where w_2 is the weight of the sample, w_1 is the weight of penetrometer filled with mercury at 1.8 psia, w_3 is the weight of the penetrometer with sample, filled with mercury at 1.8 psia, and $(w_1 + w_2 - w_3)/13.55$ represents the apparent volume of the sample.

If there are not a large number of pores which are filled with mercury at 1.8 psia, then the apparent density should approach the bulk density.

5.2.3 Real Density

The real density in cgs units, or specific gravity, as determined from mercury porosimetry data, is calculated from the following:

$$\text{Real density} = \frac{w_2}{\left(\frac{w_1 + w_2 - w_3}{13.55}\right) - v_2} \tag{25}$$

where v_2 is the penetrometer stem reading at 5000 psi, and the denominator represents the displacement volume of the solid portion of the char.

The real density determined in this way is uncorrected for closed pores or pores smaller than 0.035 μ.

5.2.4 Crystallite Density

The crystallite density in cgs units, i.e., the real density of the crystallites having some degree of ordering, can be calculated from the following:

$$\rho = \frac{n_o}{a_o \cdot c_o} \cdot \frac{mw}{6.023 \times 10^{23}} \cdot \frac{1}{10^{24}} \tag{26}$$

where

n_o = number of atoms per unit cell

n_o = 4

$a_o \cdot c_o$ = volume of a unit cell

a_o = 5.245 Å^2

c_o = height of the unit cell, in Å as determined by x-ray diffraction analysis

mw = molecular wt = 12.01 gm

6.023×10^{23} = Avogardo's number.

Then the equation for crystallite specific gravity reduces to

$$\rho = \frac{15.207}{c_o} \text{ gm/cm}^3 \tag{27}$$

where c_o is still in Å.

5.3 X-RAY DIFFRACTION ANALYSIS

The crystallite density is calculated from Eq. (27). The quantity $I_{max} \cdot \beta^*$ provides an indication of the quantity of ordered crystallite material. It is the product of the relative peak height and the peak width at half height corrected for instrumental line broadening, which in this case was the measured peak width minus 0.3.

The crystallite thickness, L_c, is given by

$$L_c = \frac{\lambda}{\beta^*} \cdot \frac{1}{\cos \theta} \tag{28}$$

where L_c is the crystallite thickness in $\mathring{A}$; λ is the wavelength of the analysing radiation, 1.5418 $\mathring{A}$; β^* is the peak halfwidth in radians corrected for instrumental line broadening, and θ is the characteristic scattering angle.

For precise analysis β^* should be corrected for b', absorption, and b'', the effect of surface roughness. The time available for this study program did not permit this more precise analysis. The crystallite length, L_a, could not be obtained from the data available.

5.4 THERMAL DIFFUSIVITY

A typical recording of the temperature history data from a specimen is shown by Fig. 12. A 40 kV pulse for firing the flash lamp imposes a voltage on the detector circuit which puts a spike on the trace. This spike is the zero point for time measurements. The laser action starts within 1 msec of this trigger pulse, and for a one-half rise time of 100 msec or longer this introduces a negligible error in the time measurement.

The time for the signal to reach one-half of its maximum value has been selected as the time base for the diffusivity measurements reported here. The one-half rise time is determined by direct measurement on the photograph. Multiplication of this distance by the scope sweep speed setting yields the one-half rise time, $\theta_{1/2}$. A variable frequency generator is used to verify oscilloscope sweep speed calibration. Diffusivity is calculated from Eq. (13)

$$\bar{\alpha} = \frac{1.38}{\pi} \frac{l^2}{\theta_{1/2}} = \frac{0.139\, l^2}{\theta_{1/2}} \tag{13}$$

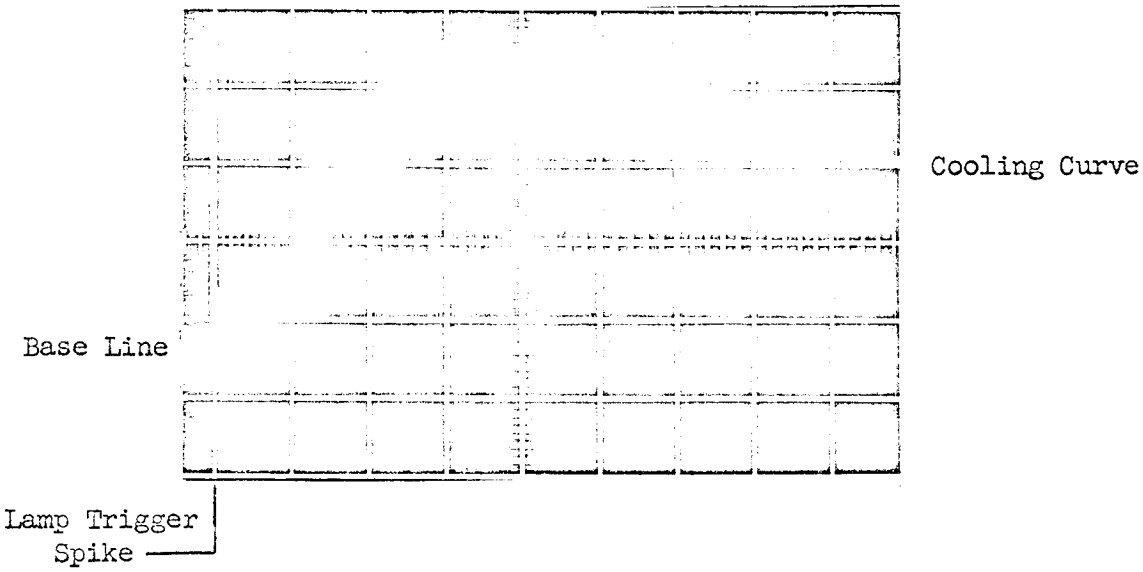

Figure 12 Typical Rear Face Time-Temperature Response Curve

where $\bar{\alpha}$ is the value uncorrected for losses. The cooling portion of the temperature response curve is used to evaluate losses during the measurement period. The signal ratio at five times $\theta_{1/2}$ to the signal ratio at $\theta_{1/2}$ is determined directly by measurement from the data record. This value is used in conjunction with Fig. 2 to calculate a correctedvalue of $\alpha\ \theta_{1/2}/l^2$. The corrected diffusivity is then

$$\alpha = \bar{\alpha} \times \frac{\left(\frac{\alpha\ \theta_{1/2}}{l^2}\right)}{0.139} \tag{29}$$

The maximum uncertainties in calculation of thermal diffusivity from the data are as follows:

$\theta_{1/2}$; 1% in measurement of one-half rise time based on a sweep speed to give a 3-cm distance from zero time.

l ; 7% for char specimens based on an uncertainty of 1% across surface asperities and a 3% deviation of the surface from peak-to-peak measurements.

These results in an uncertainty of 15% in $\bar{\alpha}$ as calculated from Eq. (13). It must be noted the major source of error lies in the determination of the thickness, l, for char specimens having an irregular surface pattern. The error may be reduced by measurement of surface profile of each sample and then calculating l on the basis of the peak-to-peak distance minus the rms value of peak-to-valley height for each surface. The scope of this program did not permit the detailed surface analysis of each specimen.

The maximum uncertainty in corrected thermal diffusivity, α, is estimated to be 20% based on 15% for $\bar{\alpha}$ and a maximum uncertainty in the loss correction of 5%.

5.5 HEAT CAPACITY

The heat capacity of the specimens was determined from enthalpy data as discussed in Sec. 3.4. The only measurements made for this program were to verify the data from Ref. 20. Enthalpy is calculated, referenced to 32° F, from the following expression:

$$\Delta H_{32} = \frac{3.5 \times F \times \Delta X}{m} \text{ (Btu/lb)} \tag{30}$$

where

- 3.5 = conversion factor for the heat of fusion-volume relationship for ice, Btu/cm^3
- F = volume measuring tube factor, cm^3/cm of height
- ΔX = total depression of the measuring tube minus the depression due to the heat content of the capsule, cm
- m = mass of the sample, lb

An equation of the form $\Delta H_{32} = a + bT^{-1} + cT + dT^2$ is fitted to the enthalpy versus temperature data by a least squares method to evaluate the coefficients. The derivation of the resultant expression is then taken to obtain the equation of heat capacity as a function of temperature.

5.6 EFFECTIVE THERMAL CONDUCTIVITY

Although the authors believe the terminology "conductance" more accurately describes the heat transfer parameter for structures such as chars, it will be referred to as "effective thermal conductivity," $\bar{k}$, in this report to prevent confusion when comparisons are made with the data and those of other investigators. The calculated values of $\bar{k}$ for each specimen tested are tabulated in Table B as a function of temperature.

Reduction of the experimentally determined thermal diffusivity data to give a value of effective thermal conductivity is accomplished by use of

$$\bar{k} = \rho \cdot C_p \cdot \alpha \tag{31}$$

where ρ is bulk density, C_p is heat capacity, and α is thermal diffusivity. All of these parameters are evaluated at the temperature for which $\bar{k}$ is to be calculated. For this program the temperatures is taken as the steady-state specimen temperature just prior to application of the pulse of radiant energy. Parker (Ref. 14) has shown the mean temperature rise of the specimen to be approximately 1.6 times the back face temperature rise which for these measurements did not exceed 20° F. This introduces a maximum uncertainty of 5% at 600° F and 2% at 1500° F in the reported temperatures for $\bar{k}$. The maximum error in evaluation of C_p from Fig. 13 is less than 2% on the basis of steady-state temperature. As no attempt was made to monitor energy for each measurement nor to evaluate absorptance of each specimen for the laser beam wavelength interval it is felt correction of mean specimen temperature is not warranted.

Room temperature bulk density, corrected for water absorption, was used for all calculations for a given sample. No corrections were applied for expansion of the specimen upon heating as the uncertainty introduced by this procedure is less than 2% based on thermal expansion data for nylon-phenolic chars from Refs. 11 and 25.

Heat capacity values were taken from Fig. 13 which graphically shows heat capacity of nylon-phenolic chars as a function of temperature. No attempt was made to correct heat capacity for changes which might occur with exposure above the formation temperature due to changes in char structures.

The estimated maximum uncertainty in calculated effective thermal conductivity values is 39% based on the following uncertainties in the terms

$$\Delta \bar{k} = \Delta \rho + \Delta C_p + \Delta \alpha \tag{32}$$

$\Delta \rho$ = 10% (due to weight loss as a function of exposure)

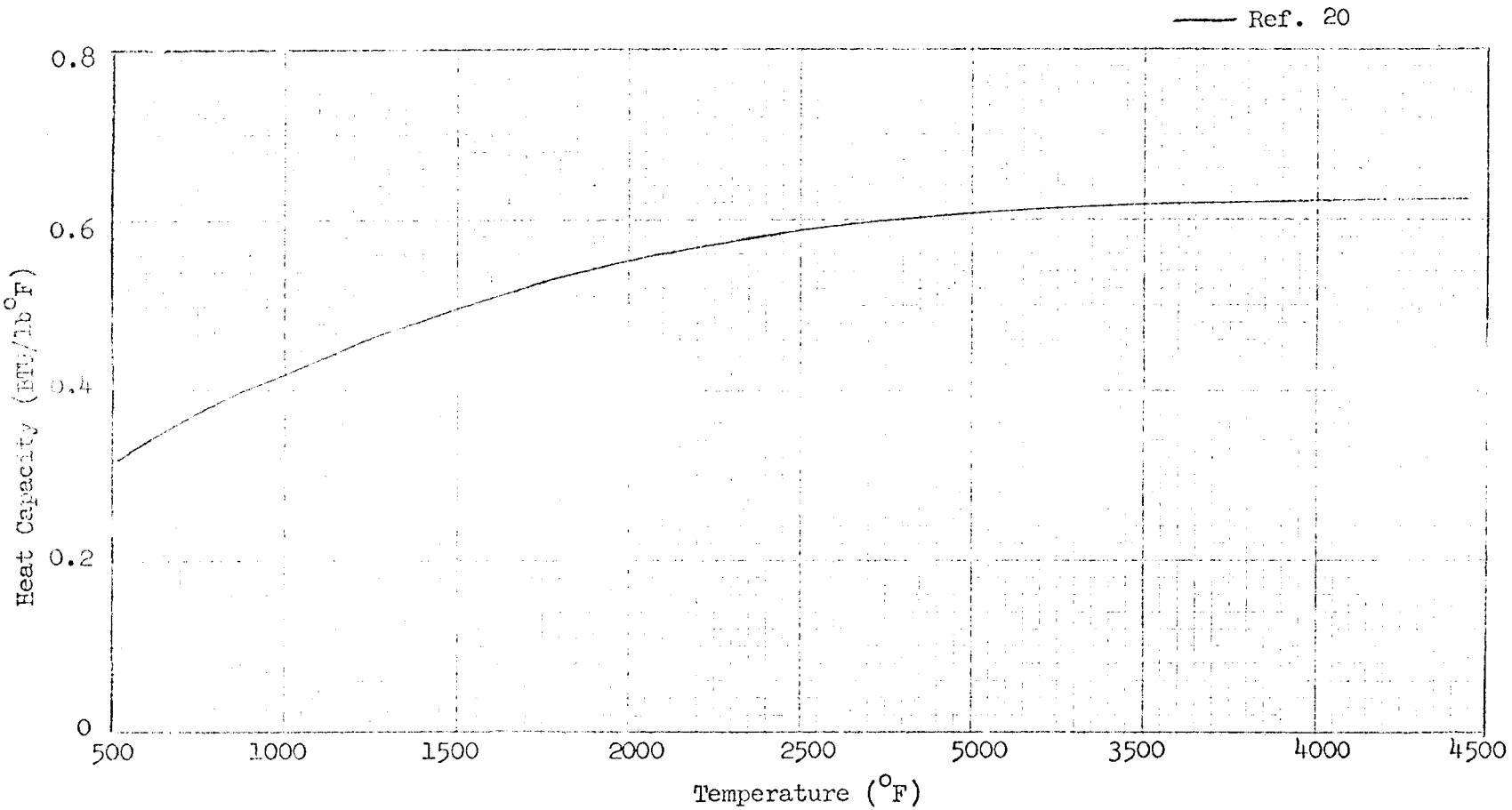

Figure 13 Heat Capacity of Laboratory Chars Formed From Nylon-Phenolic Material

$$\Delta C_p = 9\%$$

$$\Delta \alpha = 20\%$$

It must be noted these uncertainties are a function of temperature. Below the char formation temperature $\Delta \rho$ is approximately 5% and as $\Delta \alpha$ decreases with decreasing temperature, the maximum $\Delta \bar{k}$ is on the order of 15% below approximately 2000° F.

Section 6

EXPERIMENTAL RESULTS

6.1 CHAR CHARACTERIZATION

6.1.1 Microstructure

Two photomicrographs were made of each type of thermal diffusivity sample. All photomicrographs are contained in Appendix I. The series of chars prepared at 1832°F are illustrated in Figs. I-1 through I-6. In all the specimens in which nylon is present as fiber, the char is present in linearly oriented arrays. The void configuration tends to follow the original fiber configuration. Dark areas are voids; white areas are char. Medium gray areas in Fig. I-1 are mount material. In a sample of Type A, in which the original fiber diameter was 13 mils, the structure is coarse, Fig. I-1. As the fiber diameter is decreased the structure becomes finer and more regular, as in Figs. I-3, I-4,and I-5. In samples of Type A, B, and C, which were produced from the Stern & Stern nylon, Table 3, the chars do not have many small voids, Figs. I-2, I-3,and I-4. In samples of Type C and D, produced from Burlington nylon, the chars have numerous small holes, Figs. I-3 and I-4. Their appearance suggests that individual nylon filament strands separated from the body of the fiber resulting in a more intimate mixture of phenolic and nylon. As could be expected, all the chars of the nylon fiber type are strongly oriented. The layers of char are normal to the surface. In the 1832°F Zytel char, the char is randomly oriented with a random void structure, Fig. I-6.

Chars formed at 2200°F are illustrated in Figs. I-7 through I-12. (The photomicrographs were made under slightly different lighting conditions from the first series. The light gray areas are char, the medium gray areas are void filled with mount epoxy, and the black areas are voids which have not been completely penetrated

by mount material.) In general, they exhibit the same characteristics as the lower temperature chars. The coarseness of the char decreases with fiber diameter. In chars produced from nylon in the form of fibers, the structure is strongly oriented, while the Zytel char structure is random.

Chars formed at 2900°F, Figs. I-13 to I-18, are similar in nature to the low-temperature chars. The char structure is oriented with respect to the original surface. (These photomicrographs have been mounted so that the vertical elevation is parallel to the original surface.)

6.1.2 Crystal Structure

The crystalline character of these chars may be described in the following way. Data on real and crystallite density suggest that these chars consist of two phases: a glassy carbon phase in which the carbon atoms are randomly oriented and have the general characteristics of a polymer, and numerous small crystallites which have some degree of ordering, i.e., they are oriented with respect to each other and are approaching the graphite model of stacked layers of hexagonal arrays of carbon atoms. The specific gravity of glassy carbon is about 1.3 (Ref. 26). The crystallite specific gravity is about 2.0 or greater, Table 4. In a heterogeneous mixture of the two the real specific gravity would lie somewhere between the two values. The measured real specific gravity ranges from 1.4 to 1.6.

Carbonaceous chars may be said to be graphitizable as they assume a greater degree of carbon ordering with increasing temperature of formation and heat treatment. As these materials become more ordered, the following events occur:

- The interlayer spacing, the distance between the hexagonal arrays of carbon atoms, becomes smaller.
- The crystallites may become increasingly larger in overall dimensions.
- The quantity of ordered material also increases, at the expense of a reduction in disordered material.

In general, a material is not said to be truly graphitic unless it has an interlayer spacing of 3.45 Å or less. None of the chars studied have approached this value, but we have nevertheless used the terminology "becoming graphitic" to indicate both a degree of ordering and an increase in the amount of ordering.

X-ray diffraction analysis was used to evaluate the approach to graphitic structure of the polymeric chars being studied. Data are listed in terms of the following:

I_{max} – the relative peak intensity, which is a function of the amount of ordered material

β – the peak width at half height which is a function of crystallite size. As crystallite size increases the peak narrows and becomes sharper

$I_{max} \cdot \beta^*$ – the product of the relative intensity and the peak halfwidth corrected for instrumental line broadening. This quantity is a function of both the amount and degree of ordering and should increase as the material becomes more "graphitic."

Interlayer spacing – which is the distance between stacked arrays of carbon atoms within the crystal. The interlayer spacing decreases as the material becomes more ordered, to a value of 3.36 for completely graphitic material.

Crystallite density – is calculated from interlayer spacing, Sec. 5.2.4. It increases with increasing order. The crystallite density of single crystal graphite is greater than 2.2.

L_c – the crystallite thickness in angstroms should increase with increasing graphitization.

The chars of the six types of material vary in the way these parameters change with temperature. With respect to $I_{max} \cdot \beta^*$ there is considerable variation between the six types of char produced at a given temperature, Table 4. In general, the Zytel tends to form a "hard" carbon, that is it is not as graphitizable as other materials. It has much less tendency to graphitize than does material of Type B, which has almost

Table 4

X-RAY ANALYSIS OF CHAR STRUCTURE

Sample	Orientation	$I_{max.}$	β	Interlayer Spacing (A)	Crystallite Density, (gm/cc)	$(I_{max.}\beta^*)$ (a)	Crystallite Thickness L_c (A)
9-15-A-5	Top	110	8.0	3.62	2.10	846	11.8
1832°F	Side	90	7.3	3.74	2.035	630	12.9
	Avg	100	7.65	3.68	2.06	738	12.35
9-15-B-5	Top	128	7.6	3.70	2.055	935	12.0
1832°F	Side	125	8.1	3.70	2.055	975	11.8
	Avg	127.5	7.85	3.70	2.055	955	11.9
9-15-C-5	Top	133	7.3	3.70	2.055	930	12.9
1832°F	Side	61	8.5	3.77	2.02	500	11.0
	Avg	97	7.9	3.735	2.037	735	11.95
9-15-D-5	Top	78	8.0	3.64	2.085	600	11.8
1832°F	Side	61	7.9	3.64	2.085	464	11.9
	Avg	69.5	7.95	3.64	2.085	532	11.85
9-15-E-5	Top	78	8.5	3.62	2.10	640	11.1
1832°F	Side	81	8.5	3.60	2.12	664	11.1
	Avg	79.5	8.5	3.61	2.11	652	11.1
Z-1-10-9		42	7.7	3.90	1.95	311	12.2
1832°F							
Z-1-10-R		46	8.8	3.83	1.97	545	10.6
1832°F	Avg	44	8.25	3.86	1.96	428	11.4
9-15-A-3	Top	125	7.6	3.74	2.03	912	12.3
2200°F	Bottom	86	7.6	3.80	2.00	628	12.3
	Avg	106	7.6	3.77	2.015	770	12.3
9-15-B-1	Top	126	8.1	3.83	1.985	983	11.5
2200°F	Bottom	90	7.7	3.77	2.02	666	12.2
	Avg	108	7.9	3.80	2.00	825	11.85

Table 4 (Cont.)

Sample	Orientation	$I_{max.}$	β	Interlayer Spacing (A)	Crystallite Density, (gm/cc)	$(I_{max.}\beta^*)$ (a)	Crystallite Thickness L_c (A)
9-15-D-6	Top	59	8.8	3.77	2.025	495	10.6
2200°F	Bottom	58	8.3	3.64	2.085	465	11.3
	Avg.	58.5	8.5	3.70	2.055	475	10.9
9-15-E-2	Top	59	9.3	3.70	2.055	531	10.0
2200°F	Bottom	53	7.1	3.74	2.03	361	13.2
	Avg	56	8.2	3.72	2.04	446	11.6
Z-1-5		18	7.3	3.70	2.055	126	12.2
2200°F							
Z-12-R		46	8.8	3.83	1.97	391	10.2
2200°F	Avg	32	8.05	3.76	2.01	260	11.2
9-15-A-3		100	7.8	3.77	2.02	750	11.5
2900°F							
9-15-B-6		127	7.3	3.77	2.02	890	12.9
2900°F							
9-15-C-9		177	8.4	3.83	1.985	1433	11.3
2900°F							
9-15-D-9		112	9.1	3.77	2.02	985	10.2
2900°F							
9-15-E-6		70	9.2	3.70	2.05	623	12.2
2900°F							
Z-1-1-16		85	8.8	3.80	2.00	748	10.6
2900°F							

(a) $\beta^* = \beta$ Corrected for instrumental line broadening

the same chemical composition. Chars of material of Type A, which had the largest original fiber diameter, are the least sensitive to formation temperature. All chars of material A, whether produced at 1832, 2200, or 2900°F, had about the same degree of ordering. Chars of material Type C, which had the smallest original fiber diameter, were the most sensitive to temperature.

The quantity $I_{max} \cdot \beta^*$ increases with increasing temperature of formation. In 1832°F chars, it ranged from 430 for Zytel to 955 for Type B material. In 2200°F chars, it ranged from 260 for Zytel to 960 for material of Type C. (The lower degree of ordering in the Zytel-2200 in comparison with the Zytel-1832 sample, may be attributed to the shorter heat cycle, Table 2, used to produce the 2200°F char. Because this material is less graphitizable it takes longer to reach a given degree of graphitization.) In 2900°F chars, the quantity $I_{max} \cdot \beta^*$ ranged from 748 for Zytel to 1430 for char of material Type C.

The crystallite densities of the five fiber composites were approximately the same and did not vary significantly with increasing temperature of formation. The Zytel chars had a somewhat lower crystallite density, at a given formation temperature, which is further evidence that this material forms a hard coke. Crystallite specific gravities are sometimes higher for the long heat cycle, 1832°F chars, than they are for the shorter heat cycle, 2200 and 2900°F chars.

The average crystallite thickness L_c varies from 11.1 to 12.4 for 1832°F chars. The ratio of L_c to interlayer spacing suggests that these crystallites consist of approximately three stacked layers of hexagonal carbon arrays. In chars formed at 2900°F, the crystallite thickness has decreased only slightly to a range of 10.28 to 12.3 $\mathring{A}$.

The effect of thermal diffusivity tests on the degree of "graphitization" of the charred materials was quite pronounced, Table 5. In general the quantity $I_{max} \cdot \beta^*$ increased after the material was subjected to test. However, in the A-1832°F char it decreased,

TABLE 5

EFFECT OF THERMAL DIFFUSIVITY MEASUREMENTS ON CHAR PROPERTIES

Material Type		Bulk Sp. Gravity	Apparent Sp. Gravity	Real Sp. Gravity	Aminco Porosimetry Total Porosity (%)	% Pores <10μ	% Pores <1μ
a. (Specific Gravity + Aminco Porosity)							
9-15-A- 1832°F	B*	-	1.11	1.41	21.25	68	88
	A	-	1.27	1.53	17.2	84	89.5
9-15-B 1832°F	B	.44 ± .13	1.08	1.44	25.2	76	88.5
	A	.45	.80	1.49	46.2	94	99.5
9-15-C 1832°F	B	-	.63	1.66	61.6	96.5	99.5
	A	-	.57	1.46	60.6	99.2	99.5
9-15-D 1832°F	B	-	.89	1.65	46.0	75	89.5
	A	-	.65	1.49	55.3	86	92
9-15-E 1832°F	B	.65 ± .08	1.04	1.64	36.7	75	88
	A	.52	.68	1.51	54.9	80	89.5

b. X-Ray Parameters

Sample		I_{max}	β	Interlayer Spacing, A	Crystallite Sp. G. (gm/cc)	I_{max} * β	L_c
9-15-A 1832°F	B	100	7.65	3.68	2.06	735	12.35
	A	130	3.5	3.56	2.13	416	27.1
9-15-B 1832°F	B	127.5	7.85	3.70	2.055	963	11.75
	A	485	3.6	3.52	2.16	1600	25.9
9-15-C 1832°F	B	97	7.9	3.74	2.037	735	11.95
	A	465	3.7	3.54	2.15	1580	25.3
9-15-D 1832°F	B	69.5	7.95	3.64	2.085	532	11.85
	A	175	6.8	3.60	2.112	1140	13.9
9-15-E 1832°F	B	79.5	8.5	3.61	2.11	652	11.1
	A	630	2.1	3.44	2.21	1133	53.2

* B = Before Test, A = After Test

TABLE 5
(cont'd)

Sample		I_{max}	β	Interlayer Spacing, A	Crystallite Sp. G. (gm/cc)	I_{max}	*β	L_c
Z-1	B	42	7.7	3.90	1.95	311		12.2
1832°F	A	68	6.1	3.59	2.11	394		15.5
Z-1	B	18	7.3	3.70	2.055	126		12.2
2200°F	A	119	5.45	3.60	2.112	614		14.5

*B Before Test, A = After Test

apparently because crystallite size grew, but the quantity of crystalline material did not increase. In the Zytel-type chars there was little difference before and after test in the 1832°F char. In the 2200°F char there was considerable change before and after test, with a corresponding change in thermal conductance, Sec. 7. The interlayer spacing after test is lower than before test in all chars evaluated. The crystallite density increased in all cases, as did crystallite thickness.

The number of stacked hexagonal arrays after test is about 7 for 1832°F chars of materials Type A, B, and C. The 1832°F char, material Type E, had the greatest increase in crystallite thickness to approximately 15 layers. Chars of material Type D and the Zytel increased only by a layer or two.

All the materials were more ordered after test than before. In the Zytel material which is the least graphitizable, the changes were less. Only one Zytel sample, the 2200°F char showed any marked increase, and this was primarily in the amount of ordered material, rather than the degree to which it was ordered.

6.1.3 Specific Gravity

The specific gravity of the chars as determined from bulk measurements and mercury porosimetry data are listed in Table 6.

The bulk specific gravity is the ratio of the mass to the volume calculated from micrometer measurements. The apparent density is the ratio of the mass to the apparent volume of char surrounded with mercury at 1.8 psia. One could expect the bulk density to be less, because maximum dimensions are used to compute volume, and in mercury porosimetry surface depressions are filled. When this difference is greater than 20% we can assume that the apparent specific gravity is erroneous as a result of mercury penetration into pores greater than 100 μ at 1.8 psia.

TABLE 6

SPECIFIC GRAVITY OF CHARS

Material Type	Produced at 1832°F			Produced at 2200°F			Produced at 2900°F		
	Bulk	Apparent	Real	Bulk	Apparent	Real	Bulk	Apparent	Real
9-15-A	.41	1.19	1.46	.36	1.37	1.64	.36	.55	1.55
	.44	1.04	1.36	.38	1.52	1.68	.38	.54	1.44
	.42			.45	1.22	1.69	.45	.59	1.79
	.43	1.11	1.41	.40	1.37	1.67	.40	.56	1.60
9-15-B	.54	1.09	1.48	.39	.70	1.64	.39	.53	1.48
	.50	1.07	1.41	.40			.40		
	.29			.40			.40		
	.44	1.08	1.44	.40			.40		
9-15-C	.53	.64	1.67	.44	.64	1.74	.44	.48	1.45
	.52	.63	1.64	.44			.44		
	.39			.43			.43		
	.48	.63	1.66	.44			.44		
9-15-D	.64	.80	1.61	.47	.61	1.59	.47	.54	1.46
	.65	.97	1.68	.48			.48		
	.58			.43			.43		
	.62	.89	1.65	.46			.46		
9-15-E	.74	1.12	1.70	.38	.58	1.47	.40	.47	1.49
	.59	.97	1.59	.42			.42		
	.62			.36			.41		
	.65	1.04	1.64	.39			.41		
Zytel SN/1	.48	.57	1.46	.47	.56	1.53	.50	.52	1.46
	.51	.58	1.52	.43			.47		
	.50	.62	1.55	.43			.50		
	.47	.58	1.51	.44			.49		
	.47								
	.46								
	.48								

In chars produced at 1832°F, the bulk specific gravity appears to be greatest on chars of materials Type D and E. Bulk specific gravities tend to decrease with increasing temperature of formation. The apparent specific gravity of 1832°F chars indicates some mercury penetration into the pores in all cases except possibly the Zytel char. At higher formation temperatures, the differences between bulk and apparent specific gravities are less.

At a given formation temperature the real density varies with type of virgin material. For chars of Type A the real density increases with formation temperature, which is accompanied by an increase in porosity, Table 7. For chars of Types B and C, the real density increases with formation temperature of 2200°F, but decreases at a formation temperature of 2900°F, with corresponding changes in total porosity. For chars of Types C and D the real density decreases with increasing temperature, as it does with the Zytel. Since these changes are not directly reflected in x-ray parameters there are two possible explanations: (a) larger fractions of small closed voids are formed in some of these materials at high temperature, or (b) larger volumes of interstitial atoms are given off at temperatures above 1832°F. Both factors probably could contribute and may actually be part of the same phenomenon. Entrapped gases of oxygen, nitrogen, and hydrogen could cause small voids. The incomplete carbonization of chars at 1832°F has been shown in previous work (Ref. 13). The carbon content of 1832°F chars formed from nylon phenolic is about 90 ± 5 wt%. According to Mrowzowski (Ref. 27) the removal of interstitials from carbon chars may not be complete until temperatures greater than 3800°F have been reached.

Thermal diffusivity tests had the same effect on real density, Table 5, as did increasing formation temperature. In Type A, the real density increased. In all other samples it decreased, yet the extent of graphitization increased. These phenomena could only result from the removal of interstitial volatiles from the random network of carbon atoms. Since the randomly-oriented carbon atoms constitute a hard coke, the intercarbon distance could not be expected to shrink with the removal of interstitials. This is substantiated by the observation that the chars did not change dimensionally during test, but lost considerable weight.

Table 7

SUMMARY OF PORE SPECTRA DATA

Sample	Total Porosity, Vol. %(a)			Avg. Large Pore Diameters, μ			Aminco Distr. of Small Pores, %		
	A	B	C	Avg.	Sigma	n	$<50\mu$	$<10\mu$	$<1\mu$
9-15-A-1832	78.5 ±6.6 n=8	18.7 23.6 21.2	70.0 63.0 66.5	395	127	8	23.0	68	88.5
9-15-B-1832	84.0 ±4.0 n=6	26.2 24.2 25.2	68.0 63.2 66.6	300	78	10	23.0	76	88.5
9-15-C-1832	85.6 ±5.7 n=8	61.9 61.7 61.8	71.7 69.9 70.8	190	119	10	0	98.2	99.5
9-15-D-1832	75.0 ±6.0 n=6	50.1 42.0 46.0	58.8 63.0 60.9	230	25	10	5.0	74.5	87.5
9-15-E-1832	80.0 ±4.7 n=6	34.2 39.3 36.7	58.5 51.8 55.2	220	25	10	8.0	76.5	88.0
Z-1-1832	78.2 ±7.2 n=8	61.6 61.1 60.2 61.0	70.9 65.0 68.9 68.3	270	83.5	10	59.0	99.5	100.0
9-15-A-2200	67.2 ±9.5 n=8	27.6 16.8 9.3 17.9	78.0 77.4 73.5 76.3	215	94	10	31.0	75.0	93.0
9-15-B-2200	74.4 ±5.7 n=8	54.8	75.5	135	45	10	29.0	97.0	99.0
9-15-C-2200	64.9 ±7.4 n=8	63.0	74.7	96	28	10	40.0 est.	98.0	98.5
9-15-D-2200	66.2 ±5.8 n=8	61.9	71.2	155	55	10	32.0 est.	82.0	96.5

Table 7 (Cont.)

Sample	Total Porosity, Vol. %[a]			Avg. Large Pore Diameters, μ			Aminco Distr. of Small Pores, %		
	A	B	C	Avg.	Sigma	n	$<50\mu$	$<10\mu$	$<1\mu$
9-15-E-2200	77.6 ±4.4 n=8	60.3	70.2	162	77	10	22.0 est.	83.0	97.5
Z-1-2200	71.6 ±3.5 n=8	63.4	71.3	318	137	10	10.0	74.5	93.0
9-15-A-2900	66.6 ±4.0 n=8	64.3 62.5 67.1	77.1	330	172.5	10	55.0	97.0	99.8
9-15-B-2900	77.4 ±4.1 n=8	64.4	73.0	318	80.5	10	55.0	91.0	97.0
9-15-C-2900	77.0 ±4.0 n=8	66.7	69.0	160	90	10	1.0	97.5	99.0
9-15-D-2900	70.6 ±3.3 n=8	63.2	68.4	333	138	10	3.5	86.0	94.5
9-15-E-2900	68.0 ±5.9 n=8	68.0	68.7	320	167	10	1.0	86.0	95.0
Z-1-2900	71.6 ±4.6 n=8	64.5	66.5	286	115	10	10.0	93.0	99.6

(a) A = Linear Porosity – computed from quantitative metallography (% of Pores having distribution indicated in Col. 3)
B = Aminco Porosity
C = Calculation from real bulk density, See Section 5.1

6.1.4 Shrinkage Factors

The gross shrinkage factors, dimensional changes and weight changes representative of all types of chars studied, are listed in Table 8 for reference purposes.

6.1.5 Electrical Resistivity

The effective* electrical resistivity of 1832°F chars of the six types of material are listed in Table 9. The resistance was measured in the direction parallel to the surface. Samples which had the least effective resistivity were B and Z, which had a ratio of phenolic to nylon of 50%. Sample B had the most ordered crystal structure and thus should have the lowest resistivity. The Zytel sample, although relatively disordered, had a greater degree of connection throughout the pore network, Fig. I-6, and thus a better conduction path.

As the formation temperature increased to 2200°F, the effective electrical resistivity decreased for Samples C, D, and E, presumably because of an increase in ordering in the random carbon phase. The Zytel sample which graphitizes slowly had a higher electrical resistivity because of the shorter heat cycle.

At a maximum char formation temperature of 2900° F, a drop in bulk density for Sample B indicates removal of interestitial atoms presumably with some breakage of bonds and break in the conduction path. Thus the electrical resistivity should go up. Additionally, the chars are more likely to crack at higher formation temperatures. Small microcracks could easily increase the measured resistance with an increase in effective resistivity.

It should be noted that the resistance of carbon black passes through a minimum at a heat-treatment temperature of 2200° F (Ref. 28). At a formation temperature of 1832° F the specific resistance of carbon black powder is 0.24 ohm-cm, reaches a

*Uncorrected for particle geometry or solid fraction.

TABLE 8

SHRINKAGE FACTORS AND WEIGHT LOSS IN CHAR PREPARATION

Sample	% Change in diameter	% Change in thickness	% Change in volume	Weight Loss, %
9-15-A 1832°F	19.2	25.0	51.1	83.1
	19.2	26.7	52.0	82.4
	19.35	25.0	51.3	82.9
	19.25	25.6	51.5	82.8
9-15-B 1832°F	23.1	35.1	61.5	81.9
	19.4	34.9	58.0	82.0
	18.5	12.4	42.0	83.2
	20.3	27.5	53.8	82.4
9-15-C 1832°F	21.4	24.0	53.0	78.5
	21.0	23.3	52.2	79.0
	21.6	22.9	38.3	79.9
	21.3	23.4	47.8	79.1
9-15-D 1832°F	24.5	26.8	58.3	77.5
	22.4	25.1	57.0	76.8
	23.5	21.8	54.1	77.5
	22.4	29.4	58.4	78.0
	23.2	25.8	57.0	77.5
9-15-E 1832°F	30.6	28.4	69.0	81.5
	27.8	28.4	61.3	81.3
	28.9	28.1	62.7	80.8
	29.1	28.3	64.3	81.2
Z-1 1832°F	17.7	14.95	29.9	77.0
	17.9	15.15	42.8	76.7
	17.25	13.6	43.7	76.9
	17.08	16.5	35.9	77.2
	17.05	18.0	42.5	75.6
	18.2	16.5	41.2	76.6
	17.5	15.76	39.3	76.6
9-15-A 2200°F	16.6	21.0	45.1	85.0
	17.7	20.2	46.0	85.6
	18.0	16.0	43.6	85.9
	17.4	19.1	44.9	85.5
9-15-B 2200°F	15.8	30.8	51.0	84.5
	17.6	25.0	49.0	83.7
	21.1	19.0	49.6	83.9
	18.2	24.9	49.9	84.0
9-15-C 2200°F	18.0	21.1	46.9	80.0
	20.6	23.5	51.7	81.0
	20.2	20.4	49.4	80.4
	19.6	21.7	49.3	80.5

TABLE 8 (Cont.)

SHRINKAGE FACTORS AND WEIGHT LOSS IN CHAR PREPARATION

Sample	% Change in diameter	% Change in thickness	% Change in volume	Weight Loss, %
9-15-D 2200°F	19.7	15.0	45.3	79.7
	20.4	19.8	49.0	79.0
	18.5	19.8	46.6	78.8
	19.5	18.2	47.0	79.1
9-15-E 2200°F	17.4	22.6	47.1	83.0
	21.1	27.6	55.0	83.0
	11.0	28.2	43.0	82.8
	16.5	26.1	48.4	82.9
Z-1 2200°F	18.0	19.0	45.5	77.4
	17.5	16.0	42.9	78.6
	16.7	16.1	41.8	78.2
	17.4	17.0	43.4	78.1
9-15-A 2900°F	20.0	28.3	54.0	85.5
	19.5	33.3	56.8	85.6
	26.5	34.0	63.4	85.5
	22.0	31.7	58.1	85.5
9-15-B 2900°F	21.6	25.0	54.0	84.7
	22.4	22.5	53.3	83.8
	22.4	25.6	55.2	83.9
	22.1	24.3	54.2	84.1
9-15-C 2900°F	19.5	20.2	48.1	80.5
	19.7	20.5	48.7	80.1
	19.9	19.4	48.1	80.5
	19.7	20.0	48.3	80.4
9-15-D 2900°F	22.4	16.8	49.8	80.0
	22.3	19.7	51.4	79.6
	21.6	16.5	48.6	80.9
	22.1	17.7	49.9	80.2
9-15-E 2900°F	23.5	21.6	54.0	84.2
	23.4	25.3	56.0	84.0
	22.6	25.5	55.4	84.3
	23.2	24.1	55.1	84.2
Z-1 2900°F	17.5	15.0	42.2	75.4
	17.5	15.0	42.1	77.2
	18.2	17.6	45.0	75.7
	17.7	16.5	43.1	76.1

TABLE 9

EFFECTIVE ELECTRICAL RESISTIVITY OF CHARS

Material Type	Prepared at 1832°F Resistivity (ohm-cm)	Prepared at 2200°F Resistivity (ohm-cm)	Prepared at 2900°F Resistivity (ohm-cm)
9-15-A	.232	---	---
9-15-B	.170	.137	.219
9-15-C	.234	.192	---
9-15-D	.261	---	---
9-15-E	.231	.185	---
Z-1-1	.172	.317	---

minimum of 0.15 ohm-cm at a formation temperature of 2200°F, and increases to 0.26 at a heat-treatment temperature of 2900°F. This minimum in resistivity is accompanied by a maximum change in hydrogen content.

6.2 CHAR PORE SPECTRA

Char pore spectra data were summarized in Table 7 and are listed in detail in Table A. The total porosity in volume percent was calculated in three ways, Sec. 3.1. Total porosity Type A was calculated from quantitative stereology. The volume calculated was that volume of voids which were greater than 100 μ. Total porosity Type B was calculated from Aminco mercury porosimetry data and includes only the ratio of voids 100 to 0.035 μ in size to apparent volume. This value should be lower than porosity measurement B. Neither measurements A or B give the total volume percent porosity. They are not additive, because the two fractions, as determined, can overlap.

Total porosity, Type C, calculated from the difference between real density and bulk density gives the most reliable estimate of void fraction. It may be noted that in many instances, the linear porosity, A, is greater than the total porosity, C. This suggests an uncorrected shape factor was present or that the selected photomicrographs were not quite representative of the bulk sample.

The average large pore diameter determined from quantitative stereology is listed, along with σ which indicates the distribution in large pore diameter. The large pore diameter increases with the original fiber diameter. Variation in nylon-to-phenolic ratio has little effect on the average fiber diameter.

The distribution of small pores as determined by mercury porosimetry is also listed. This distribution varies considerably from sample to sample. A more detailed account of this distribution is given in Table A.

For 1832°F chars, the distribution of small pores after thermal diffusivity tests is listed in comparison with before test data in Table 5. The major effects noted are that the volume fraction of large pores in the range 100 to 10 μ is greater after test. For Samples B, D, and E, the volume fraction of all pores 100 to 0.035 μ is greater. This apparently results from the outgassing or weight loss observed before and after tests. It is probably associated with the loss of impurities such as N, H, and O in the form of hydrocarbon fragments such as $-CH_3$, $-CH_2CH_3$, $-CHO$, $-NH_3$, or as the vapor species N_2, H_2, and O_2.

6.3 THERMAL DIFFUSIVITY

Eighteen char samples were tested to measure their thermal diffusivity. An additional three tests were conducted to study the effect of the measurement environment, i.e., time at temperature, on the thermal diffusivity of three of the eighteen samples. The specimens tested are listed in Table 10.

Table 10
THERMAL DIFFUSIVITY TESTS

Formation Temperature (°F)	Material Designation	Remarks
1832	9-15A	2 heating cycles
	9-15B	1 heating cycle
	9-15C	1 heating cycle
	9-15D	1 heating cycle
	9-15E	3 samples, 2 heating cycles on one
	Zytel	1 heating cycle
2200	9-15C	1 heating cycle
	Zytel	1 heating cycle
2900	9-15A	2 samples, 1 heating cycle each
	9-15B	1 heating cycle
	9-15C	2 samples, 2 heating cycles on one
	9-15D	1 heating cycle
	9-15E	1 heating cycle
	Zytel	1 heating cycle

In each case the initial test temperature was in the range of 550 to 700°F. The maximum test temperature varied from 3000 to 4600°F. No useful data were obtained above 4600°R due to difficulties encountered with the radiometer above this point. A second radiometer consisting of an S-1 response photomultiplier tube was tried. However, the problems of the magnetic fields caused by the high current furnace power supply were such that satisfactory operation of this second detector was not achieved during the period of the contract. The majority of the tests were terminated in the temperature range of 3500 to 4000°F due to the changes which were occurring in the sample structure due to heating. This is described in detail in the discussions of the results for each type of char.

The results of all the tests are given in Table B. Figures 14 through 20 graphically show the variation of thermal diffusivity with temperature.

6.3.1 Chars Formed at 1832°F Maximum

The results of the measurements on chars formed at 1800°F are shown by Figs. 14 through 16 for all six types of materials.

The differences in diffusivity between types of materials are discussed in Sec. 7 because sample to sample density variations must be considered in such a comparison.

The most important result from these tests is the change in diffusivity after exposure to elevated temperatures during the test period. The diffusivity of the 9-15A char (Fig. 14) changed by a factor of more than three after reaching a maximum temperature of 4500°F. This increase in diffusivity may be correlated with the change in structure as shown in Table 5. The real density increased and the crystallite dimension, L_c, doubled. This coupled with the decrease in β^* shows the presence of a more ordered structure having larger crystallites. One would expect the diffusivity therefore to increase as the thermal conductivity has increased. From Ref. 22, data of Jamieson, et al, show an increase of approximately threefold in the

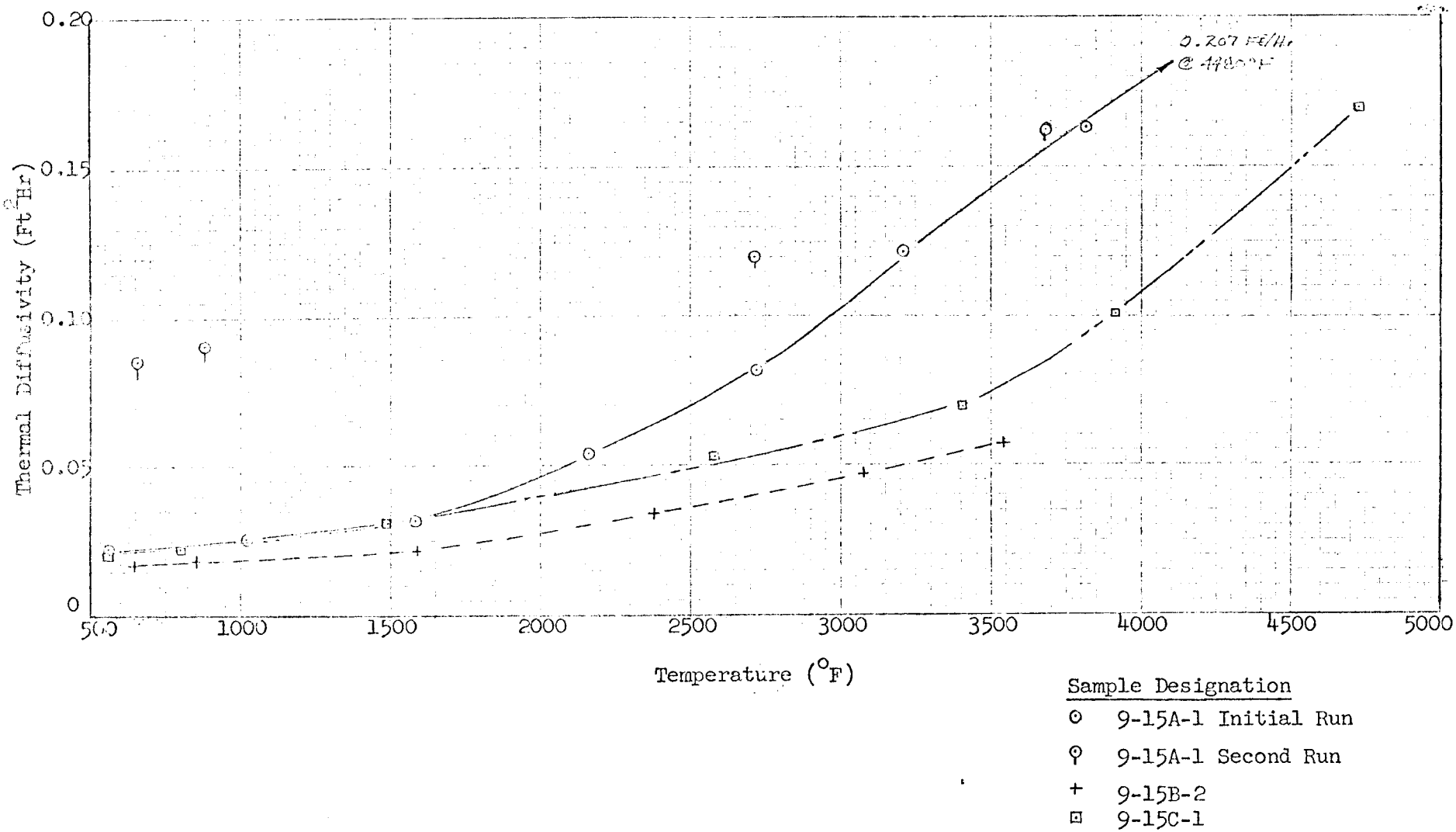

Figure 14 Thermal Diffusivity of Laboratory Chars Formed at 1832 °F Maximum from 9-15A, 9-15B and 9-15C Materials

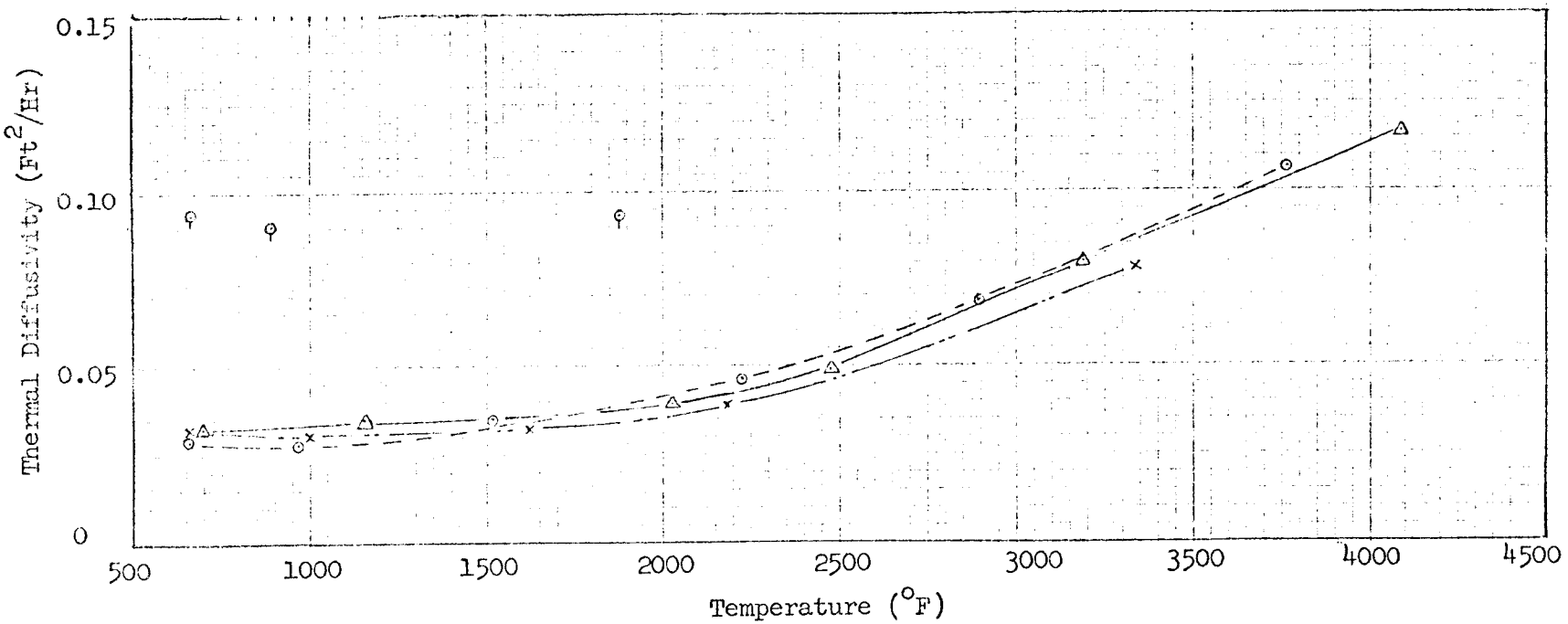

Figure 15 Thermal Diffusivity of Laboratory Chars Formed at 1832 °F Maximum from 9-15E Materials

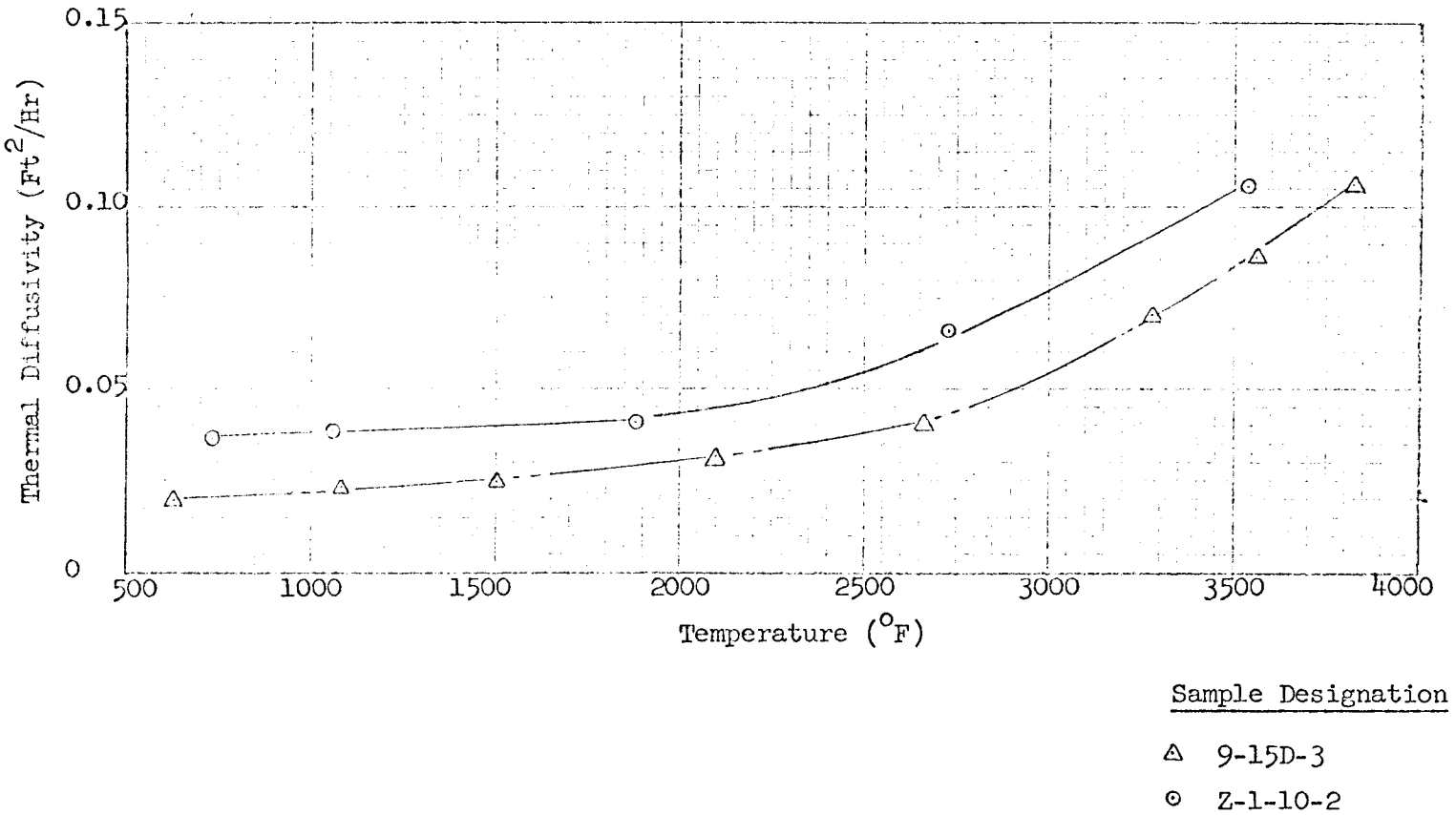

Figure 16 Thermal Diffusivity of Laboratory Chars Formed at 1832° F Maximum from 9-15D and Zytel Materials

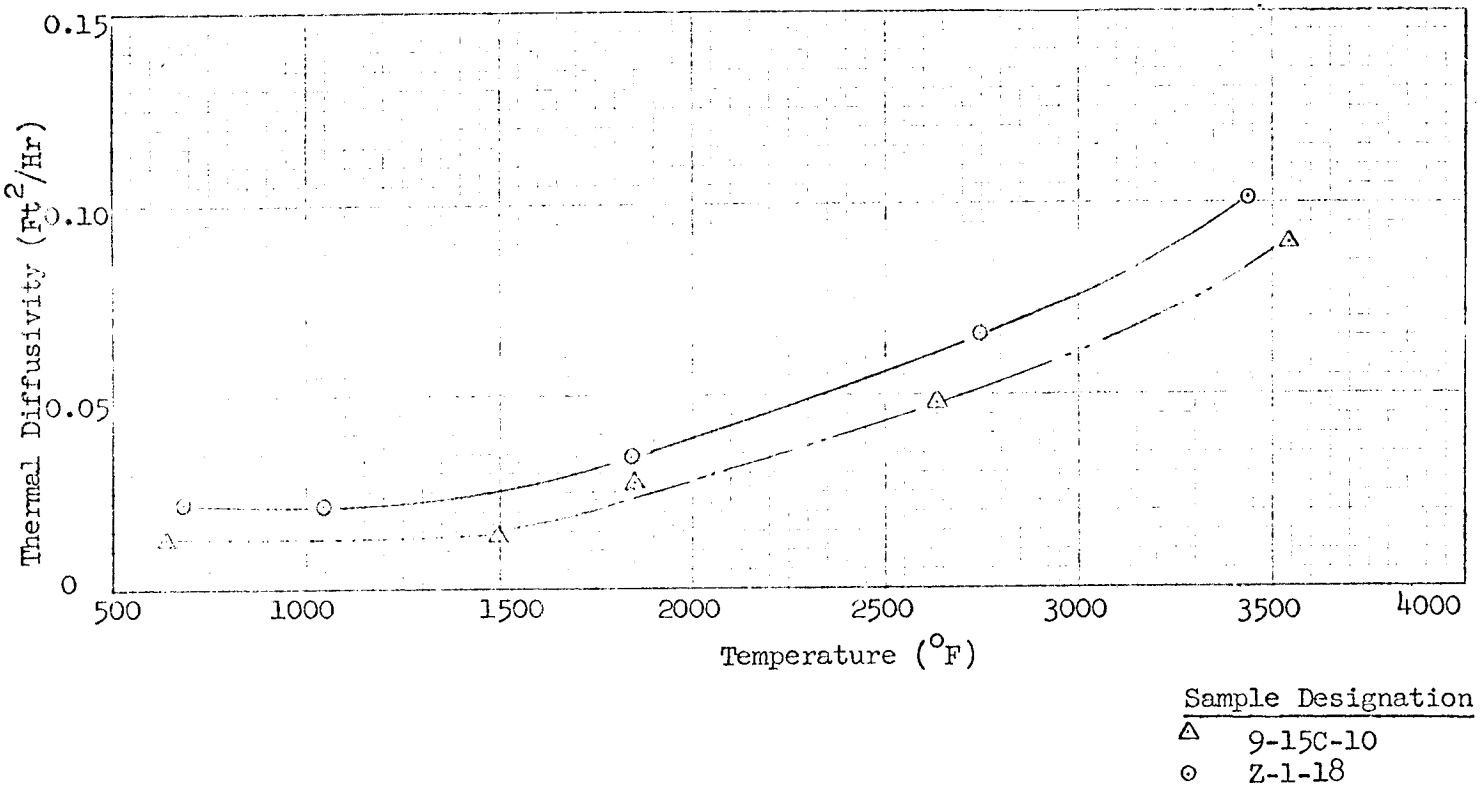

Figure 17 Thermal Diffusivity of Laboratory Chars Formed at 2200°F Maximum from 9-15C and Zytel Materials

thermal conductivity of an experimental graphite was achieved by doubling the crystallite size. Further discussion of the changes in the char after heat treatment during the test is contained in Sec. 6.1.

A similar change in diffusivity was observed with a sample of the 9-15E material (Fig. 15). Again, a very large increase in L_c was noted with a decrease in β^*.

6.3.2 Chars Formed at 2200°F Maximum

The two samples of 2200°F chars which were tested showed a lower value of diffusivity than their corresponding types formed at 1832°F. This is attributed to the larger void fraction present in the 2200°F chars as shown by Table 7, porosity C and $I_{max}\beta^*$.

6.3.3 Chars Formed at 2900°F Maximum

The thermal diffusivity was measured for char specimens, from each material type, which were formed at 2900°F. Figures 18 through 20 illustrate the results of these measurements. A large change in diffusivity was observed during the second test of a Zytel char which had been subjected to a maximum temperature of 4300°F during the initial test (Fig. 20). Similarly, a 9-15C char showed an increase in α after heating to 4300°F. In both cases the diffusivity was approximately doubled. No post test x-ray analysis was performed on either specimens.

6.4 HEAT CAPACITY

Enthalpy measurements were made on one sample each of an 1832° F char and a 2900° F char. Since these data checked the enthalpy data used for the computation of heat capacity shown by Fig. 13, no measurements were made on additional char specimens.

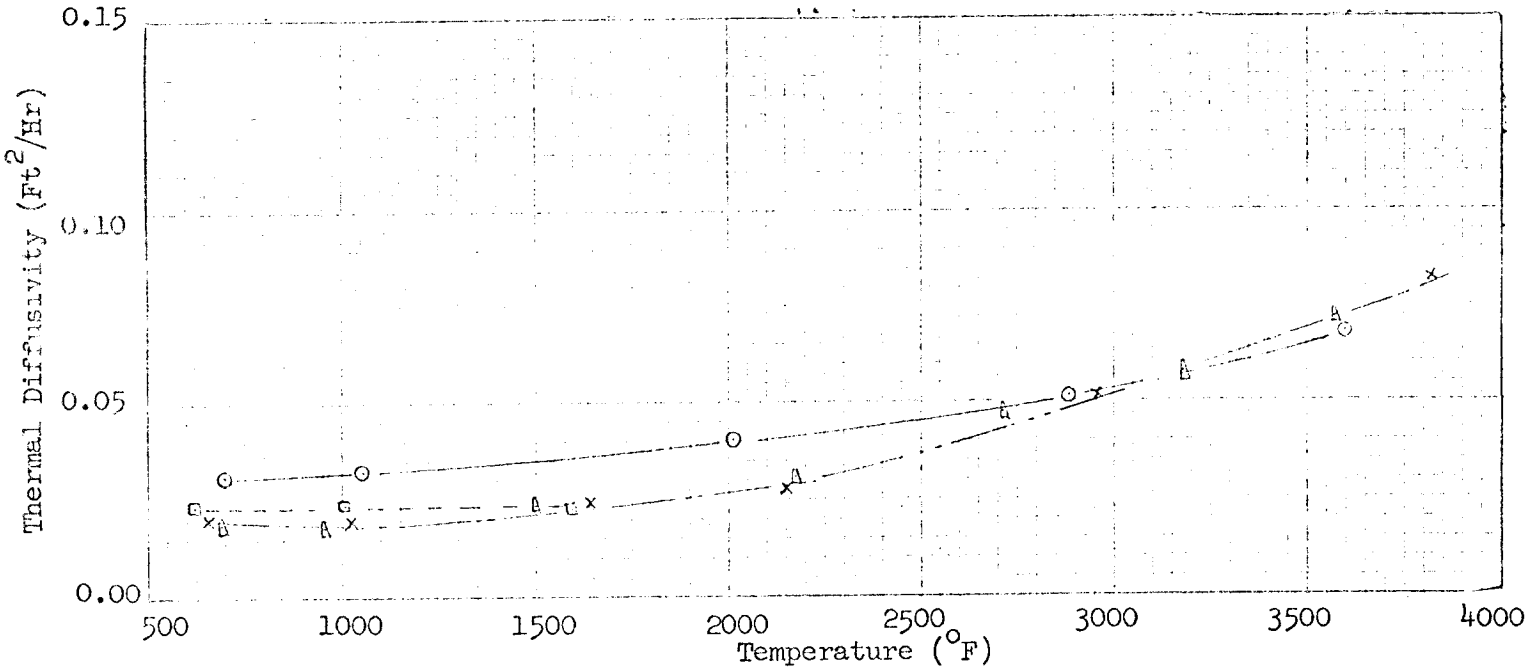

Sample Designation	
A	9-15A-4
×	9-15A-6
⊡	9-15B-5
⊙	9-15D-4

Figure 18 Thermal Diffusivity of Laboratory Chars Formed at 2900°F Maximum from 9-15A, 9-15B, and 9-15D Materials

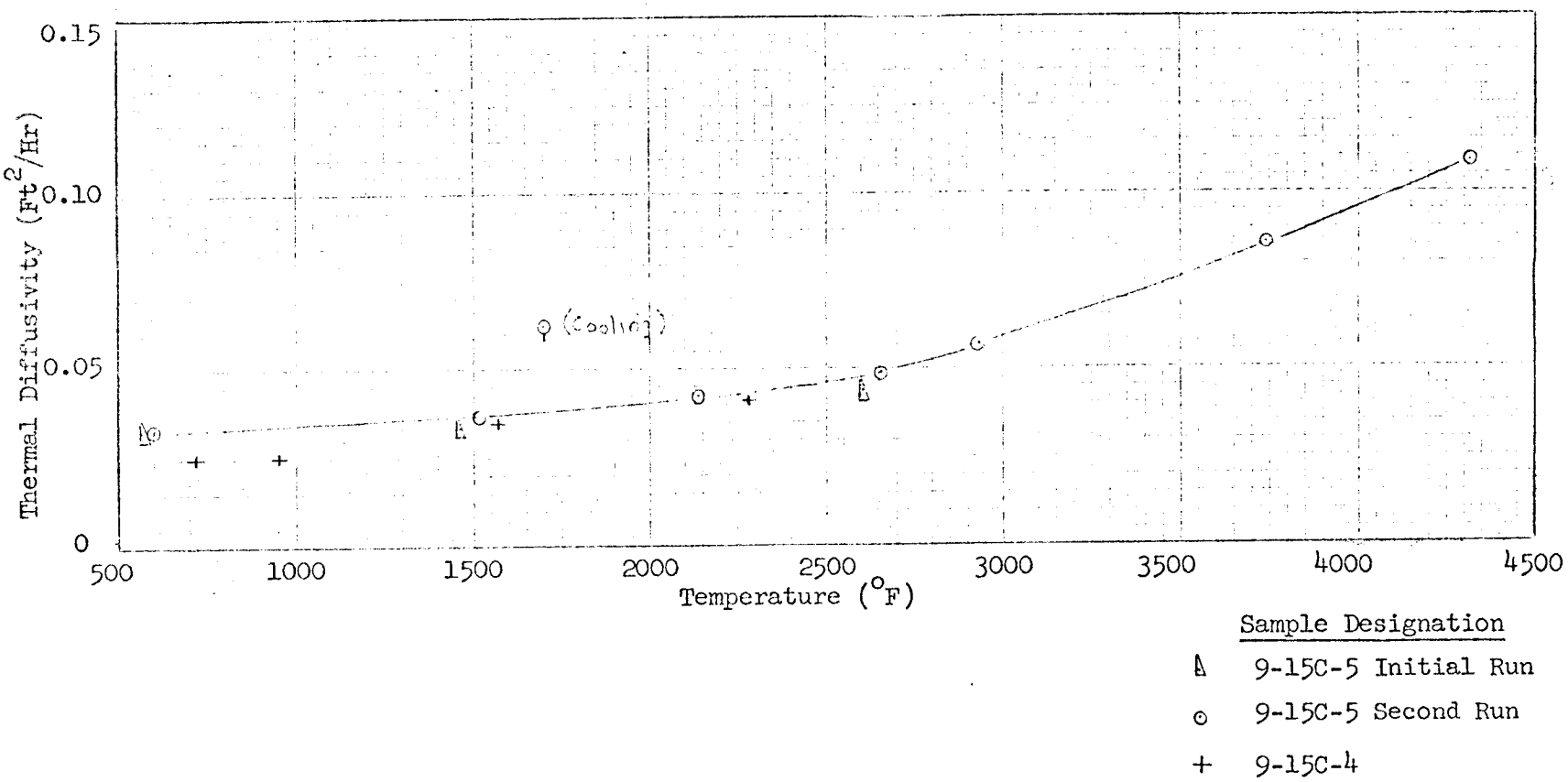

Figure 19 Thermal Diffusivity of Laboratory Chars Formed at 2900 °F Maximum from 9-15C Material

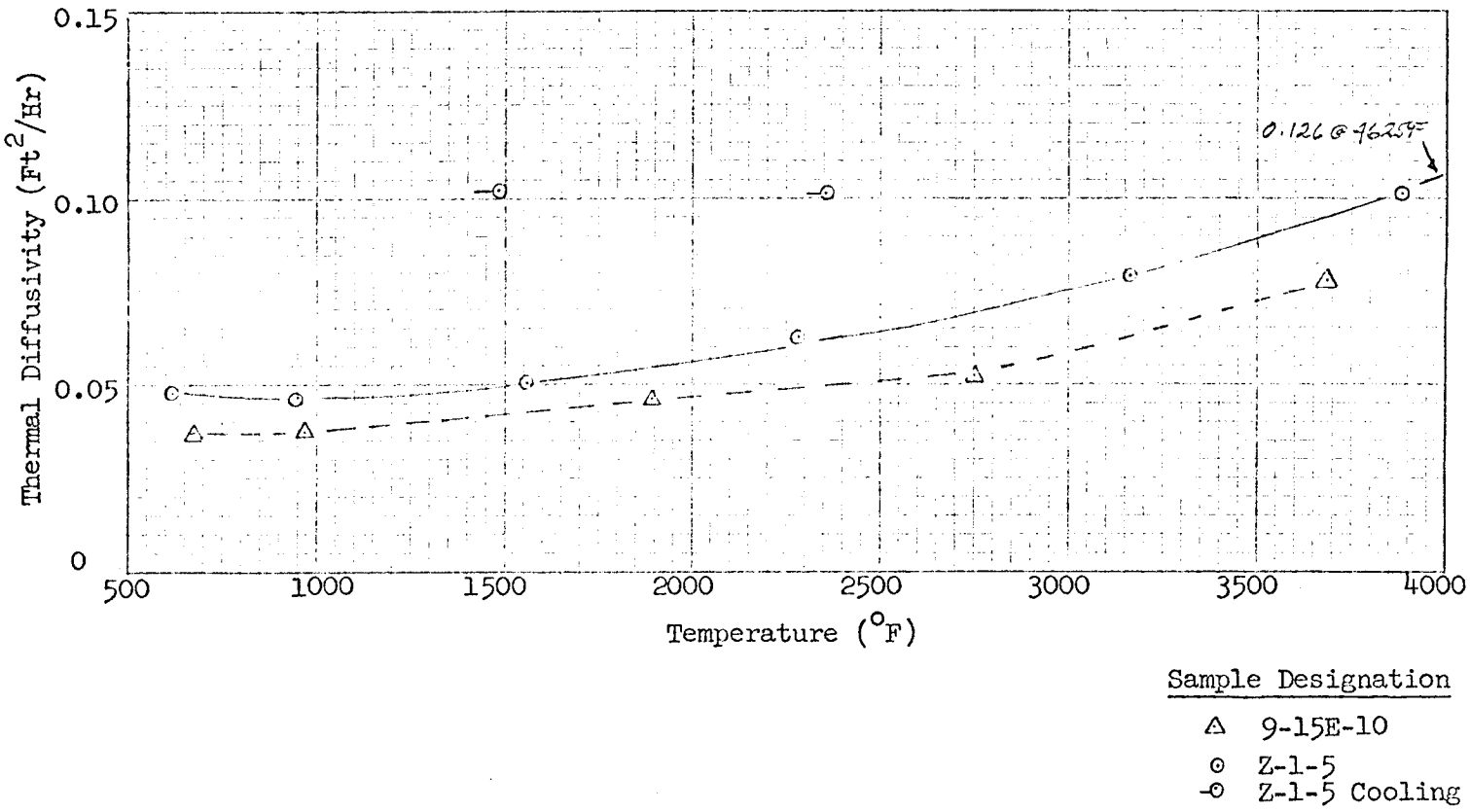

Figure 20 Thermal Diffusivity of Laboratory Chars Formed at 2900°F Maximum from 9-15E and Zytel Materials

The experimental results are as follows:

Char Type	Temperatures (° F)	Enthalpy Btu/lb	Enthalpy, Fig. 13 Btu/lb
	500	110	110
	1000	290	300
1832° F	1500	520	525
	2500	1030	1070
2900° F	500	105	110
	1500	500	525
	2500	1000	1070

The results for the 2900° F char indicate the material may have a slightly lower heat capacity than that given by Fig. 13. This may be due to a more ordered or graphitic type structure. As the calculated heat capacity for this material falls within 7% of that given by Fig. 13, and as the scope of this program did not include a thorough study of char heat capacity, no further work was done in this regard. However in view of the changes in thermal diffusivity with sample heat treatment, the heat capacity function should be examined in more detail.

Section 7
EFFECTIVE THERMAL CONDUCTIVITY

An effective thermal conductivity, as discussed in Sec. 5.6, was calculated for each specimen from the thermal diffusivity data. These values are tabulated in Table B. Figures 21 through 26 show the influence of temperature on the conductivity of representative specimens.

The change in diffusivity with repeated tests is the result of a change in the thermal conductivity of the structure with heat treatment as shown by Fig. 21. An increase in $\bar{k}$ of approximately 300% was observed at 600° F. This correlates with the change in structure as shown by Table 5. Also, the rate of change of conductivity with temperature appears to be less after the initial heating cycle. This indicates the temperature dependency shown by the initial test of a sample is due, to a large extent, to a change in structure and, consequently, solid-phase conductivity rather than radiative transport processes. The conductivity to the char formation temperature is probably dependent upon radiative transport and solid-phase conduction where the solid conductivity varies with nearly a first power of temperature relationship. However, above this temperature range, the solid phase contribution is a function of a structure change with an attendant change of conductivity as a function of both time and temperature.

No attempt was made to correlate the data with a specific theoretical model for conductivity of porous structure having a continuous solid phase. However, trends in conductivity as a function of parameters such as void fraction and structure may be seen from the data. In general, the conductivity attributable to the continuous solid phase may be expressed as a function

$$k_s = \phi [k_T, (1 - \delta), \overline{F}] \tag{33}$$

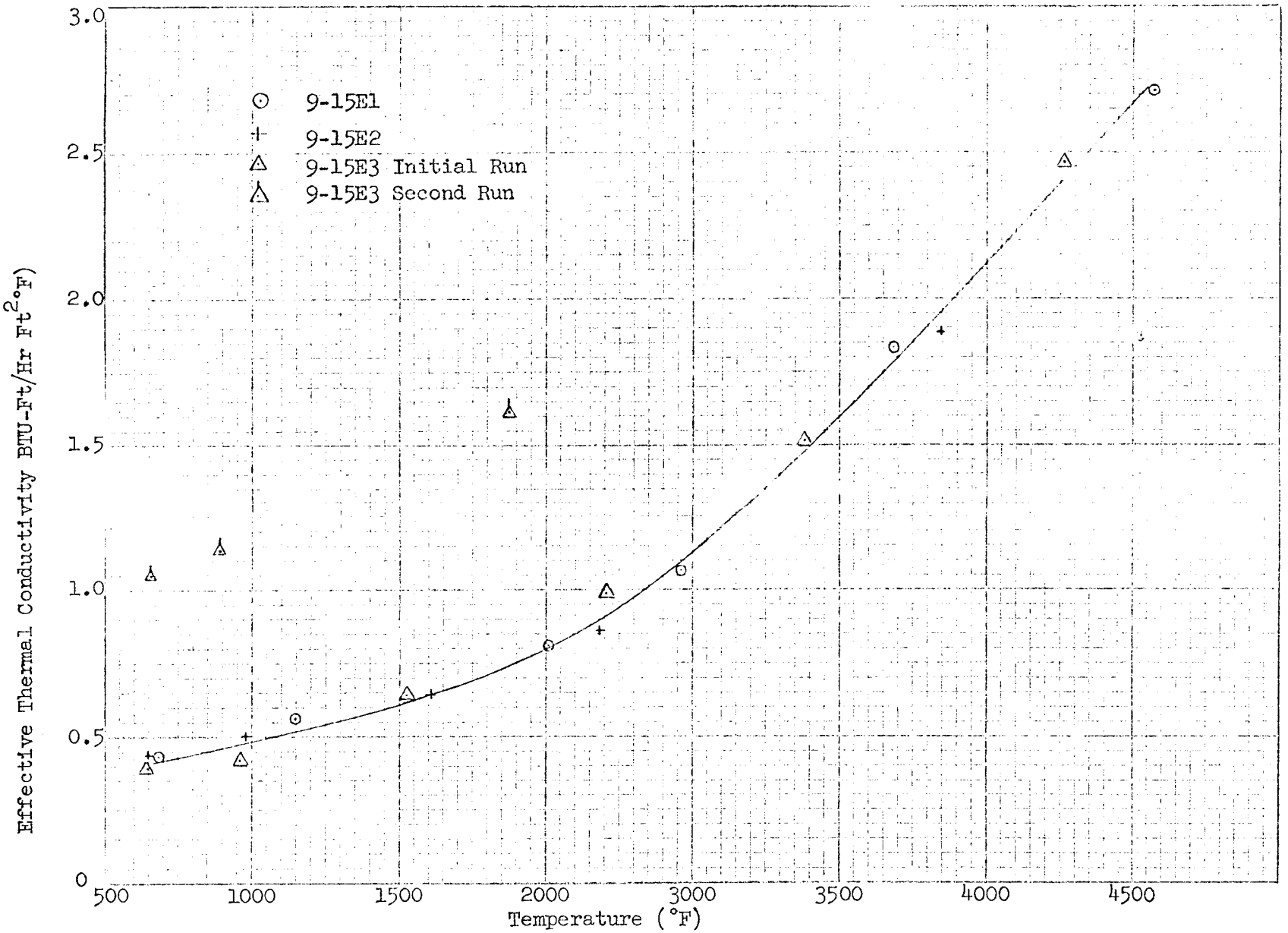

Figure 23. Effective Thermal Conductivity of Chars formed at 1832°F from 9-15E Material showing Variation from Sample to Sample

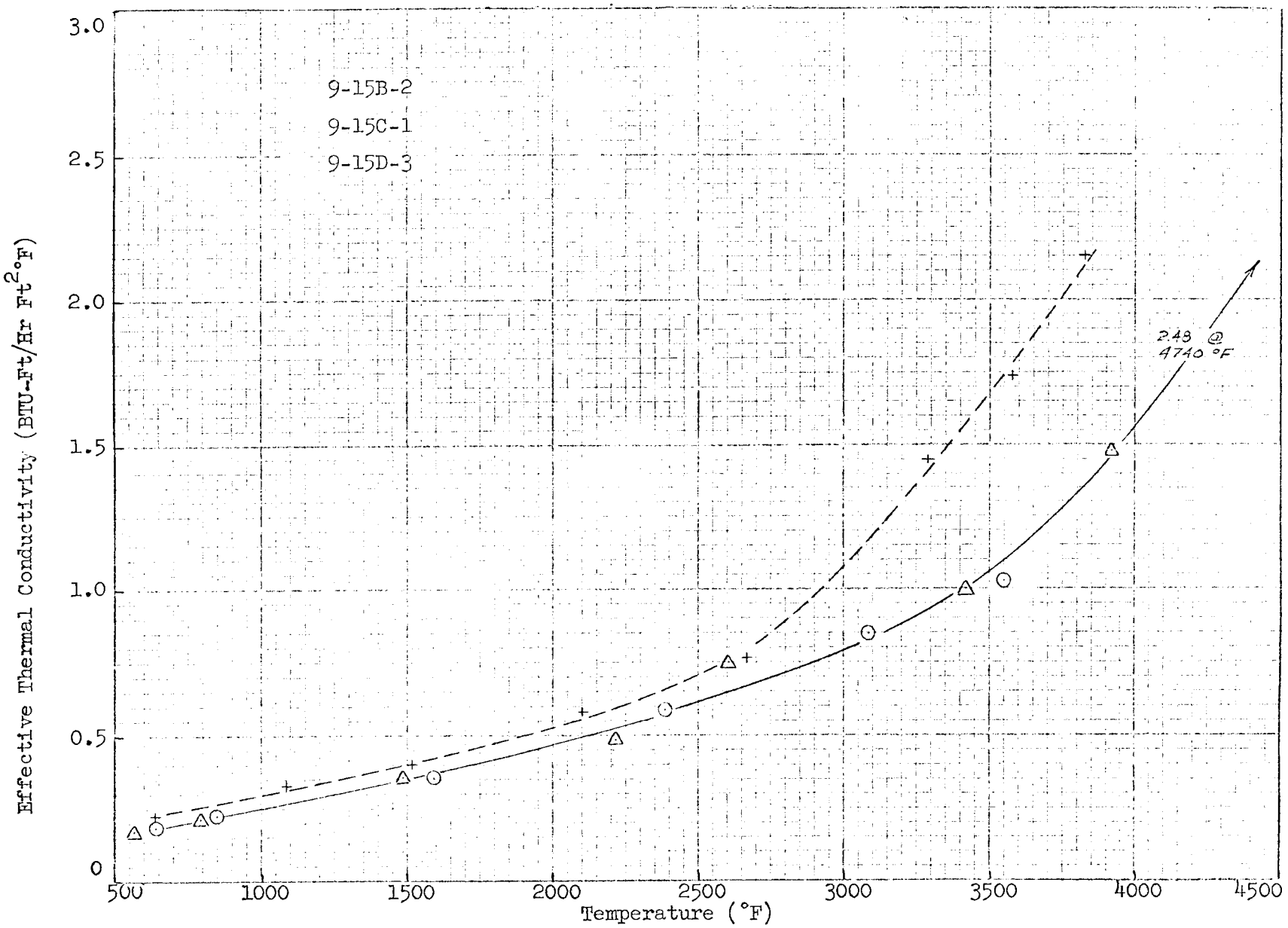

Figure 22. Effective Thermal Conductivity of Laboratory Chars formed at 1832°F Maximum from 9-15B, 9-15C, and 9-15D Materials

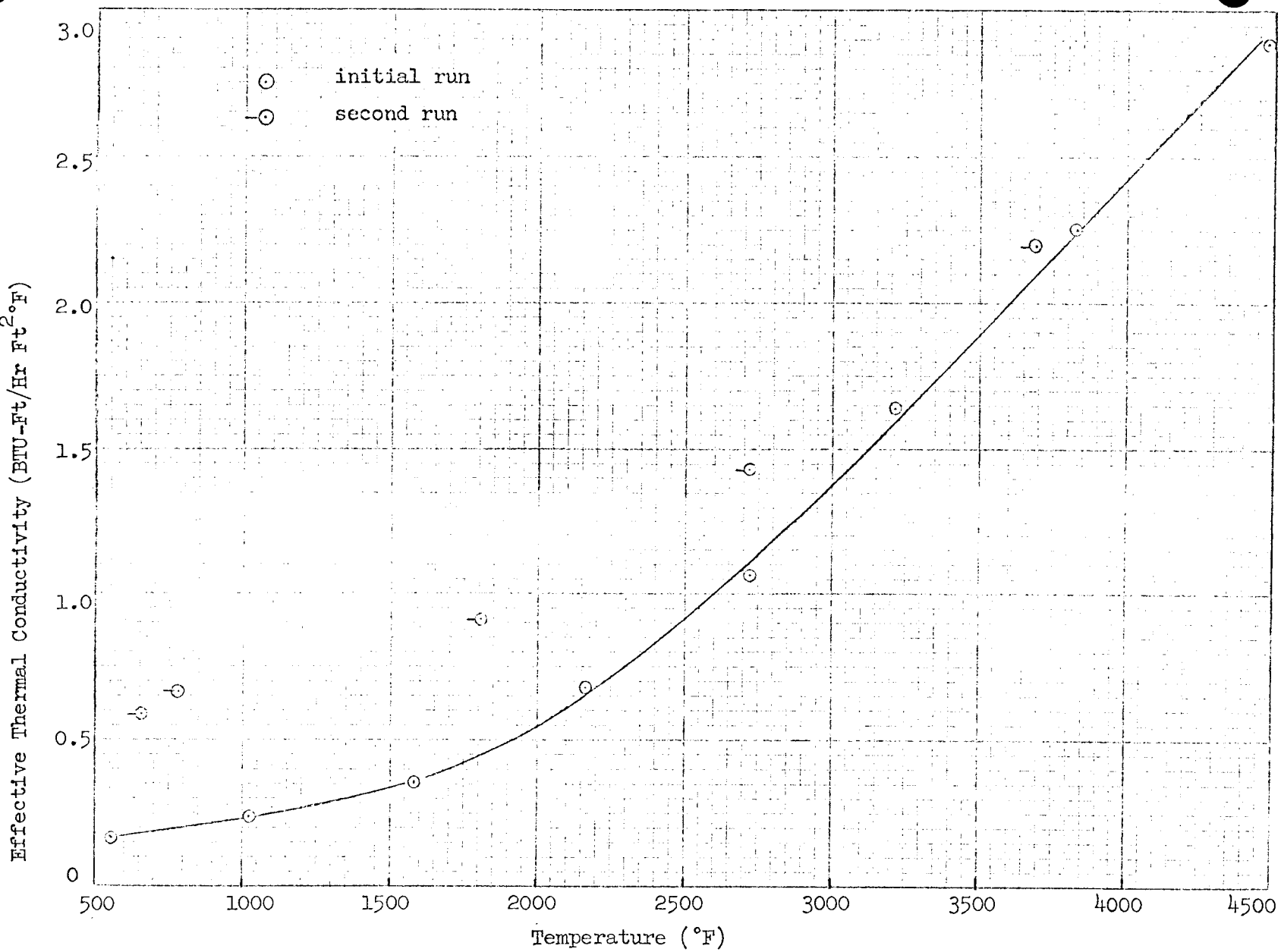

Figure 21. Effective Thermal Conductivity of Laboratory Chars formed at 1832°F from 9-15A Material

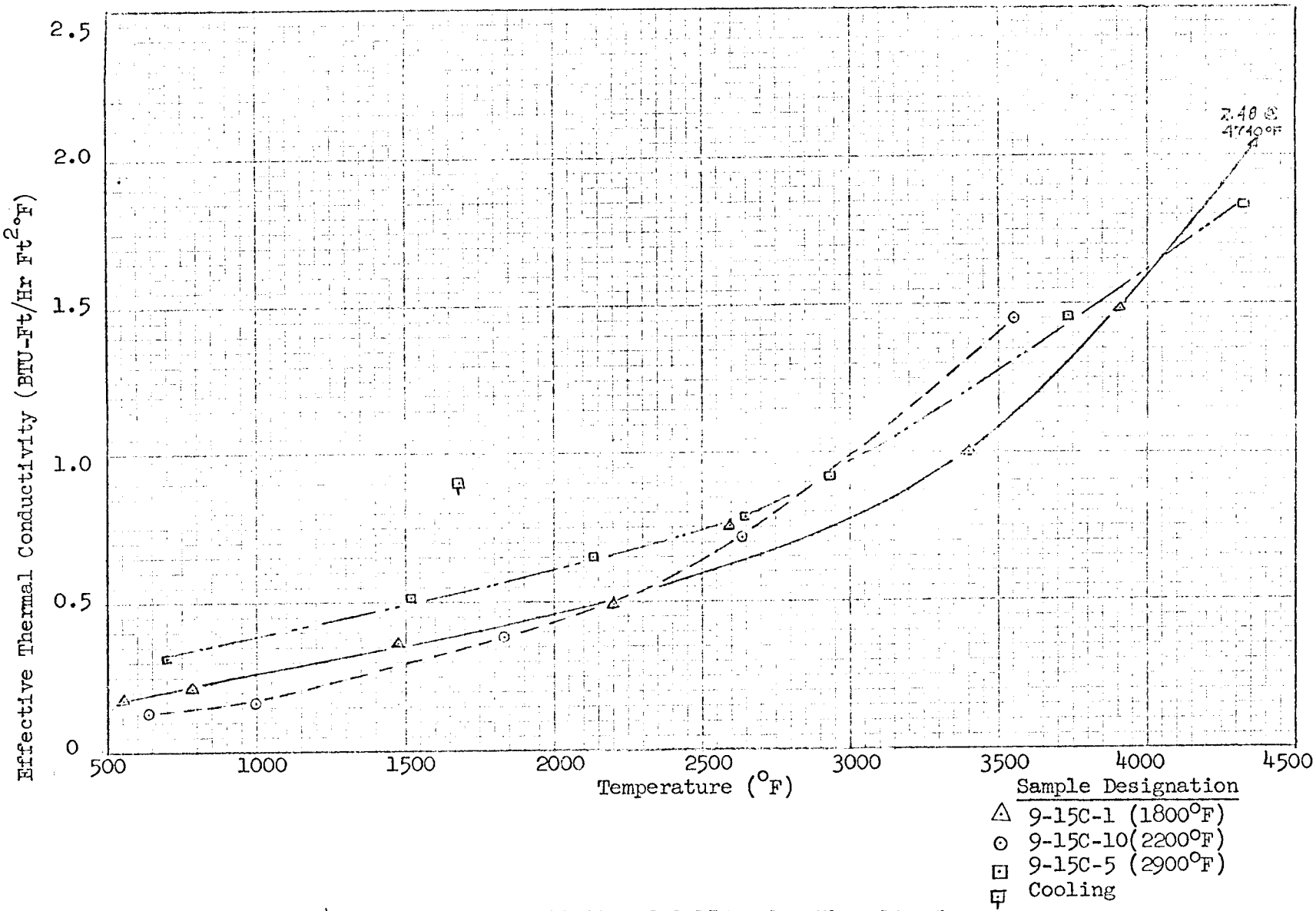

Figure 24. Thermal Conductivity of 9-15C Nylon Phenolic Chars as a Function of Char Formation Temperature

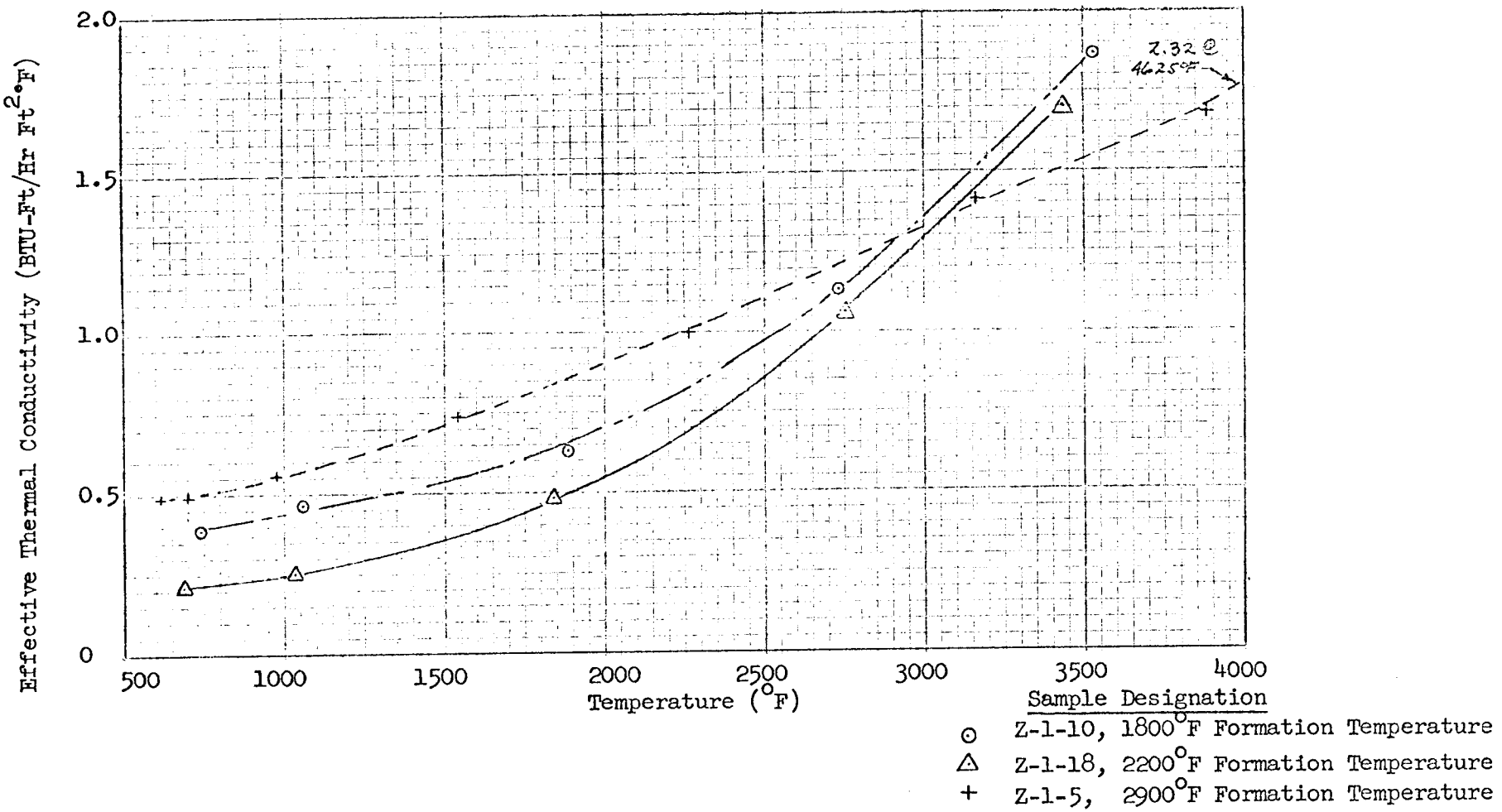

Figure 25. Effective Thermal Conductivity of Laboratory Chars formed from Zytel as a Function of Formation Temperature

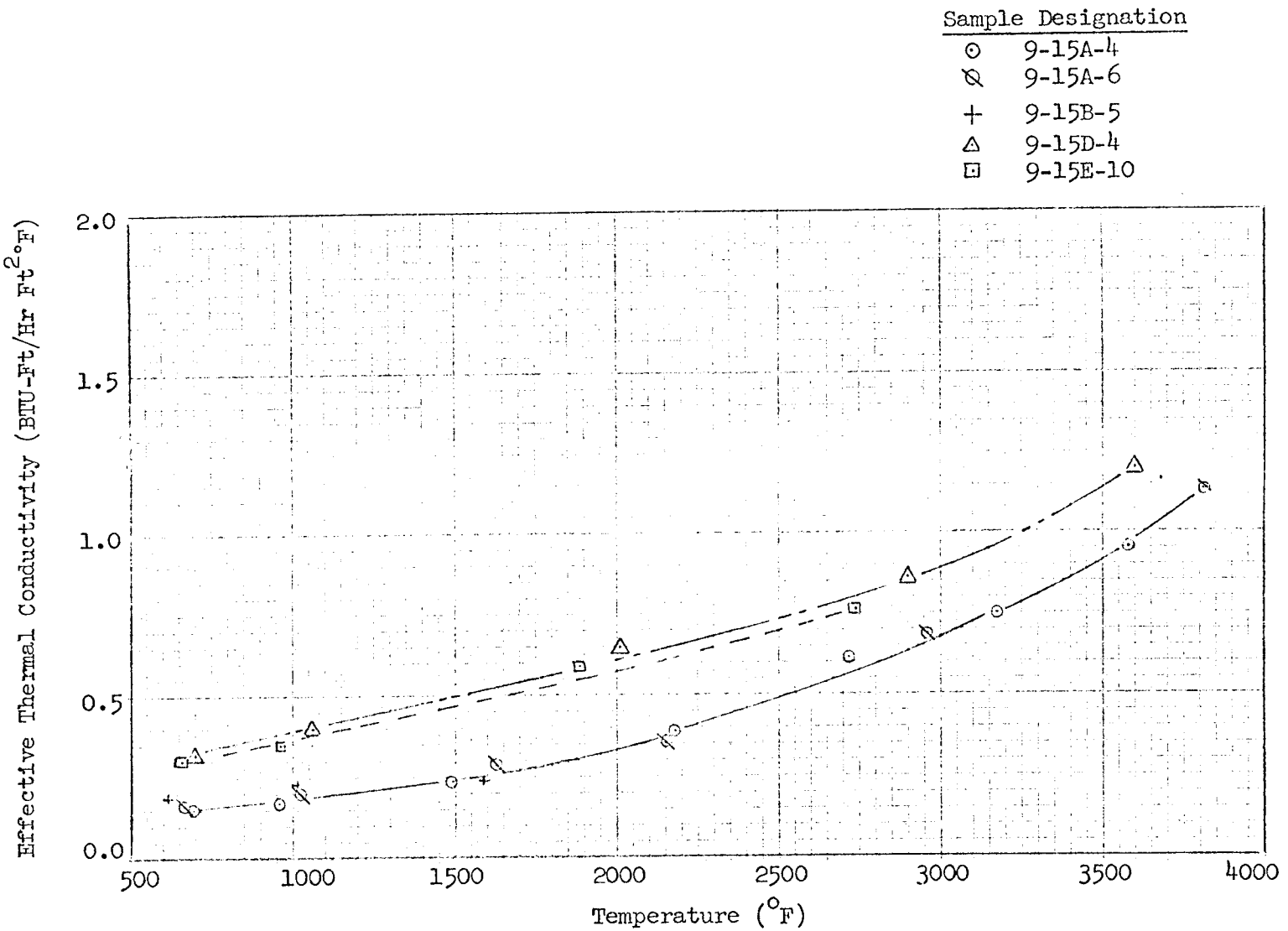

Figure 26. Effective Thermal Conductivity of Chars formed at 2900°F from 9-15A, 9-15B, 9-15D, and 9-15E Materials

where

k_s = solid phase conductivity term

k_T = thermal conductivity of the solid constituent

$(1 - \delta)$ = fraction of solids

$\bar{F}$ = geometrical factor accounting for dimensions of the solid path and restrictions to heat transport

In a complex structure such as a char a true k_T does not exist because the structure is composed of several solid phase constituents such as disordered carbon and crystallites.

From the data, it can be shown that the effective thermal conductivity, which in its simplest form* may be treated as a sum of the solid phase and gas phase conductivities and a radiation conductivity, is at low temperatures proportional to $(1 - \delta)$ and the structure parameters from x-ray analysis. The trend of increasing conductivity with increasing solid fraction and ordering of the structure may be observed in Table 11. The data are evaluated at 600 and 1500° F. Evaluation of the exact structure is beyond the scope of this program. However, using the criterion of true density, ρ_r, as an indication of the degree of ordering of the carbon system one can establish the relationship where the solid conductivity is a function of $(1 - \delta)$ and ρ_r.

The average pore size does not appear to have a significant effect on conductivity. This would of course not be true for measurements made in an atmosphere in which the pores are filled with a gas. Under these conditions the size and shape of the voids and the relationship of a characteristic void dimension to the mean free path of the contained gas would have a pronounced effect on conductivity at lower temperature.

*In an exact analysis the interactions of conduction and radiation must be considered.

Table 11

EFFECTIVE THERMAL CONDUCTIVITY

Char Temp.	Type	k $\left(\frac{\text{Btu-Ft.}}{\text{hr-ft}^2\text{-}^\circ\text{F}}\right)$ 600° F	1500° F	$(1-\delta)$	ρ_r (gm/cm^3)	$I_{max}{}^*\beta$	$(1-\delta)\rho_r$	Av. Pore Dia. (μ)
	9-15A	0.18	0.35	0.33	1.41	738	0.47	395
	9-15B	0.18	0.35	0.33	1.44	955	0.48	300
1800	9-15C	0.18	0.36	0.29	1.66	735	0.48	190
	9-15D	0.23	0.40	0.39	1.65	532	0.64	230
	9-15E	0.41	0.64	0.45	1.64	652	0.73	220
	9-15A	0.14	0.26	0.23	1.60	750	0.37	330
	9-15B	0.19	0.27	0.27	1.48	890	0.40	318
2900	9-15C	0.30	0.46	0.31	1.45	1433	0.45	160
	9-15D	0.31	0.52	0.32	1.46	985	0.47	333
	9-15E	0.29	0.47	0.31	1.49	623	0.46	320

Examination of the data for the 9-15C and Zytel materials as a function of formation temperature shows the lowest conductivity occurs for the 2200° F chars. The x-ray data for Zytel clearly shows the least graphitic and ordered structure at this formation temperature, with increasing ordering at 1832° F and 2900° F. The conductivity data also follow in this increasing order. The 9-15C chars exhibited this increase in conductivity with formation temperatures of 2200° F, 1832° F, and 2900° F. Again, the x-ray data for the 2900° F char show the most order. This is not as clear for the other chars in which case the degree of order is approximately the same for both 1832 and 2200° F. However, the solid fraction, $(1-\delta)$ is larger for the 1832° F char and results in a larger conductivity.

Section 8

CONCLUSIONS AND RECOMMENDATIONS

8.1 CONCLUSIONS

Thermal conductivities of laboratory chars were found to change significantly when the materials were exposed to temperatures above their formation temperature during the thermal property test period. An increase in conductivity by a factor of two to three was observed in the 600 to 700° F temperature range for chars which had been heated to temperatures beyond their formation temperature. This increase is due principally to a more graphitic and ordered structure which occurs upon heating during the testing process.

Changes in properties other than thermal conductivity, such as heat capacity and coefficient of expansion, might also be expected to occur during any testing process in which the specimen is exposed to temperatures above its formation temperature for any appreciable period of time.

The following effects of the thermal measurements procedure were noted during post test examination of the samples:

- An increase in the fraction of pores in the 10 to 100-μ range
- An increase in the extent of graphitization as indicated by an increase in the degree of ordering and in the volume of ordered material; a decrease in interlayer spacing; an increase in crystallite thickness; and an increase in the number of stacked hexagonal carbon arrays in a given crystallite
- A loss in weight which is attributed to the loss of impurities such as O, N, H with possible loss of associated carbon

A correlation was shown between thermal conductivity and char parameters of void fraction and degree of graphitization for measurements made below the formation temperature. The pore size parameter showed no measurable effect on the conductivity values obtained during the program. This is attributed to (a) the pore size range investigated was not large and(b) measurements were made in vacuum so there was no gas phase contribution to the effective thermal conductivity. The influence of pores in the range of 10 to 1000μ would be predominant in the process of heat transport by gas phase conduction.

Six types of materials, five of nylon fiber in phenolic and the sixth of nylon powder in phenolic were used to produce chars of varying pore diameter for correlation with measurements of thermal conductance. It was found the average large pore diameter varied as the average diameter of the original fiber filament. The ratio of nylon-to-phenolic did not appreciably affect the average pore diameter but did affect the bulk density or total porosity of the char. The effect of temperature of formation on pore spectra, at the heat rates used to produce crack free chars was moderate even though the temperature was varied from 1832 to 2900° F. A change in atmospheric pressure from 15 psia to 0.15 psia had a noticeable effect. The number of pores in the 100 to 10μ range was larger at the lower pressure, presumably because a larger percentage of volatile hydrocarbons was removed during the degradation process. The crystalline character of the six types of materials was quite different. At a given temperature of formation the degree of crystallite ordering and the amount of ordering varied between the six samples. The degree and amount of ordering increased with temperature of formation and heat treatment time, as would be expected. The crystallite density and average crystallite thickness did not vary greatly between any of the samples or at successively increasing temperatures.

The flash method was shown to be suitable for measurement of the thermal diffusivity of char specimens. An improved low noise radiometer is needed for reliable measurements above 4500° F. However, the experimental apparatus performed acceptably in all other aspects.

8.2 RECOMMENDATIONS

The course of the experimental work suggested certain specific areas for further investigations:

- The characteristics of the materials should be more precisely controlled. Material made up of nylon powder rather than fiber is superior for this type of investigation because it forms a more isotropic char and one which has less tendency to crack. Undoubtedly, suitable higher heat-rate chars could be produced from this material. A wider variation in pore spectra variations could be accomplished by change in powder size.
- The techniques of char characterization for a more precise delineation of char properties should be extended and refined. A better understanding of the thermal energy transport phenomena in the complex char structure may be obtained from experimented data only with a precise knowledge of the character of the structure. A complete x-ray analysis should be used to give a better picture of all constituents and their arrangement in the total solid phase. The effects of heat treatment after formation should also be examined.
- A thorough study should be given to the measurement procedures used for determining properties of materials such as chars which undergo change in their structure by heat treatment during the test period. The diffusivity method appears to offer the best solutions at this time for thermal properties work as with present techniques the heating period for a single measurement point can be reduced to approximately 10 to 15 min. Even shorter times may be possible with modified apparatus. With suitable refinements, the technique may also be used to measure heat capacity of chars in a manner similar to that described by Parker in Ref. 1.

Section 9

REFERENCES

1. W. J. Parker, R. J. Jenkins, C. P. Butler, and G. L. Abbott, "Flash Method of Determining Thermal Diffusivity. Heat Capacity and Thermal Conductivity," J. Appl. Phys. 32, 1961

2. Lockheed Missiles & Space Company, Proposal for an Experimental Study of the Thermal Conductance of Polymer Chars, LMSC-893405, Sunnyvale, Calif., 16 Apr 1964

3. R. Nagler, Jet Propulsion Laboratory, Pasadena, Calif., Meeting of JPL and LMSC Personnel, Palo Alto, Calif., 4 Dec 1964

4. American Instrument Co., Inc., "Porosity Determinations of a Broad Variety of Materials," Data to accompany Aminco Porosimeter Bulletin 2330, 8030 Georgia Ave., Silver Spring, Md., Nov 1961

5. -----, "Pore Structure Analysis," Bulletin 2330-A, 8030 Georgia Ave., Silver Spring, Md., Jul 1964

6. -----, "Aminco-Winslow Porosimeter, Cat. No., 5-7107, Instruction No. 597," 8030 Georgia Ave., Silver Spring, Md., Aug 1960

7. N. M. Winslow and J. J. Shapiro, "An Instrument of Pore-Size Distribution by Mercury Penetration," ASTM Bulletin No. 236, Feb 1959, pp. 39–44

8. E. E. Underwood, "Quantitative Metallography," Parts I and II Metals Engineering Quarterly, published by ASM, Aug and Nov 1962

9. Unpublished Data, Materials Science Laboratory, W. Bradshaw, et al., Palo Alto, Calif.

10. R. H. Bragg and C. M. Packer, "Effect of Absorption and Incoherent Scattering on X-ray Line Profiles," Rev. Sci. Instr. 34, No. 11, pp. 1202–1207

11. Lockheed Missiles & Space Company, Quarterly Progress Report From Metallurgy and Ceramics, Orgn. 53-36, Research Directive M-1, Char Layer Studies, Period: 15 Nov 1961 to 15 Feb 1962, by W. Bradshaw, Palo Alto, Calif. (U)

12. W. Bradshaw, J. Robinson, and A. Gleason, "X-ray Diffraction Characteristics and Microstructure of the Chars of an Ablating Composite," Paper No. 36, presented at the Sixth Biennial Conference on Carbon, Pittsburgh, Pennsylvania, 17–21 Jun 1963 (U)

13. Lockheed Missiles & Space Company, Progress Report From Metallurgy, Materials Research Laboratory, Orgn. 52-30, Experimental Memos 1108-05, -06, -07, Physical Properties, Sublimation and Erosion of Char Layers, Period: 15 Nov 1962 to 15 Feb 1963, W. Bradshaw, Palo Alto, Calif. (U)

14. W. J. Parker, "Flash Method of Measuring Thermal Diffusivity," Proceeding of The Third Thermal Conductivity Conference, Oct 1963

15. J. A. Cape and G. W. Lehman, "Temperature and Finite Pulse Time Effects in the Flash Method for Measuring Thermal Diffusivity," J. Appl. Phys. 34, 1963

16. R. D. Cowan, "Proposed Method of Measuring Thermal Diffusivity at High Temperature," J. Appl. Phys. 32, 1961

17. Carslaw and Jaeger, Conduction of Heat in Solids, 2nd ed., Oxford University Press, 1959

18. R. D. Cowan, "Pulse Method of Measuring Thermal Diffusivity at High Temperatures," J. Appl. Phys. 34, 1963

19. D. E. Ginnings and R. J. Corruccini, J. Research N.B.S. 38, 1947

20. Lockheed Missiles & Space Company, Theory for the Thermophysical Performance of Charring Organic Heat-Shield Composites, by K. M. Kratsch, L. F. Hearne, and H. R. McChesney, LMSC-803099, 2-60-63-7, Sunnyvale, Calif., 18 Oct 1963

21. J. P. Moore, et al., "Comparison of the Thermal Conductivity, Electrical Resistivity, and Seebeck Coefficient of a High Purity Iron and Armco Iron to 1000°C," from Proceedings of the Fourth Conference on Thermal Conductivity, Oct 1964

22. A. Goldsmith, et al., "Thermophysical Properties of Solid Materials," WADC Technical Report TR 58-476, 1960, Wright Air Development Division, Air Research and Development Command, USAF, Wright-Patterson Air Force Base, Ohio

23. Industrial Graphite Engineering, National Carbon Co., Div. Union Carbide Corp., Copyright 1959

24. Westech Plastic and Chemical Company, Shipping Memo, "Panel Composition of Material Produced From P'O' 24-78505," 25 Oct 1964, Menlo Park, Calif.

25. Southern Research Institute, Some Thermophysical Properties of Reinforced Plastics, 5507-1331-1X, Birmingham, Ala., Aug 1962 (C)

26. S. Yamada and H. Sato, "Some Physical Properties of Glassy Carbon," Nature 193, Jan 1962, pp. 261–262

27. S. Mrozowski, "Kinetics of Graphitization," Paper 31, pp. 264–270 of Kinetics of High-Temperature Processes, J. Wiley and Sons, New York, 1959

28. A. R. Ubbelohde and F. A. Lewis, Graphite and its Crystal Compounds, p. 88, Clarendon Press, Oxford, England, 1960

TABLE A

PORE SPECTRA DATA

Material:	9-15A	A_5-Duplicate
Preparation Temp:	1832°F	0.0351 gms.
Sample No.:	A_5	0.008 cc
Sample W_t.:	0.0574 gms.	23.6
Measured Pore Volume:	0.009 cc	
Volume % Porosity:	18.7	

Pore Size,* μ	Vol.%*	Pore Size, μ	Vol. %
97.5	0	97.5	0
62.5	0	62.5	12.4
46.1	22.3	46.0	25.0
36.5	33.4	36.5	37.5
30.2	44.5	30.2	50.0
25.7	44.5	25.7	50.0
19.9	44.5	22.4	62.5
17.2	55.6	8.7	62.5
11.5	66.7	5.9	75.0
5.8	66.7	2.0	75.0
3.5	77.8	1.6	87.5
1.9	88.8	0.56	87.5
0.57	88.8	0.38	100
0.38	100	0.035	100
0.035	100		

Material:	9-15B	
Preparation Temp:	1832°F	
Sample No.:	B5	B_5-Duplicate
Sample Wt.	0.0708 gms.	0.0442 gms.
Measured Pore Volume:	0.017 cc	0.010 cc
Volume % Porosity:	26.2	24.2

Pore Size, μ	Vol. %	Pore Size, μ	Vol. %
97.5	0	97.5	0
45.0	41.2	62.5	10.0
30.0	58.9	46.1	20.0
22.0	64.7	36.5	40.0
17.0	70.6	30.2	50.0
11.4	76.5	25.7	60.0
8.6	82.3	17.2	60.0
5.8	82.3	11.5	70.0
3.5	82.3	8.7	80.0
2.9	88.2	1.6	80.0
1.6	88.2	0.83	90.0
0.84	94.2	0.058	90.0
0.16	94.2	0.035	100
0.058	100		
0.035	100		

*Volume % of measured pores > indicated diameter in Pore Size

TABLE A

PORE SPECTRA DATA (cont.)

Material:	9-15C		
Preparation Temp:	1832°F		
Sample No:	C6		C_6-Duplicate
Sample Wt:	0.0719 gms.		0.0752 gms.
Measured Pore Volume:	0.070 cc		0.077 cc
Volume % Porosity	61.9		61.7

Pore Size, μ	Vol. %	Pore Size, μ	Vol. %
97.5	0	97.5	0
39.0	75.7	62.5	3.9
26.5	88.6	42.7	32.5
20.0	92.8	33.3	67.5
15.9	94.3	26.5	80.6
10.8	97.2	23.0	84.5
8.3	97.2	20.0	91.0
4.25	97.2	18.0	93.5
2.5	98.7	15.9	93.5
0.17	98.7	10.8	94.8
0.058	100.	8.3	96.3
0.035	100.	5.6	97.5
		3.4	98.7
		1.6	98.7
		0.056	100.
		0.035	100.

Material:	9-15D		
Preparation Temp.	1832°F		
Sample No.:	D_4		D_4-Duplicate
Sample Wt.:	0.0626 gms.		0.0739 gms.
Measured Pore Volume:	0.039 cc		0.032 cc
Volume % Porosity:	50.1		42.0

Pore Size, μ	Vol. %	Pore Size, μ	Vol. %
97.5	0	97.5	0
46.1	15.4	62.0	3.1
28.5	56.4	45.8	6.3
21.5	64.1	35.5	31.2
17.0	69.2	29.0	43.7
11.0	77.0	25.0	46.2
8.4	79.4	21.8	56.3
5.7	84.6	19.4	59.4
3.5	87.2	16.5	65.7
1.6	87.2	11.3	68.8
0.57	89.8	8.5	75.1
0.29	89.8	5.7	81.3
0.17	92.3	3.5	84.3
0.058	93.4	1.9	84.3
0.035	100	1.6	87.5
		0.29	87.5
		0.17	90.8
		0.059	96.9
		0.035	100

TABLE A

PORE SPECTRA DATA (cont.)

Material:	9-15E		
Preparation Temp:	1832°F		
Sample No:	E_4	E_4 - Duplicate	
Sample Wt:	0.0589	0.0861 gms.	
Measured Pore Volume:	0.018 cc	0.035 cc	
Volume % Porosity:	34.16	39.28	

Pore Size, μ	Vol. %	Pore Size, μ	Vol. %
97.5	0	97.5	0
46.1	0	46.1	0
30.2	11.1	29.1	45.7
22.4	27.8	22.0	51.4
17.2	38.9	16.7	57.2
11.5	50.0	11.2	65.8
8.7	55.6	8.5	68.5
5.8	61.1	5.8	74.4
3.5	66.7	4.3	77.2
1.6	66.7	3.4	77.2
0.57	72.2	1.9	80.2
0.29	77.8	1.6	80.2
0.17	83.4	0.57	82.8
0.058	94.5	0.29	85.7
0.035	100	0.17	91.5
		0.058	97.2
		0.035	100

Material:	Zytel-1		
Preparation Temp:	1832°F		
Sample No:	-10_{21}	-10_{22} -Duplicate	
Sample Wt.:	0.1182 gms.	0.1040	
Measured Pore Volume:	0.1280	0.1100 cc	
Volume % Porosity:	61.1	61.6	

Pore Size, μ	Vol. %	Pore Size, μ	Vol. %
97.5	0	97.5	0
46.0	58.2	46.0	69.5
32.4	93.0	33.6	91.4
26.9	94.8	28.2	94.5
23.3	96.9	24.3	96.0
20.6	97.7	21.4	97.3
18.4	98.5	18.8	97.7
16.6	98.8	17.0	98.2
14.7	98.8	15.0	98.7
10.3	99.3	10.5	98.7
5.5	99.3	8.1	99.3
4.17	99.7	2.8	99.3
1.56	99.7	1.58	99.7
0.56	100	0.17	99.7
0.035	100	0.058	100
		0.035	100

TABLE A

PORE SPECTRA DATA (cont.)

Material:	9-15A		
Preparation Temp:	2200°F		
Sample No:	f		2-Duplicate
Sample Wt:	0.0652 gms		0.0667 gms.
Measured Pore Volume:	0.008 cc		0.0150 cc
Vol. % Porosity:	16.75		27.55
Pore Size, μ	Vol. %	Pore Size, μ	Vol. %
97.5	0	97.5	0
62.5	25.0	46.1	33.1
46.0	37.5	30.2	53.3
25.7	37.5	22.5	60.0
22.4	50.0	17.2	66.7
19.8	62.5	11.5	73.3
17.2	62.5	8.7	80.0
11.5	75.0	6.95	80.0
2.9	75.0	5.8	86.7
1.7	87.5	2.91	86.7
0.56	100	1.59	93.4
0.035	100	0.29	93.4
		0.17	100
		0.035	100

Material:	9-15B
Preparation Temp:	2200°F
Sample No:	3
Sample Wt:	0.0662 gms.
Measured Pore Volume:	0.0538 cc
Vol. % Porosity:	54.80

Pore Size, μ	Vol. %
97.5	0
40.7	70.3
27.8	79.5
20.9	83.3
16.2	87.0
11.1	90.8
8.36	92.6
6.80	92.6
5.67	94.5
4.28	94.5
2.87	96.4
1.59	96.4
0.56	98.2
0.19	98.2
0.058	100
0.035	100

PORE SPECTRA DATA (cont.)

Material:	9-15C
Preparation Temperature:	2200°F
Sample No:	3
Sample Wt:	0.0853 gms.
Measurement Pore Volume:	0.0840 cc
Volume % Porosity:	63.0

Pore Size,	Vol. %
97.5	0
38.1	76.2
25.7	90.5
19.9	94.2
15.5	97.5
8.22	98.8
0.17	98.8
0.058	100
0.035	100

TABLE A

PORE SPECTRA DATA (cont.)

Material:	9-15D
Preparation Temperature:	2200°F
Sample No:	5
Sample Wt.:	0.0965 gms.
Measurement Pore Volume:	0.092 cc
Volume % Porosity:	61.9

Pore Size, μ	Vol. %
97.5	0
39.8	56.5
27.0	65.0
20.4	69.5
15.8	74.0
10.8	80.5
8.3	84.7
6.7	89.2
5.6	92.5
4.2	93.5
3.4	95.5
1.6	96.9
0.56	98.0
0.17	98.0
0.058	99.0
0.035	100

Material:	9-15E
Prep. Temp.	2200°F
Sample No:	3
Sample Wt:	0.0794 gms.
Meas. Pore Vol:	0.082 cc
Vol. % Porosity:	60.3

Pore Size, μ	Vol. %
97.5	0
41.7	39.0
26.9	69.5
20.4	73.1
15.8	76.8
10.9	82.9
8.3	89.0
6.7	92.7
5.6	94.0
4.2	96.5
3.4	97.5
1.6	97.5
0.56	98.7
0.29	98.7
0.17	100
0.035	100

Material:	Zytel-1
Prep. Temp:	2200°F
Sample No:	13
Sample Wt:	0.0971 gms.
Meas. Pore Vol:	0.1100 cc
Vol. % Porosity:	63.4

Pore Size, μ	Vol. %
97.5	0
34.4	87.2
24.3	94.5
19.1	96.2
15.1	97.2
10.5	98.3
2.80	98.3
1.60	99.2
0.17	99.2
0.058	100
0.035	100

TABLE A

PORE SPECTRA DATA (Cont.)

Material:	9-15E
Prep. Temp.:	2900°F
Sample No.:	E7
Sample Wt.:	0.0769 gms.
Measured Pore Volume:	0.110 cc
Volume % Porosity:	68.0

Pore Size, μ	Vol. %
97.5	0
62.4	0
46.1	0.9
36.4	5.5
27.4	43.7
19.9	67.3
15.4	75.4
10.7	83.6
8.1	88.2
5.5	92.0
4.2	92.8
2.8	93.7
1.57	94.5
0.56	96.3
0.29	98.2
0.17	99.1
0.058	100
0.035	100

Material:	Zytel-1
Prep. Temp.:	2900 °F
Sample No.:	-16
Sample Wt.:	0.1010 gms.
Measured Pore Volume:	0.1260 cc
Volume % Porosity:	64.5

Pore Size, μ	Vol. %
97.5	0
62.4	1.6
46.2	7.9
29.2	73.0
24.0	89.7
18.6	95.3
14.6	97.0
10.4	98.5
8.0	99.3
5.5	99.3
4.2	100
0.035	100

TABLE A

PORE SPECTRA DATA (cont.)

Material:	9-15A	
Prep. Temp:	2900°F	
Sample No:	16	$9\text{-}15_2$ - Duplicate
Sample Wt:	0.0708 gms.	0.0658 gms.
Meas. Pore Vol:	0.082 cc	0.076 cc
Vol. % Porosity:	64.3	62.5

Pore Size, μ	Vol. %	Pore Size, μ	Vol. %
97.5	0	97.5	0
48.6	78.1	38.0	85.5
37.2	85.4	26.1	92.2
30.7	89.0	20.1	94.7
25.7	90.3	15.6	97.5
22.4	92.7	10.8	97.5
19.9	95.2	8.3	98.8
18.8	95.2	4.25	98.8
15.7	96.3	2.86	100
10.5	97.7	0.035	100
8.1	98.9		
5.5	100		
0.035	100		

Material:	9-15A
Prep. Temp:	2900°F
Sample No:	A_1 - triplicate
Sample Wt:	0.0825 gms.
Meas. Pore Vol:	0.094 cc
Vol. % Porosity:	67.1

Pore Size,	Vol. %
97.5	0
47.3	76.5
36.4	84.0
29.6	87.0
25.4	90.0
19.5	93.6
15.3	95.8
10.7	98.0
8.2	99.0
4.2	99.0
2.84	100
0.035	100

TABLE A

PORE SPECTRA DATA (cont'd)

Material:	9-15B
Prep. Temp:	2900°F
Sample No:	B_8
Sample Wt:	0.0707 gms.
Meas. Pore Vol:	0.086 cc
Vol % Porosity:	64.4

Pore Size, μ	Vol. %
97.5	0
62.5	3.5
39.8	57.2
26.1	83.6
19.9	89.5
15.6	93.0
10.8	97.7
8.2	97.7
5.6	98.9
4.2	100
0.035	100

Material:	9-15C
Prep. Temp:	2900°F
Sample No:	C_8
Sample Wt.	0.0925
Meas. Pore Vol:	0.128 cc
Vol. Porosity:	66.7

Pore Size, μ	Vol. %
97.5	0
62.4	0.7
46.1	1.6
29.7	64.0
24.3	80.5
18.6	90.0
14.8	93.8
10.4	97.6
8.0	98.4
5.5	99.3
0.17	99.3
0.058	100
0.035	100

Material:	9-15D
Prep. Temp:	2900°F
Sample No:	D_6
Sample Wt.	0.0984 gms.
Meas. Pore Vol:	0.116 cc
Vol. % Porosity:	63.2

Pore Size, μ	Vol. %
97.5	0
62.4	0.86
46.1	1.70
34.3	23.3
26.1	56.9
19.7	69.8
15.4	77.5
10.8	83.6
8.1	88.0
5.5	91.2
4.2	93.0
2.8	94.0
1.57	94.0
0.56	95.7
0.29	97.5
0.17	98.3
0.058	99.2
0.035	100

TABLE A

PORE SPECTRA DATA, (Cont.)

Material 9-15A

Prep. Temp.:	1832°F
Post Thermal Diffusivity Tests	
Sample No.	A,(10)
Sample Wt.	.1142 gms.
Meas. Pore Vol.	.0155 cc
Vol. % Porosity	17.2

Pore Size,	Vol. %
97.5	0
62.5	32.2
44.9	58.2
35.7	64.5
29.7	74.3
25.4	77.5
22.2	77.5
19.7	80.7
17.0	83.8
11.4	87.2
8.6	90.3
5.8	90.3
2.9	90.3
1.6	93.7
.56	96.8
.29	96.8
.17	100.0
.035	100.0

Material: 9-15B

Prep. Temp:	1832°F
Post Thermal Diffusivity Tests	
Sample No.	B,(10)
Sample Wt.	.0954
Meas. Pore Vol.	.055 cc
Vol. % Porosity	46.2

Pore Size,	Vol. %
97.5	0
53.1	68.2
39.8	79.2
32.4	83.6
27.4	86.3
23.7	88.2
20.8	89.2
18.6	91.0
16.1	91.8
11.0	95.5
8.4	96.4
5.7	97.3
4.3	98.2
2.9	98.2
1.6	98.2
.56	99.2
.29	99.2
.17	100.0
.035	100.0

Material 9-15C

Prep. Temp.	1832°F
Post Thermal Diffusivity Tests	
Sample No. C, (10)	
Sample Wt.	.1287 gms.
Meas. Pore Vol.	.136 cc
Vol. % Porosity	60.6

Pore Size, μ	Vol. %
97.5	0
38.0	94.2
31.2	94.2
26.5	95.7
23.0	96.3
20.4	97.0

Material 9-15C cont'd.

Pore Size, μ	Vol. %
18.2	97.5
16.4	98.2
14.5	98.6
10.2	99.0
7.9	99.4
1.6	99.4
.17	99.4
.058	100
.035	100

PORE SPECTRA DATA (cont.)

Material:	9-15D
Prep. Temp.:	1832°F
Post Thermal Diffusivity Test	
Sample No.	D_3(10)
Sample Wt.	.1383 gms.
Total Pore Vol.	.118 cc
Vol. % Porosity:	55.3

Pore Size, μ	Vol %
97.5	0
46.0	66.1
35.7	70.3
29.7	73.0
25.0	75.0
21.9	76.7
19.5	77.9
17.3	79.2
15.2	80.5
10.5	86.4
8.1	87.3
5.5	89.0
4.2	89.4
2.8	90.3
1.6	91.2
.56	92.8
.29	93.7
.17	95.8
.058	98.7
.035	100.0

Material:	9-15E, (10)
Prep. Temp.:	1832°F
Post Thermal Diffusivity Tests	
Sample No. E,(10)	
Sample Wt.: 1400 gms.	
Total Pore Vol: .1125 cc	

Pore Size, μ	Vol %
97.5	0
60.3	6.7
38.9	49.3
30.7	64.0
25.7	68.0
22.4	70.2
19.7	72.0
17.7	73.3
15.5	74.6
10.7	80.8
8.2	82.2
5.6	85.3
4.2	87.2
2.8	88.9
1.6	89.8
.56	92.5
.29	94.3
.17	95.2
.058	99.6
.035	100

TABLE B

CHAR THERMAL DIFFUSIVITY TEST DATA AND CALCULATED THERMAL CONDUCTIVITY

Sample Description[a]	Time[b] (hr)	Temperature (°F)	θ 1/2[c] (sec)	$\bar{\alpha}$[d] (Ft^2/Hr)	$\bar{S}$	α (Ft^2/Hr)	K[e] BTU/Ft Hr Ft^2 °F
	1832°F Formation Temperature						
9-15A-1	0.8	565	2.40	0.029	0.111	0.023	0.17
Thickness, 1.167×10^{-2} Ft	1.6	1025	2.12	0.033	0.112	0.026	0.24
Weight, 2.80×10^{-4} lb	2.2	1580	1.50	0.046	0.095	0.031	0.35
Bulk density, 22.3 lb/Ft^3	3.0	2160	0.88	0.078	0.097	0.054	0.68
	3.7	2725	0.54	0.126	0.089	0.081	1.07
	4.3	3220	0.36	0.189	0.089	0.121	1.64
	5.2	3825	0.26	0.263	0.086	0.163	2.25
	5.7	4480	0.20	0.339	0.085	0.207	2.89
	6.5	1700	Cooling to room temperature				
9-15A-1 Rerun after	0.3	655	0.75	0.091	0.130	0.085	0.59
cooling	0.7	785	0.71	0.096	0.130	0.090	0.67
Thickness, 1.167×10^{-2} Ft.	1.5	1810	0.60	0.114	0.104	0.086	0.91
Weight, 2.52×10^{-4} lb	2.8	2715	0.38	0.180	0.093	0.120	1.43
Bulk density, 20.0 lb/Ft^3	3.3	3695	0.26	0.263	0.087	0.162	2.20
9-15B-2	0.3	640	2.35	0.021	0.113	0.017	0.18
Thickness, 1.00×10^{-2} Ft.	1.0	850	2.25	0.022	0.118	0.019	0.22
Weight, 2.86×10^{-4} lb.	1.7	1595	1.65	0.030	0.108	0.024	0.35
Bulk density, 29.4 lb/Ft^3	2.5	2385	0.95	0.053	0.090	0.034	0.59
(after test, 28.1 lb/Ft^3	3.1	3080	0.46	0.108	0.067	0.048	0.85
	3.7	3550	0.38	0.131	0.060	0.057	1.03
	4.3	4100	No	data			
9-15C-1	0.8	560	2.60	0.027	0.113	0.022	0.17
Thickness, 1.19×10^{-2} Ft	1.3	795	2.45	0.029	0.113	0.023	0.21
Weight, 2.82×10^{-4} lb	1.6	1495	1.72	0.041	0.105	0.031	0.36
Bulk density, 23.6 lb/Ft^3	2.2	2590	0.90	0.078	0.096	0.054	0.75
	2.5	3415	0.68	0.104	0.092	0.069	1.00
	3.0	3915	0.48	0.147	0.096	0.102	1.49
	3.5	4740	0.34	0.207	0.114	0.170	2.48

TABLE B (cont'd)

Sample Description[a]	Time[b] (hr)	Temperature (°F)	θ 1/2[c] (sec)	$\bar{\alpha}$[d] (Ft^2/Hr)	$\bar{S}$	α (Ft^2/Hr)	K[e] BTU-Ft / Hr Ft^2 °F
9-15D-3	2.0	630	2.70	0.025	0.112	0.020	0.23
Thickness, 1.167×10^{-2} Ft	3.5	1080	2.30	0.030	0.110	0.024	0.33
Weight, 3.52×10^{-4} lb	4.0	1506	1.90	0.036	0.096	0.025	0.40
Bulk density, 32.6 lb/Ft^3	4.3	2100	1.38	0.050	0.090	0.032	0.59
	4.5	2660	0.98	0.067	0.085	0.041	0.77
	4.7	3280	0.60	0.114	0.088	0.072	1.45
	5.0	3560	0.54	0.126	0.095	0.086	1.73
	5.3	3825	0.48	0.142	0.105	0.107	2.16
9-15E-1	2.5	680	1.50	0.041	0.112	0.033	0.43
Thickness, 1.10×10^{-2} Ft	-	1150	1.45	0.042	0.116	0.035	0.55
Weight, 3.56×10^{-4} lb	-	2010	1.10	0.055	0.099	0.039	0.81
Bulk density, 37.6 lb/Ft^3	-	2460	0.85	0.071	0.096	0.049	1.07
	-	3190	0.49	0.124	0.090	0.080	1.84
	-	4080	0.34	0.178	0.090	0.115	2.71
	4.5	4925	No	Data			
9-15E-2	1.3	650	1.60	0.037	0.123	0.033	0.44
Thickness, 1.08×10^{-2} Ft	2.1	990	1.50	0.039	0.109	0.031	0.50
Weight, 3.50×10^{-4} lb	3.3	1615	1.30	0.045	0.098	0.032	0.64
Bulk density, 39.1 lb/Ft^3	3.7	2180	0.95	0.062	0.088	0.039	0.86
(after test, 36.2 lb/Ft^3)	4.2	3345	0.40	0.146	0.075	0.079	1.89
9-15E-3	0.5	650	1.70	0.035	0.118	0.030	0.38
Thickness, 1.08×10^{-2} Ft	1.0	965	1.65	0.036	0.106	0.027	0.42
Weight, 3.50×10^{-4} lb	1.7	1505	1.35	0.047	0.103	0.035	0.65
Bulk density, 37.6 lb/Ft^3	3.0	2210	0.85	0.069	0.093	0.046	0.99
(after test, 34.3 lb/Ft^3)	4.6	2885	0.55	0.107	0.087	0.067	1.51
	5.8	3765	0.32	0.184	0.080	0.106	2.47
	Cool and rerun						
	0.6	658	0.55	0.107	0.121	0.093	1.05
	1.5	897	0.55	0.107	0.116	0.090	1.14
	2.5	1876	0.49	0.120	0.107	0.093	1.62

TABLE B (cont'd)

Sample Description[a]	Time[b] (Hr)	Temperature (^{o}F)	θ 1/2[c] (sec)	$\bar{\alpha}$[d] (Ft^2/Hr)	$\bar{S}$	α (Ft^2/Hr)	K[e] $\frac{BTU\,Ft}{Hr\,Ft^2\,{}^{o}F}$
Z-1-10-2	0.6	740	1.80	0.047	0.110	0.037	0.39
Thickness, 1.30×10^{-2} Ft	1.4	1055	1.70	0.050	0.109	0.039	0.48
Weight, 2.15×10^{-4} lb	2.0	1890	1.35	0.063	0.091	0.041	0.63
Bulk Density, 28.5 lb/Ft^3	2.5	2735	0.90	0.094	0.092	0.066	1.13
(after test, 27.6 lb/Ft^3)	3.0	3535	0.46	0.184	0.080	0.106	1.87
	2200 ^{o}F Formation Temperature						
9-15C-10	0.7	640	3.30	0.020	0.100	0.015	0.13
Thickness, 1.30×10^{-2} Ft	1.5	1000	2.95	0.023	0.091	0.015	0.16
Weight, 2.04×10^{-4} lb	2.0	1855	1.50	0.045	0.086	0.028	0.38
Bulk density, 26.1 lb/Ft^3	2.3	2636	0.83	0.081	0.080	0.047	0.72
(after test, 25.5 lb/Ft^3)	2.8	3540	0.43	0.156	0.080	0.090	1.45
Z-1-18	0.5	685	2.80	0.028	0.113	0.023	0.21
Thickness, 1.24×10^{-2} Ft	1.1	1045	2.50	0.031	0.096	0.021	0.25
Weight, 2.21×10^{-4} lb	1.6	1846	1.40	0.055	0.083	0.033	0.48
Bulk density, 27.2 lb/Ft^3	2.1	2757	0.65	0.118	0.077	0.065	1.06
(after test, 25.8 lb/Ft^3)	2.7	3439	0.44	0.175	0.080	0.101	1.70
	3.0	4000	No	Data			
	2900 ^{o}F Formation Temperature						
9-15A-4	1.1	696	2.60	0.024	0.112	0.019	0.15
Thickness, 1.12×10^{-2} Ft	2.0	960	2.32	0.027	0.098	0.019	0.17
Weight, 1.70×10^{-4} lb	3.0	1495	1.70	0.037	0.085	0.023	0.24
Bulk density, 21.3 lb/Ft^3	4.0	2180	1.13	0.055	0.080	0.032	0.39
(after test, 21.0 lb/Ft^3)	4.6	2715	0.75	0.084	0.080	0.048	0.61
	5.5	3175	0.58	0.108	0.075	0 058	0.75
	6.0	3580	0.50	0.125	0.080	0.072	0.95

TABLE B (cont'd)

Sample Description [a]	Time [b] (hr)	Temperature (°F)	θ 1/2 [c] (sec)	$\bar{\alpha}$ [d] Ft^2/Hr	$\bar{S}$	α Ft^2/Hr	K^e $\frac{BTU\text{-}Ft}{Hr\ Ft^2\ °F}$
9-15A-6	2.1	668	2.10	0.026	0.112	0.021	0.16
Thickness, 1.04×10^{-2} Ft	4.1	1025	1.85	0.030	0.099	0.022	0.20
Weight, 1.63×10^{-4} lb	4.6	1635	1.40	0.039	0.091	0.025	0.29
Bulk density, 22.1 lb/Ft^3	5.1	2148	1.10	0.050	0.08	0.029	0.35
(after test, 21.8 lb/Ft^3)	5.6	2955	0.60	0.091	0.08	0.052	0.69
	6.0	3820	0.38	0.145	0.08	0.083	1.14
9-15B-5	0.5	620	2.00	0.030	0.112	0.025	0.19
Thickness, 1.10×10^{-2} Ft	0.8	1015	1.85	0.033	0.102	0.024	0.23
Weight, 1.51×10^{-4} lb	1.3	1595	1.67	0.037	0.090	0.024	0.28
Bulk density, 23.2 lb/Ft^3							
(after test 23.0 lb/Ft^3)							
9-15C-4	4.3	710	2.45	0.030	0.116	0.025	0.22
Thickness, 1.21×10^{-2} Ft	5.4	940	2.25	0.032	0.108	0.025	0.27
Weight, 2.07×10^{-4} lb	6.3	1565	1.60	0.046	0.106	0.035	0.46
Bulk density, 26.6 lb/Ft^3	7.0	2280	1.30	0.056	0.100	0.041	0.62
9-15C-5							
Thickness, 1.22×10^{-2} Ft	0.5	587	1.85	0.041	0.115	0.034	0.30
Weight, 2.16×10^{-4} lb	1.0	1455	1.45	0.052	0.090	0.034	0.46
Bulk density, 27.4 lb/Ft^3	1.5	2600	1.00	0.075	0.080	0.043	0.69
Re Run of 9-15C-5	0.3	599	1.75	0.043	0.112	0.035	0.32
	1.1	1514	1.45	0.052	0.101	0.038	0.51
	2.0	2137	1.15	0.065	0.090	0.042	0.65
	2.7	2652	0.95	0.079	0.085	0.048	0.78
	3.5	2930	0.80	0.094	0.083	0.056	0.92
	5.5	3730	0.50	0.150	0.080	0.086	1.46
	5.8	4310	0.40	0.188	0.080	0.108	1.83
	6.5	1690	0.78	0.096	0.091	0.063	0.90
9-15D-4	1.2	700	2.00	0.041	0.110	0.032	0.32
Thickness, 1.27×10^{-2} Ft	2.5	1055	1.85	0.044	0.105	0.033	0.40
Weight, 2.23×10^{-4} lb	3.4	2004	1.30	0.063	0.095	0.041	0.65
Bulk density, 28.0 lb/Ft^3	4.3	2895	0.86	0.095	0.083	0.051	0.86
(after test, 27.1 lb/Ft^3)	5.0	3600	0.55	0.148	0.065	0.069	1.20

TABLE B (cont'd)

Sample Description[a]	Time[b] (hr)	Temperature (°F)	0 1/2[c] (sec)	$\bar{\alpha}$[d] Ft^2/Hr	$\bar{S}$	$\bar{\alpha}$ (Ft^2/Hr)	K[e] BTU-Ft / Hr Ft^2 °F
9-15E-10	1.0	655	1.50	0.046	0.110	0.036	0.30
Thickness, 1.17 x 10^{-2} Ft	1.5	960	1.35	0.050	0.101	0.037	0.35
Weight, 1.72 x 10^{-4} lb	2.0	1890	1.03	0.066	0.095	0.045	0.59
Bulk Density, 24.1 lb/Ft^3	2.5	2745	0.74	0.092	0.080	0.053	0.76
(after test, 23.9 lb/Ft^3)	3.5	3680	0.50	0.136	0.080	0.078	1.16
Z-1-5	1.4	620	1.40	0.058	0.113	0.047	0.49
Thickness, x 10^{-2} Ft	2.5	973	1.35	0.061	0.106	0.046	0.56
Weight x 10^{-4} lb	3.0	1550	1.15	0.071	0.098	0.050	0.74
Bulk density, lb/Ft^3	3.2	2260	0.85	0.096	0.091	0.063	1.00
(after test lb/Ft^3)	4.0	3162	0.59	0.138	0.070	0.075	1.41
	4.5	3885	0.48	0.170	0.075	0.101	1.85
	4.8	4625	0.35	0.233	0.075	0.126	2.32
	5.0	2352	0.58	0.140	0.100	0.101	1.72
	5.5	1475	0.66	0.124	0.114	0.102	1.47

Notes

[a] Bulk density based on micrometer dimensions; corrected for adsorbed water.

[b] Time to complete measurements at given temperatures.

[c] Time for back face temperature to reach 1/2 maximum value.

[d] Corrected for Losses

[e] $k = \alpha \cdot \rho \cdot C_p$; C_p from Figure 13

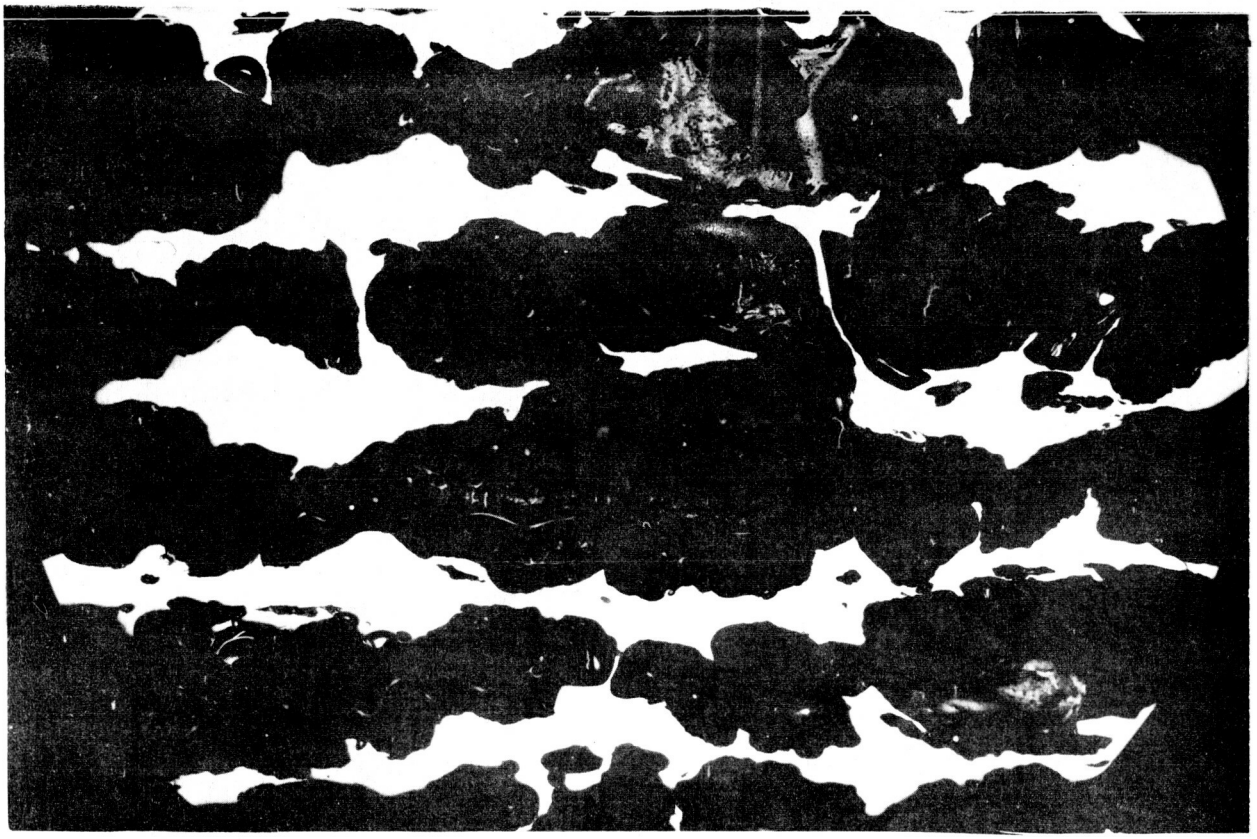

a. M-8468, 50X

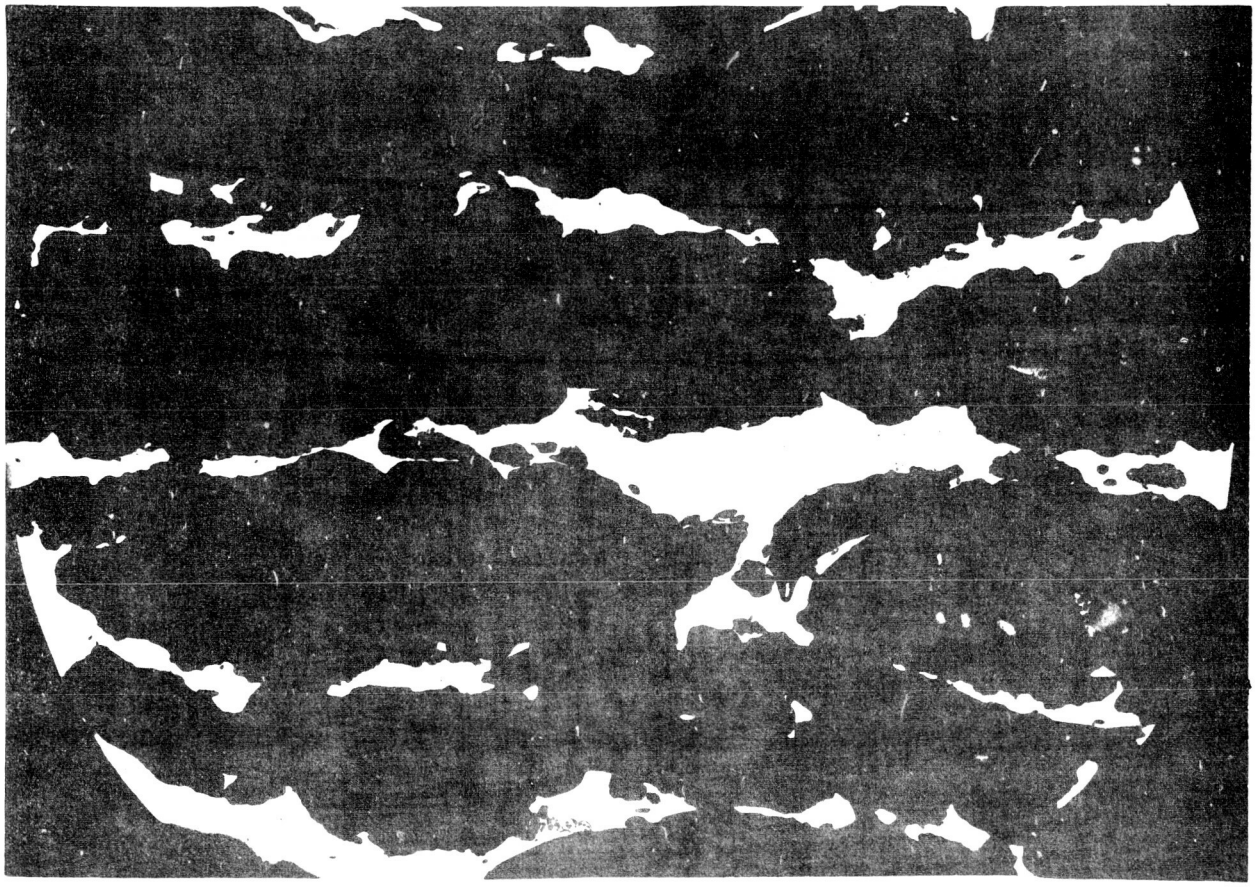

b. M-8468, 50X

Figure 4-1. [illegible] Laboratory Char Sample X-15-A-4

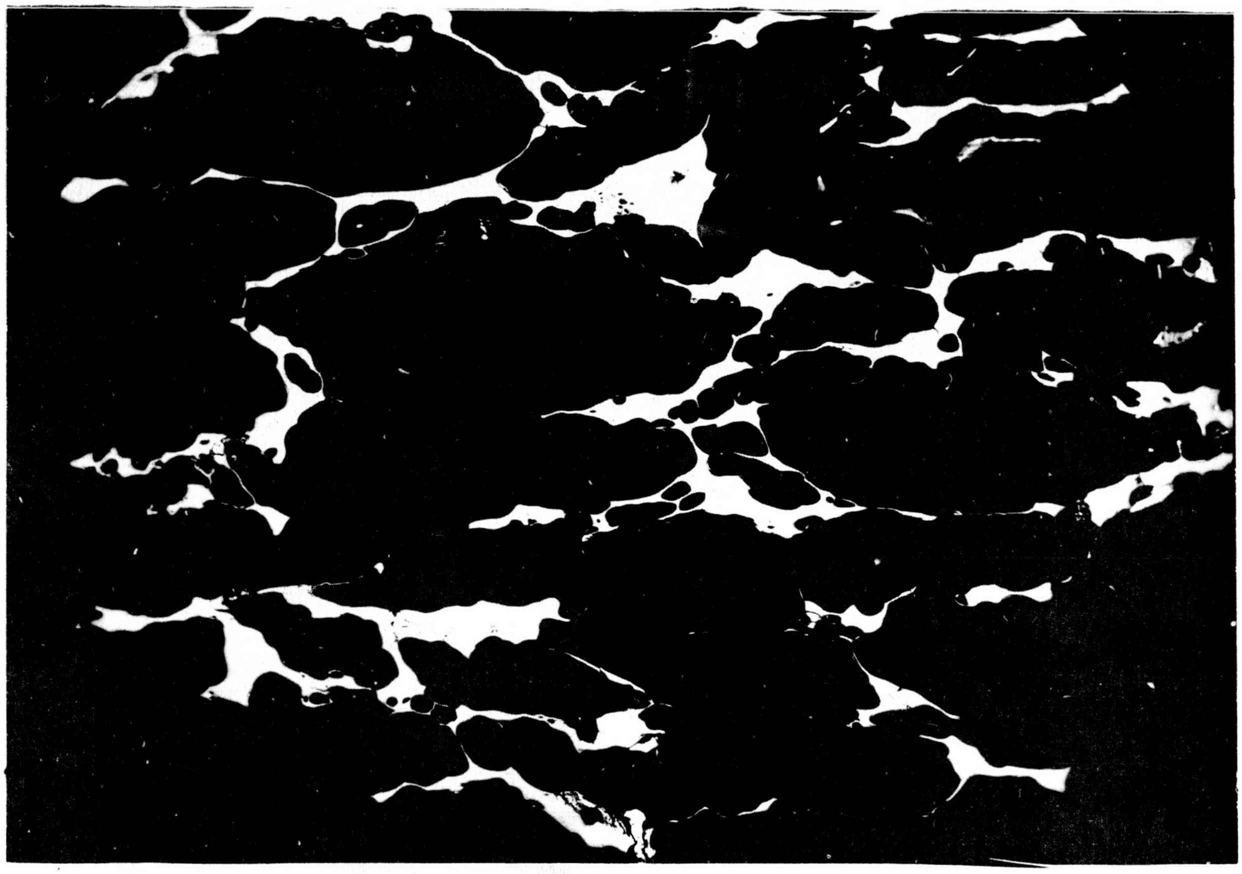

a. M-8469, 50X

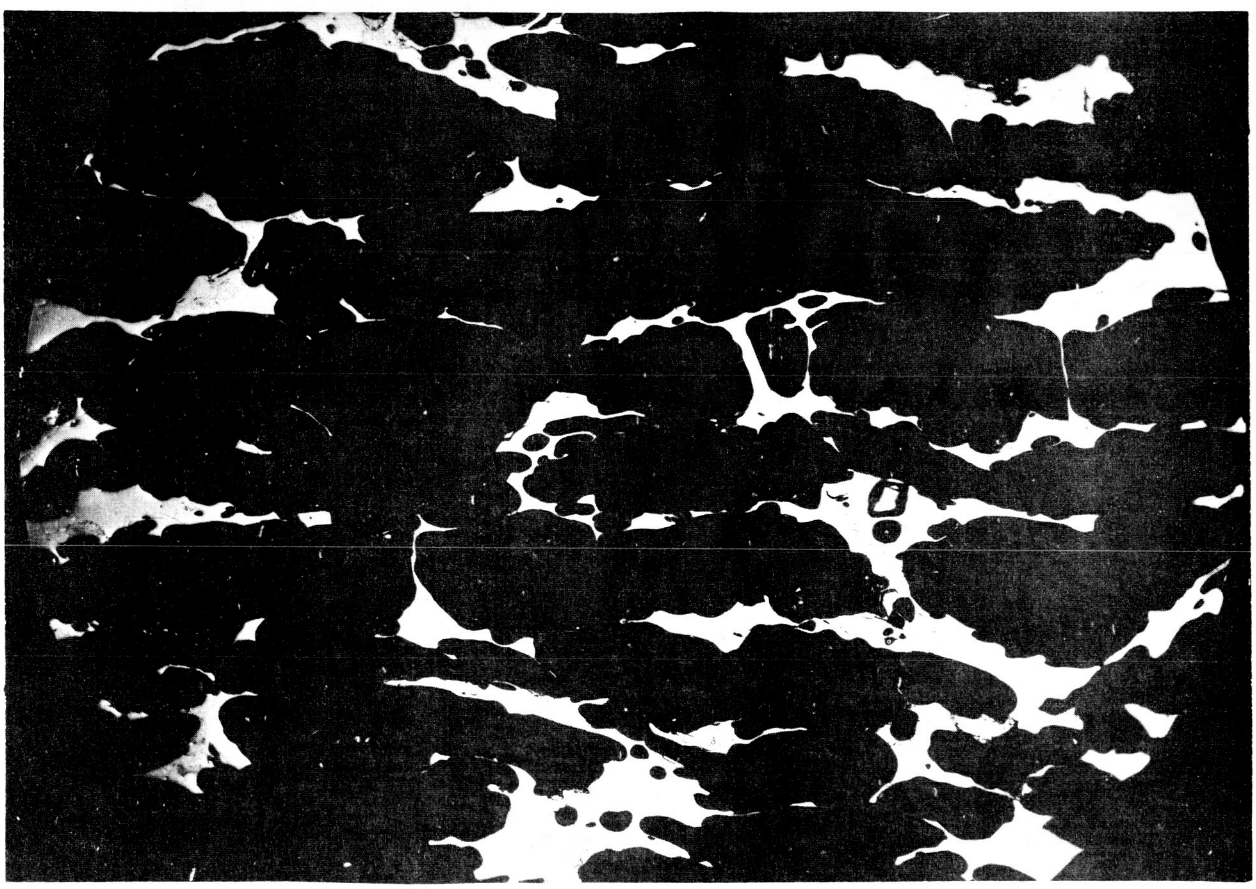

[illegible]

Figure I-[illegible] [illegible] [illegible]tory Char Sample 9-15-8-4

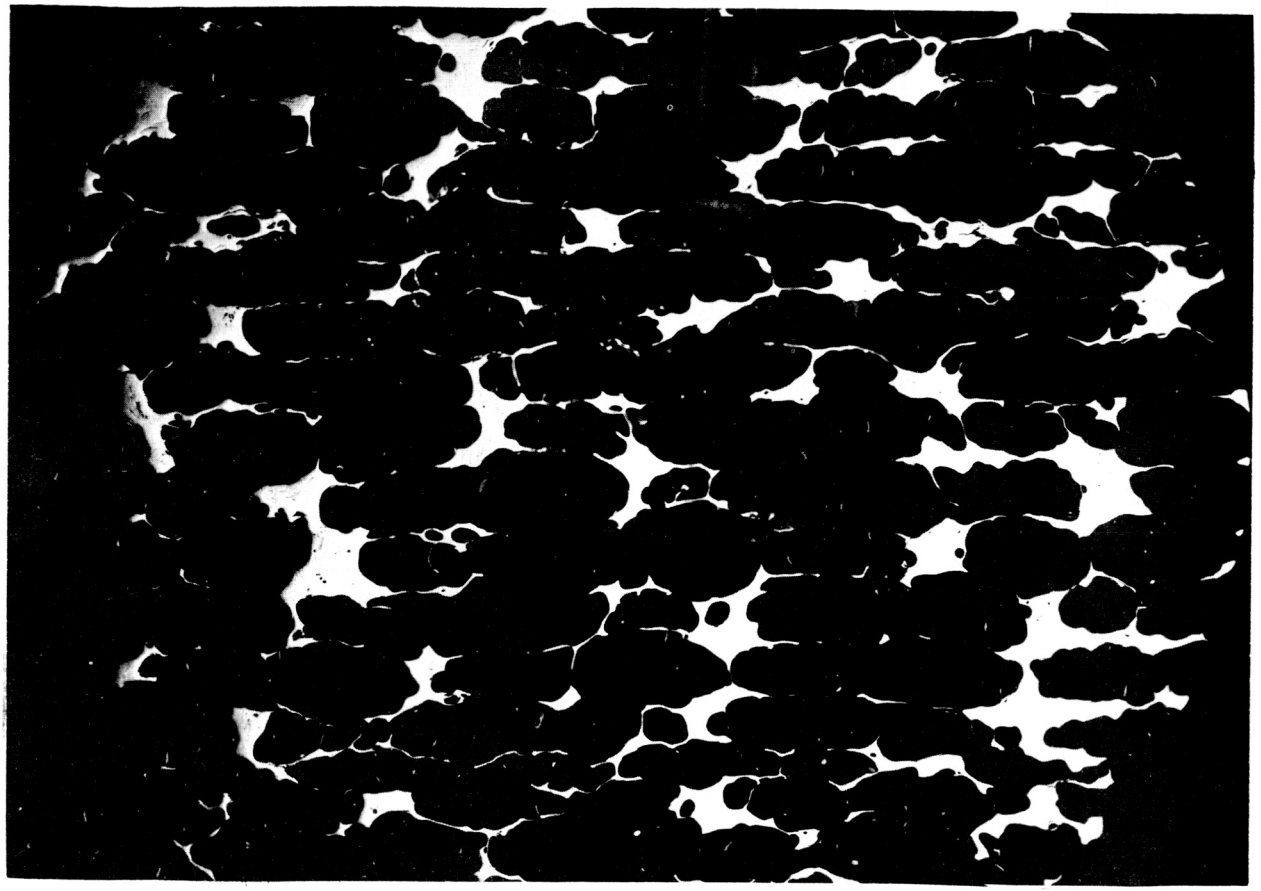

a. M-8471, 50X

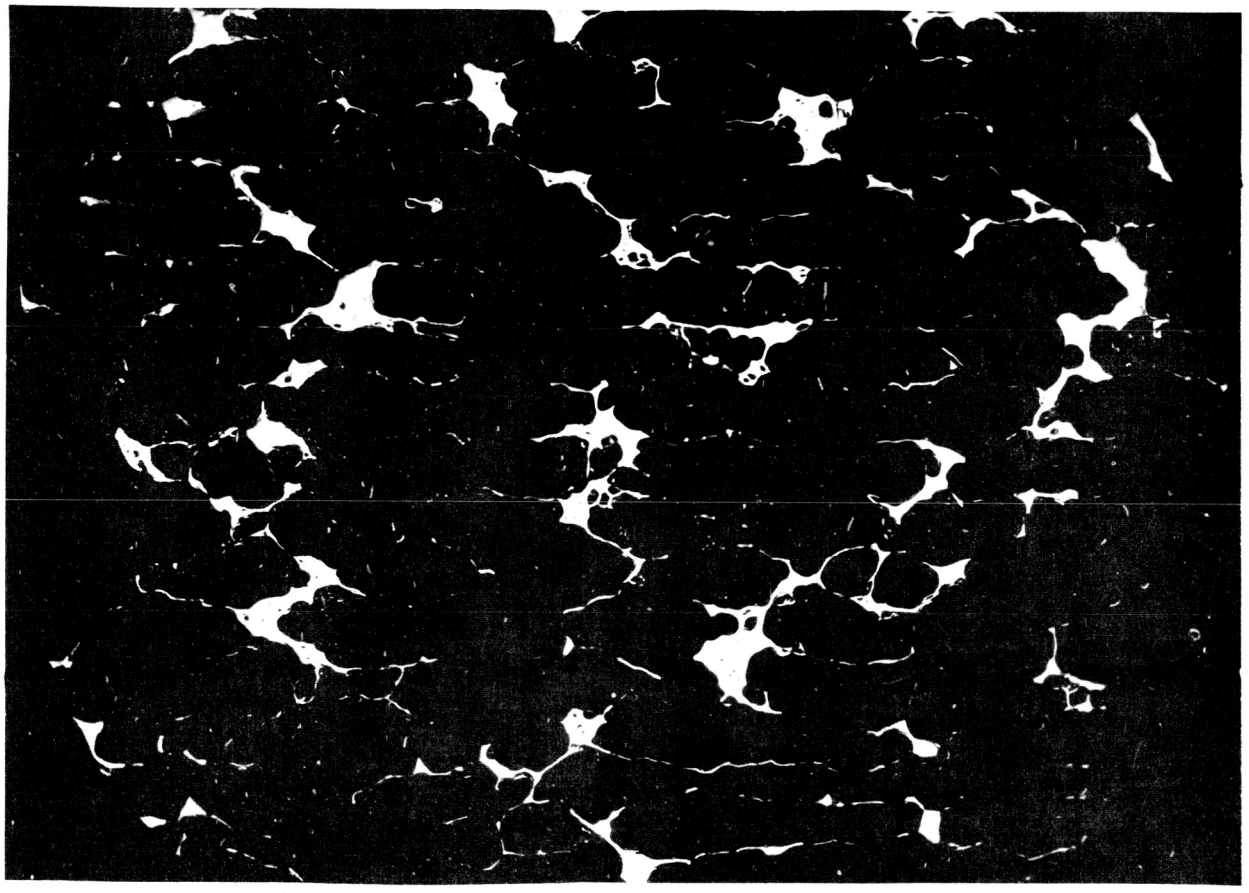

M-8472, 50X

Figure 1-3 1832°F [illegible] Quar Sample [illegible]

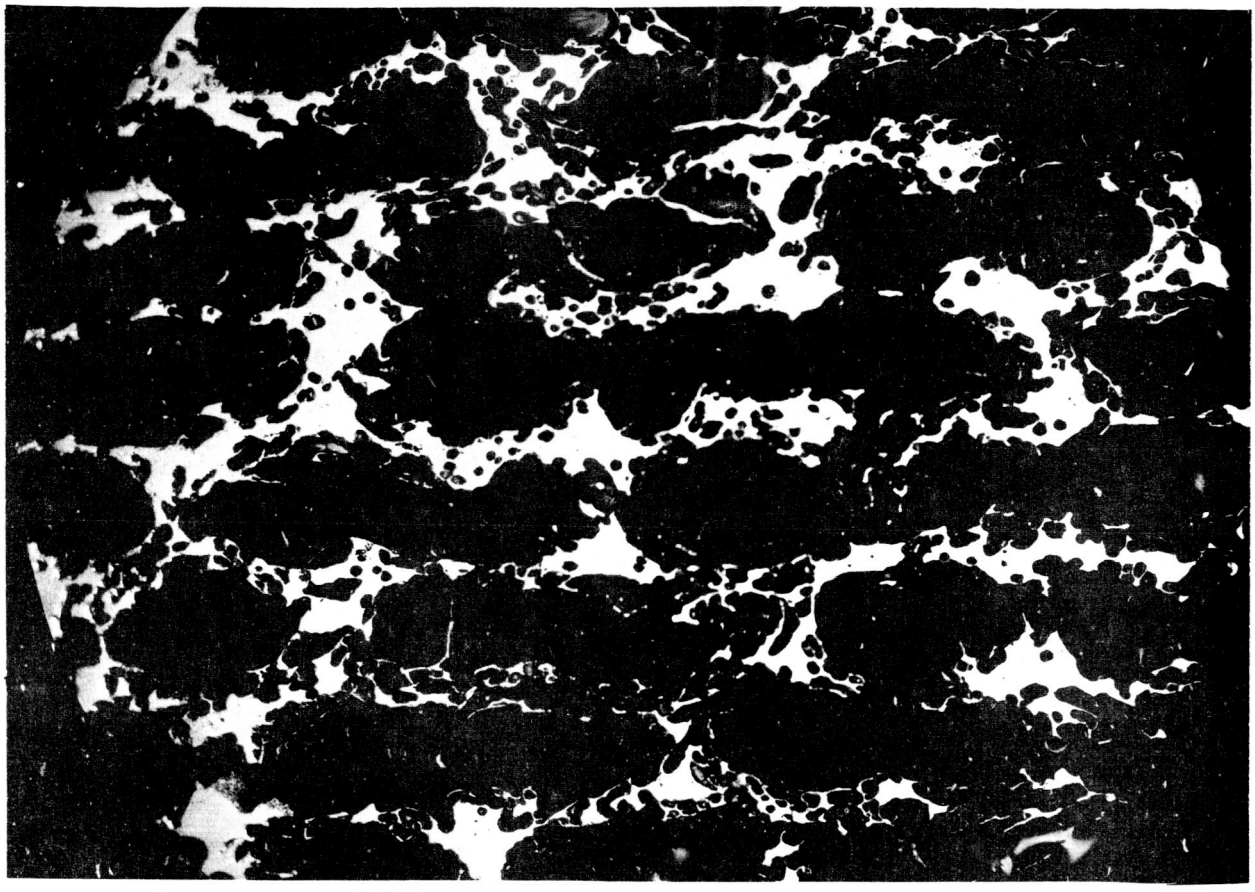

a. M-8473, 50X

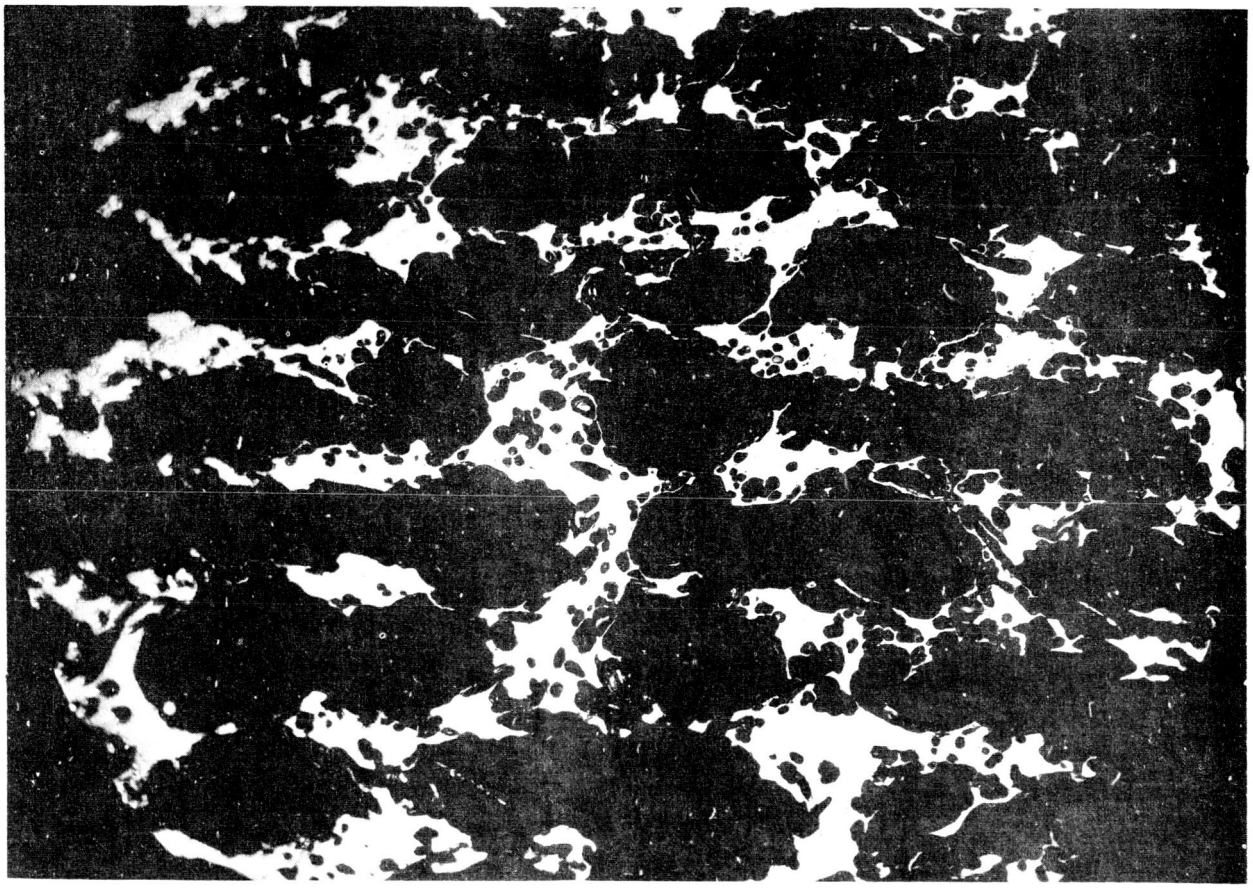

b. M-8474, 50X

Figure 7-4 1800°F Laboratory Char Sample 7-1-0-0-4

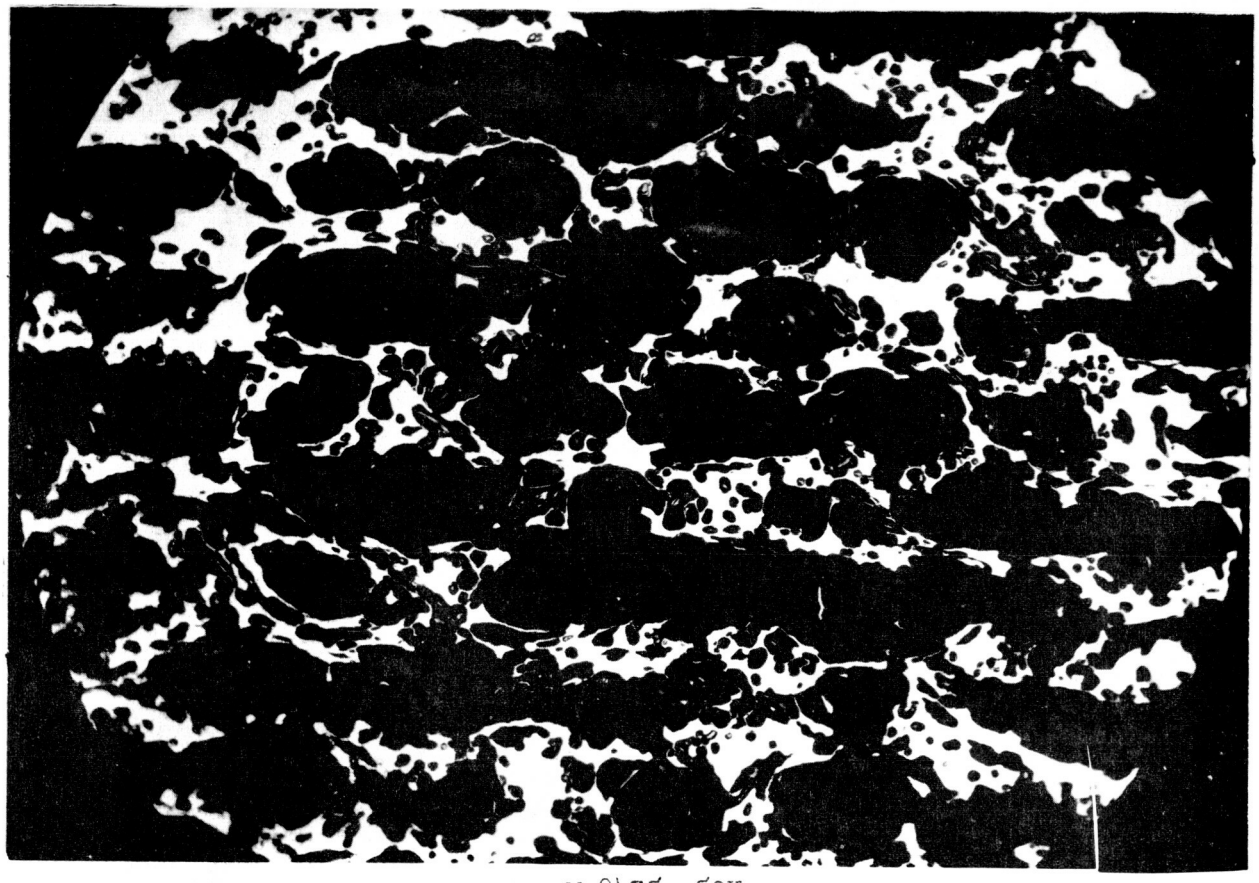

a. M-8475, 50X

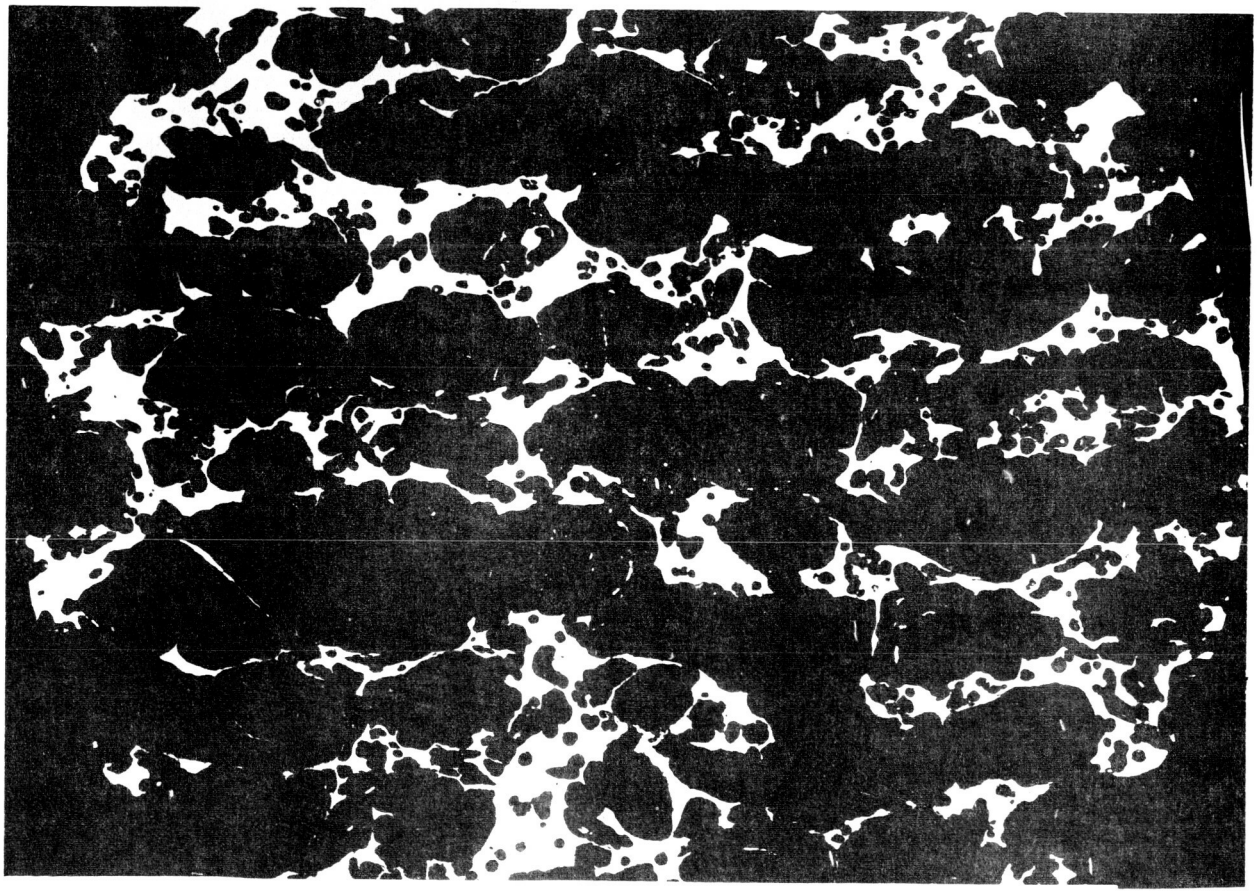

b. M-8476, 50X

Figure I-5 1832°F Laboratory Char Sample 9-15-E-4

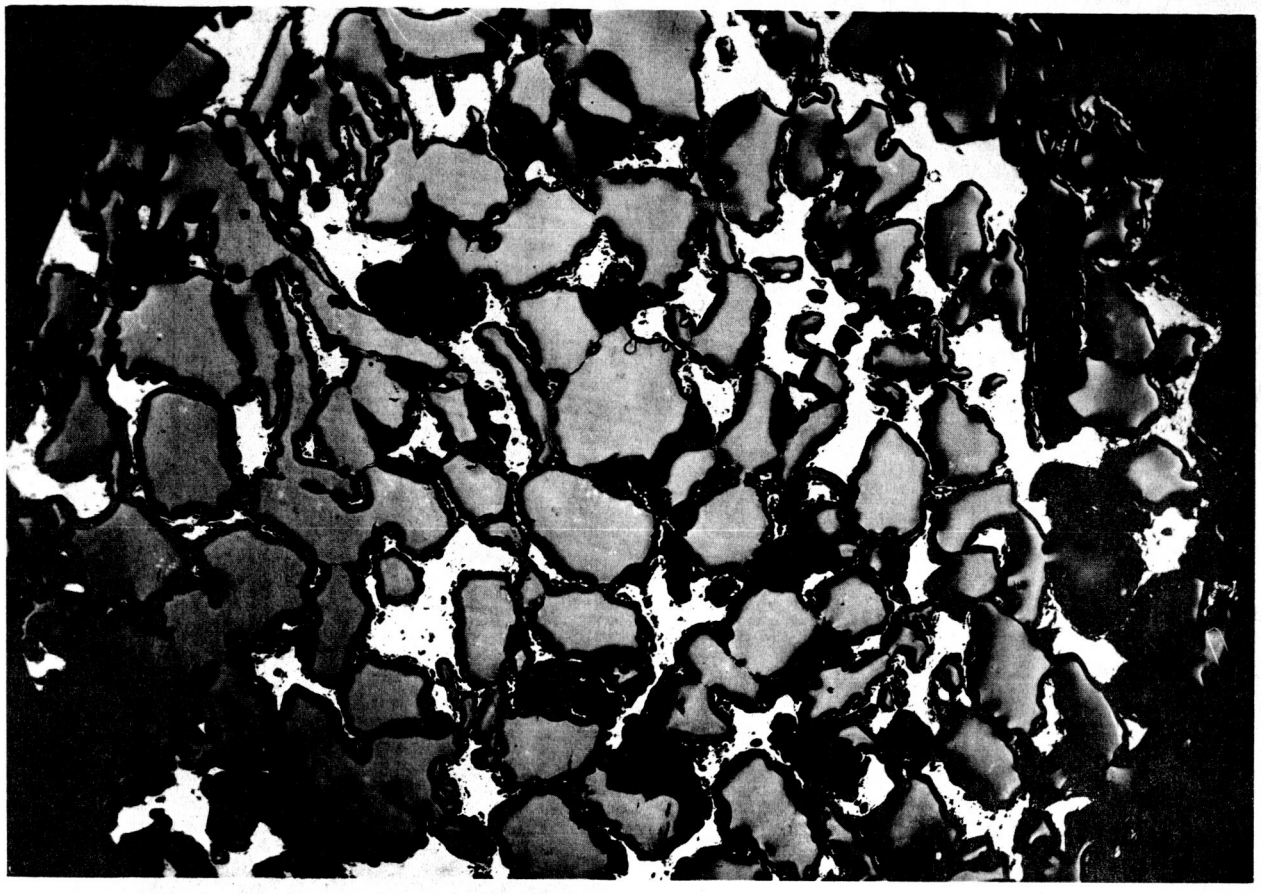

a. M-8843, 50X

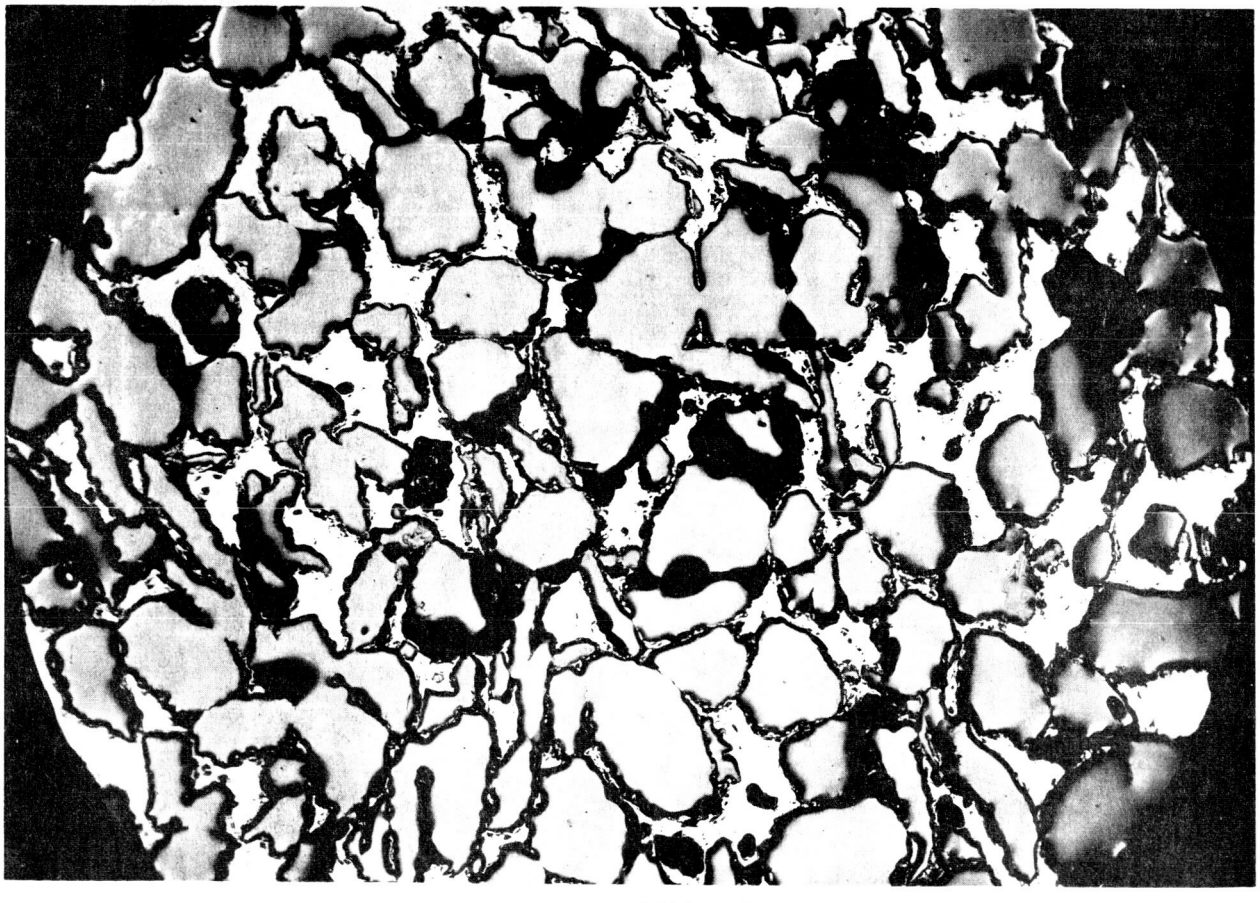

b. M-8844, 50X

Figure I-6 1832°F Laboratory Char Sample Z-1-10-8

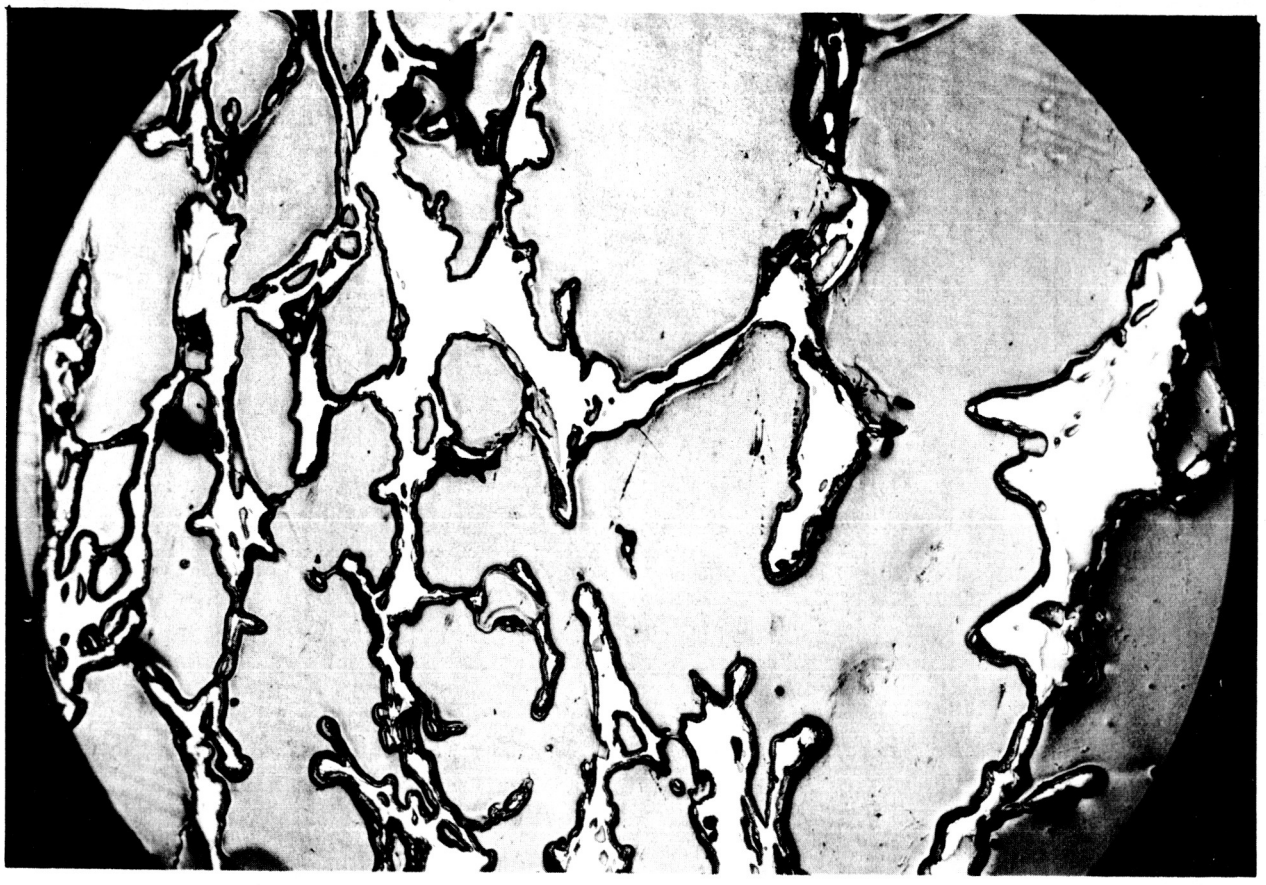

a. M-8663, 100X

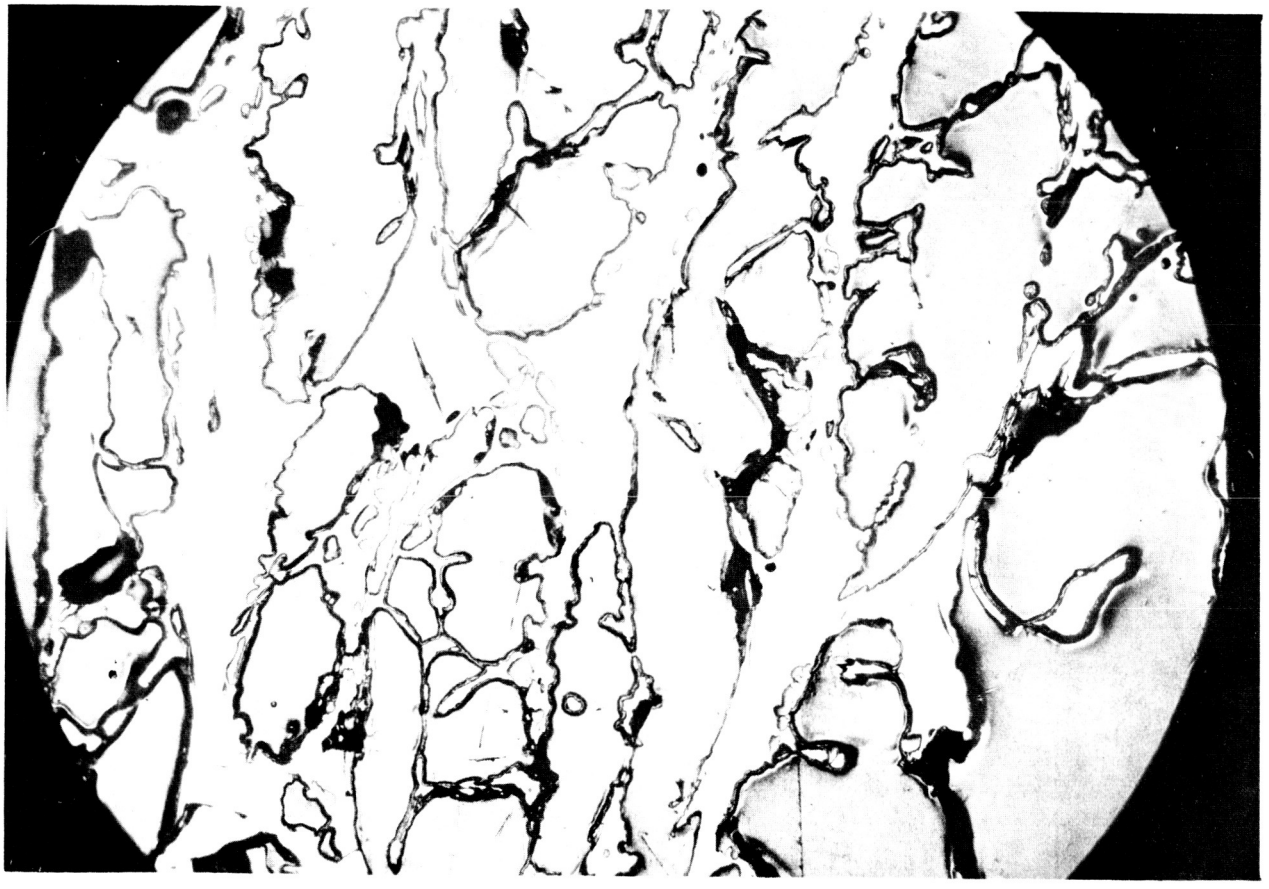

b. M-8664, 100X

Figure I-7 2200°F Rapid-Heat Char Sample 9-15A

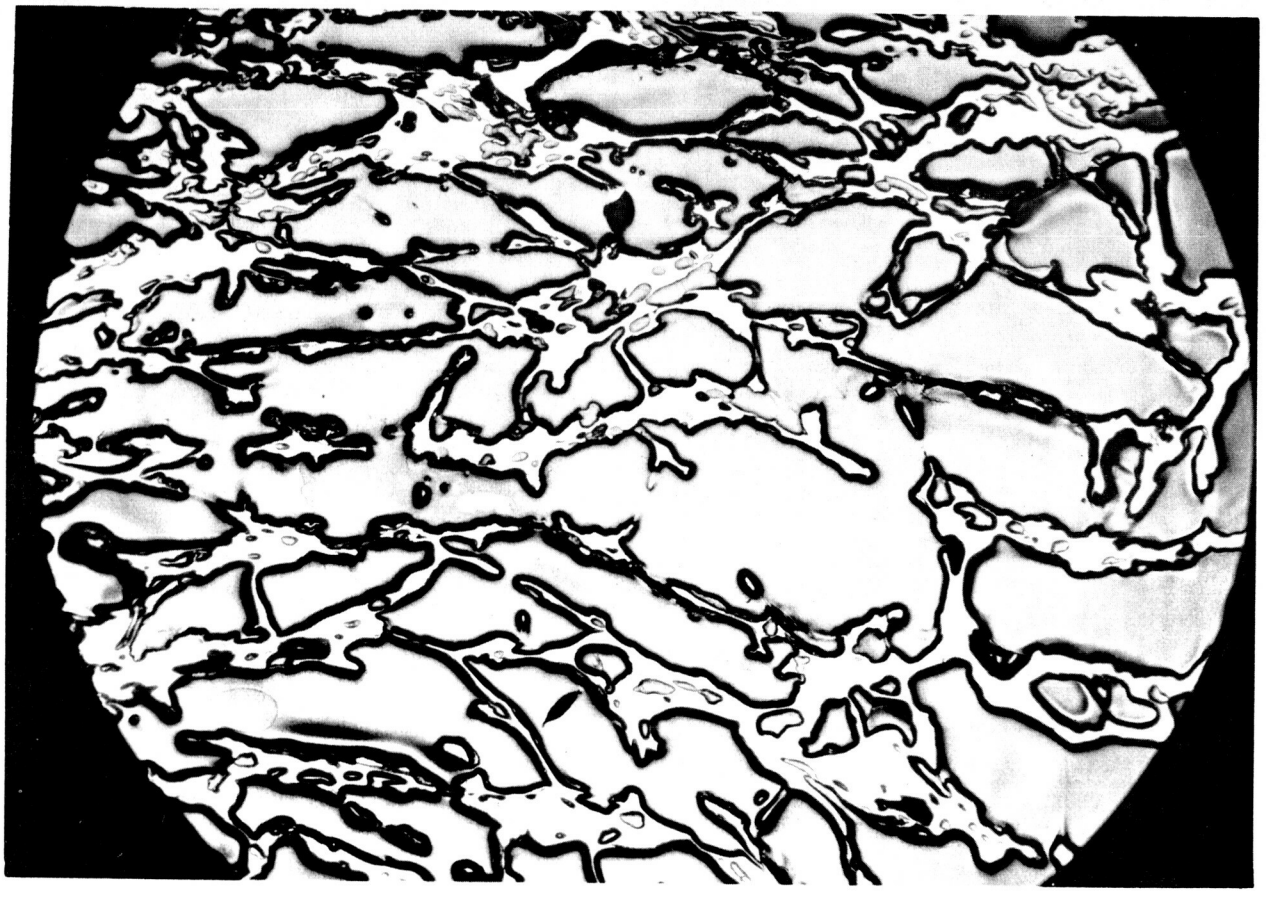

a. M-8666, 100X

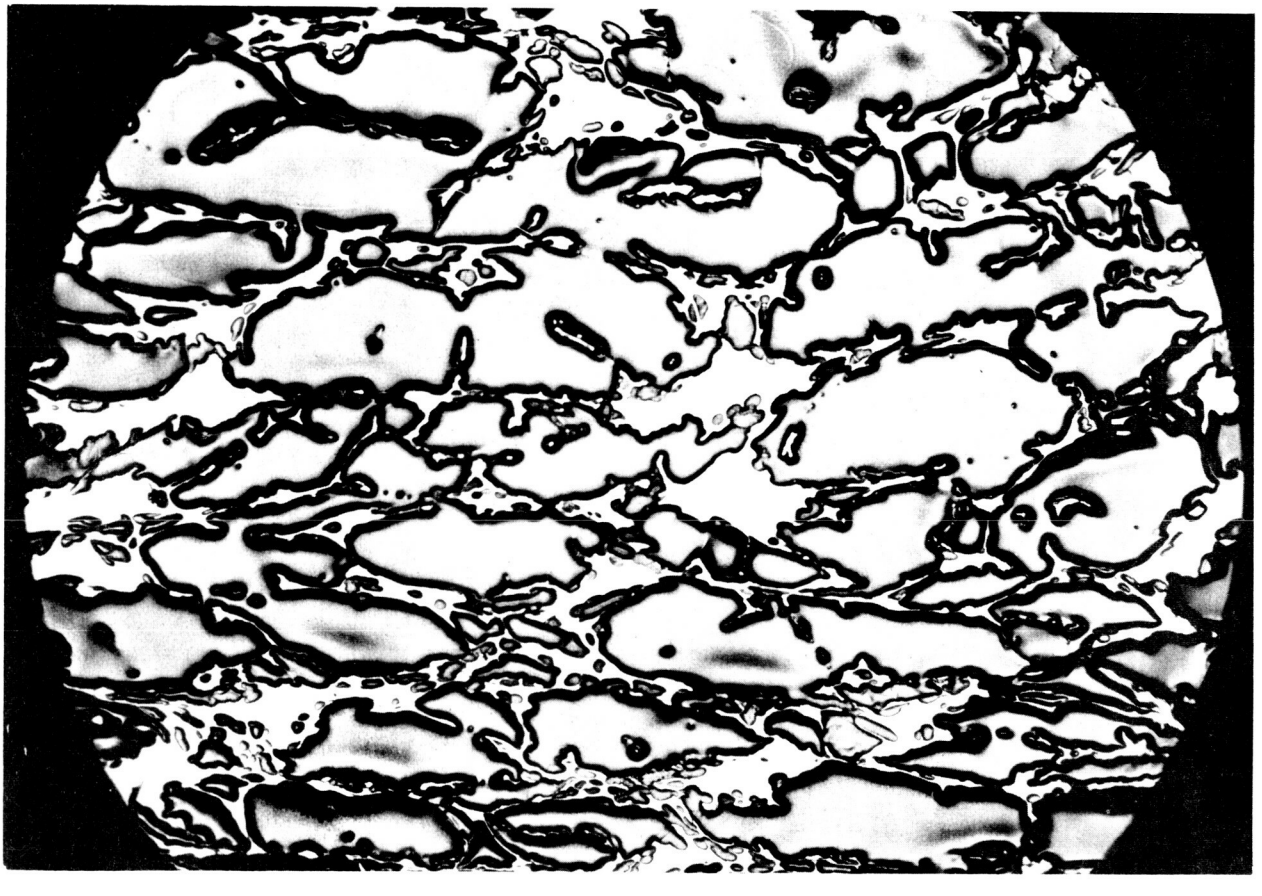

b. M-8667, 100X

Figure I-8 2200°F Rapid-Heat Char Sample 9-15B

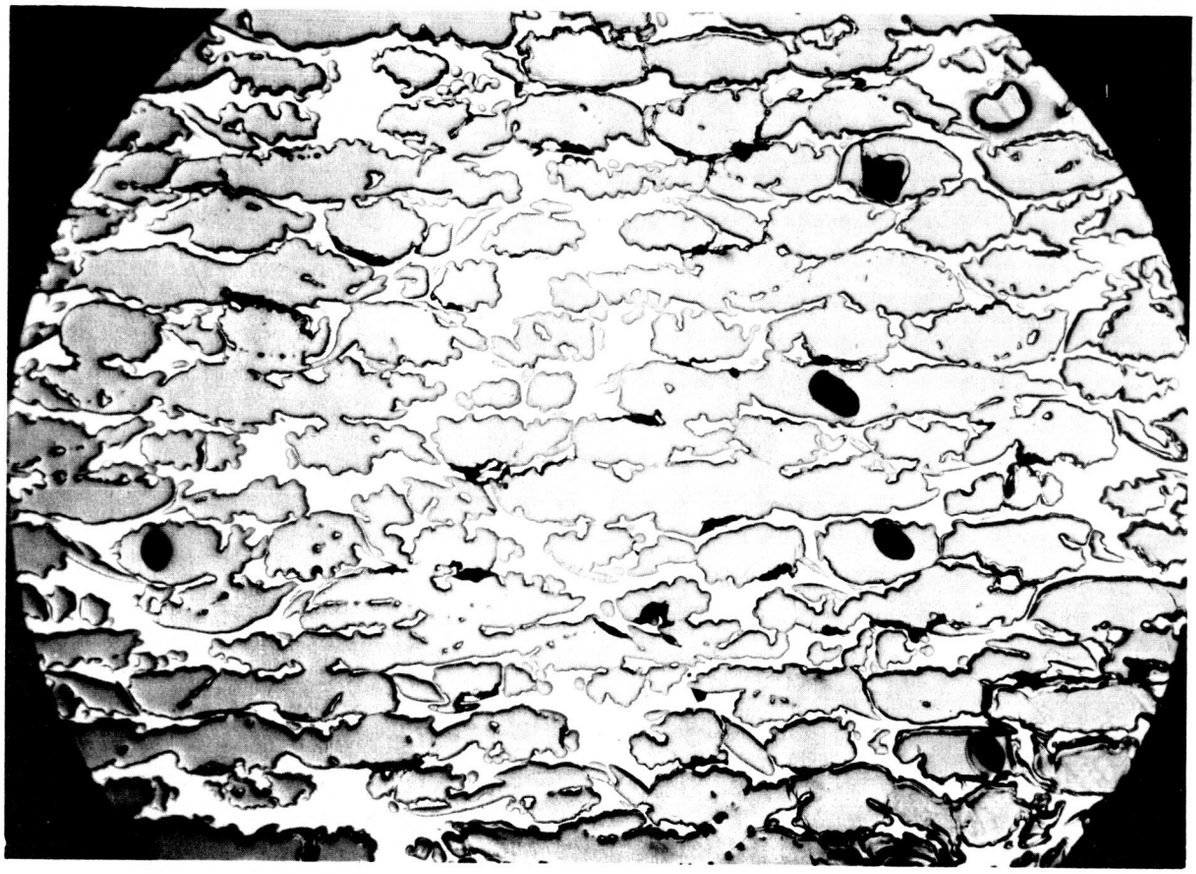

a. M-8668, 100X

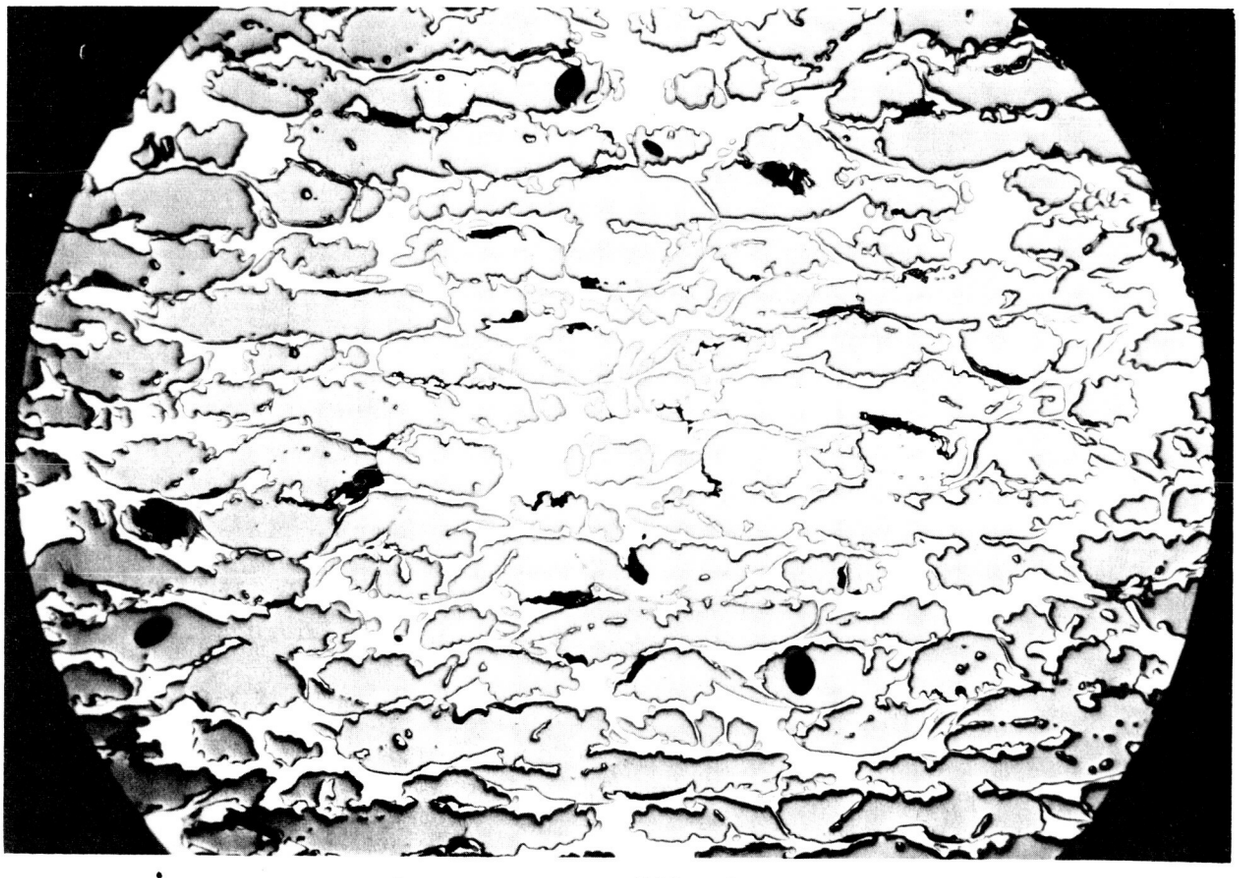

b. M-8669, 100X

Figure I-9 2200°F Rapid-Heat Char Sample 9-15C

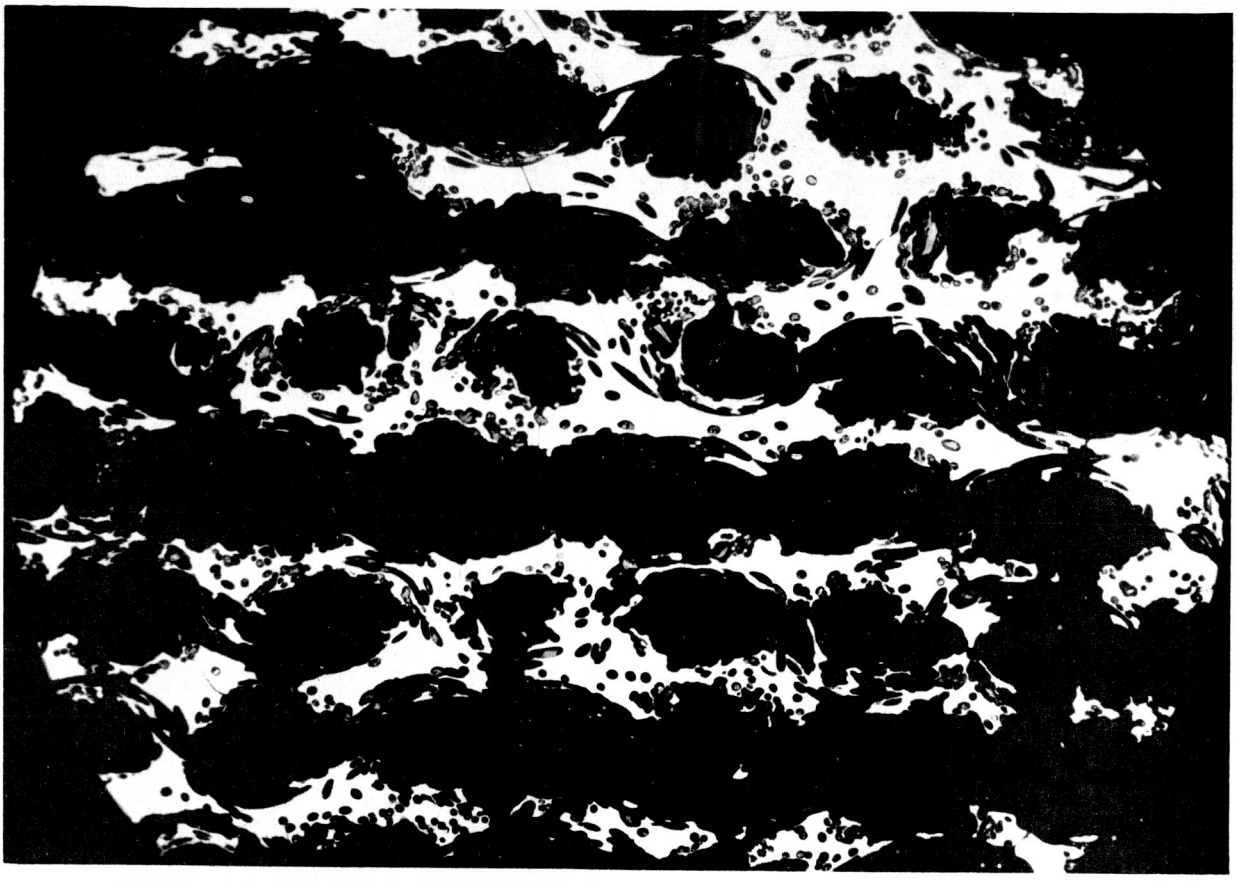

a. M-8670, 100X

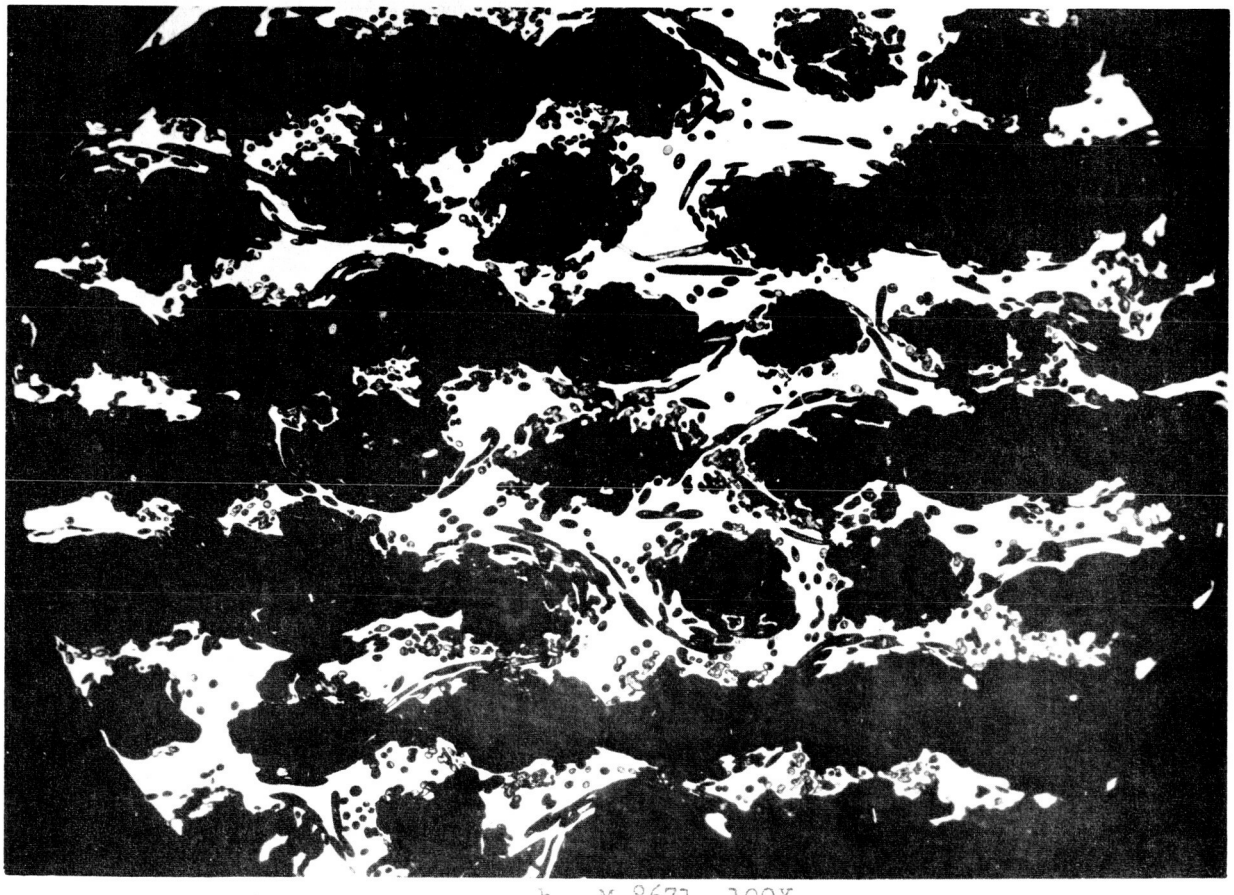

b. M-8671, 100X

Figure I-10 2200°F Rapid-Heat Char Sample 9-15D

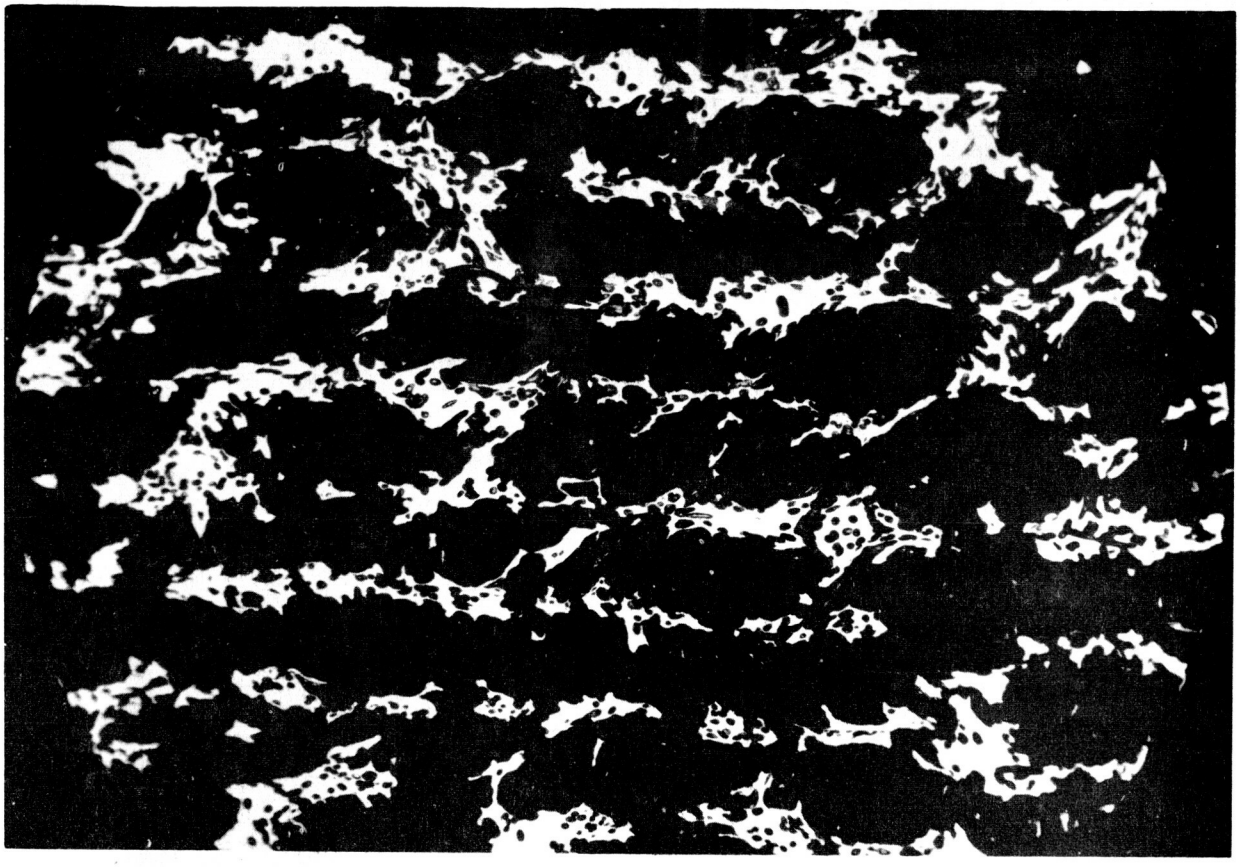

a. M-8672, 100X

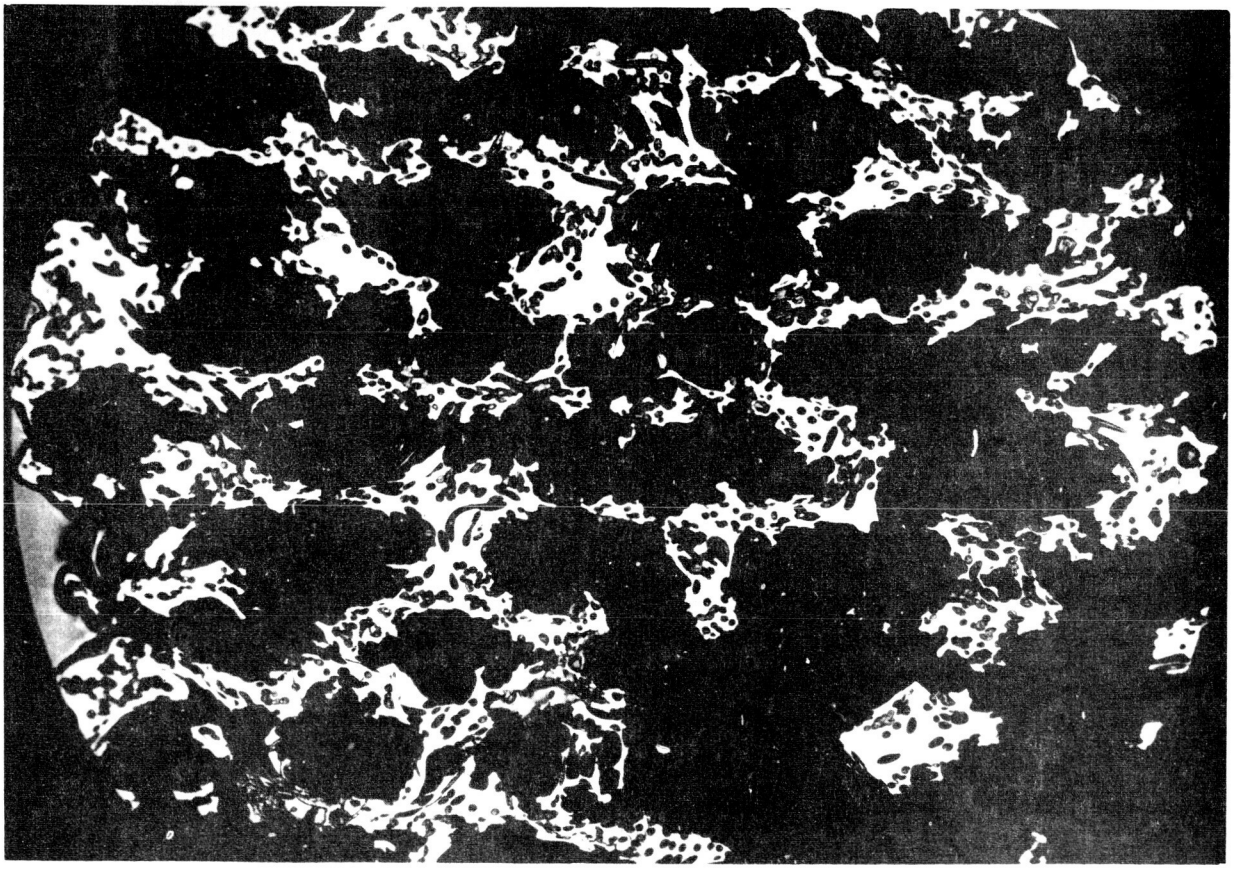

b. M-8673, 100X

Figure I-11 2200°F Rapid-Heat Char Sample 9-15E

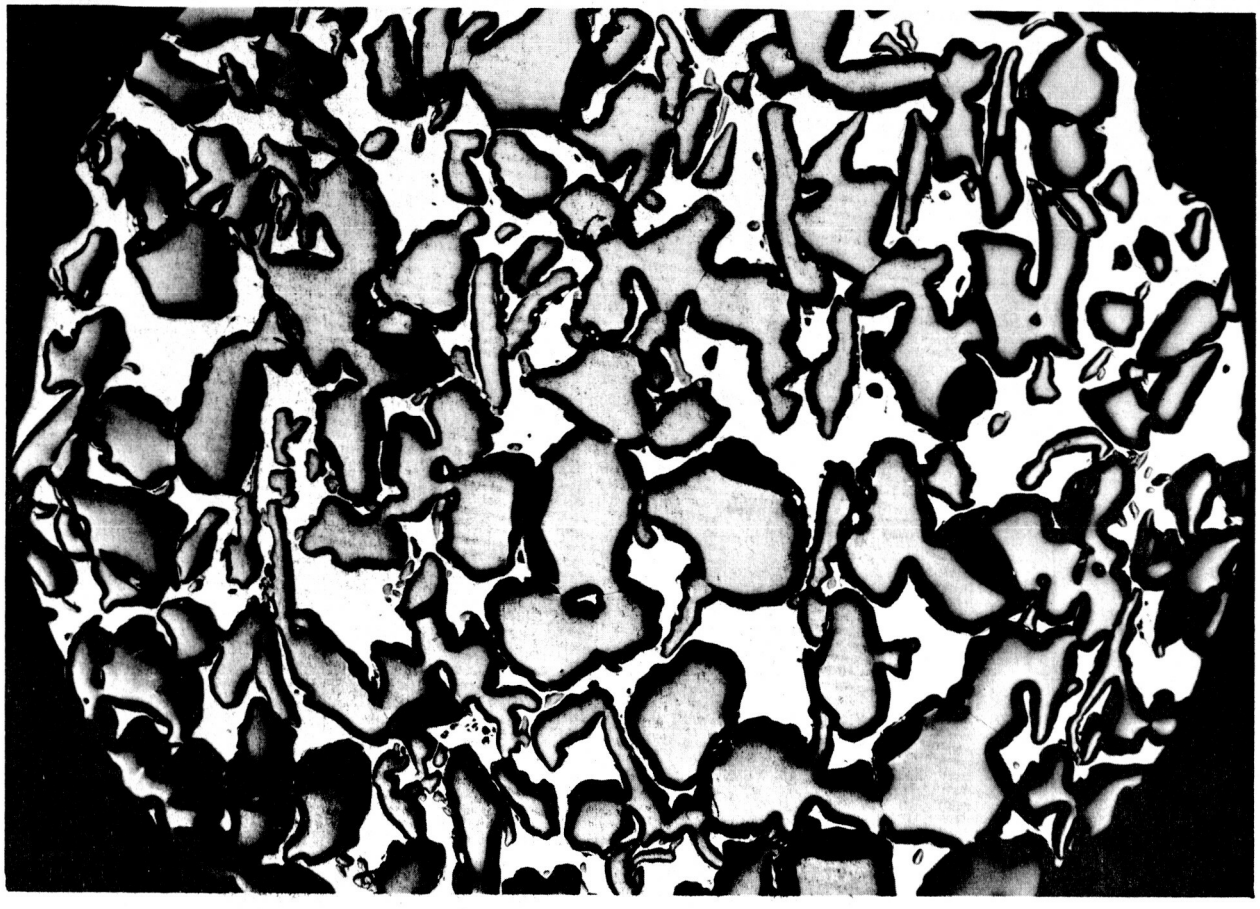

a. M-8845, 50X

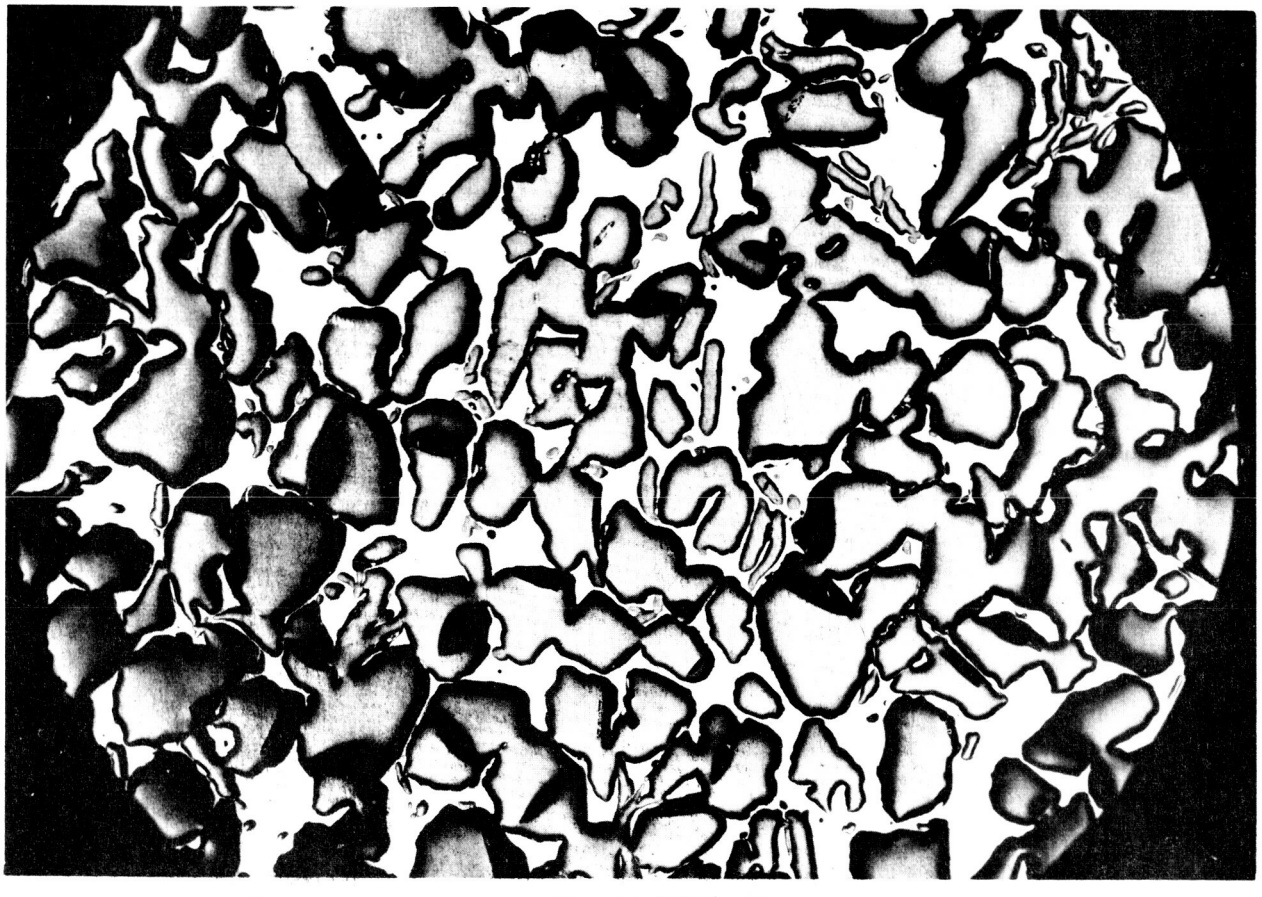

b. M-8846, 50X

Figure I-12 2200°F Rapid-Heat Char Sample Zytel SN/1

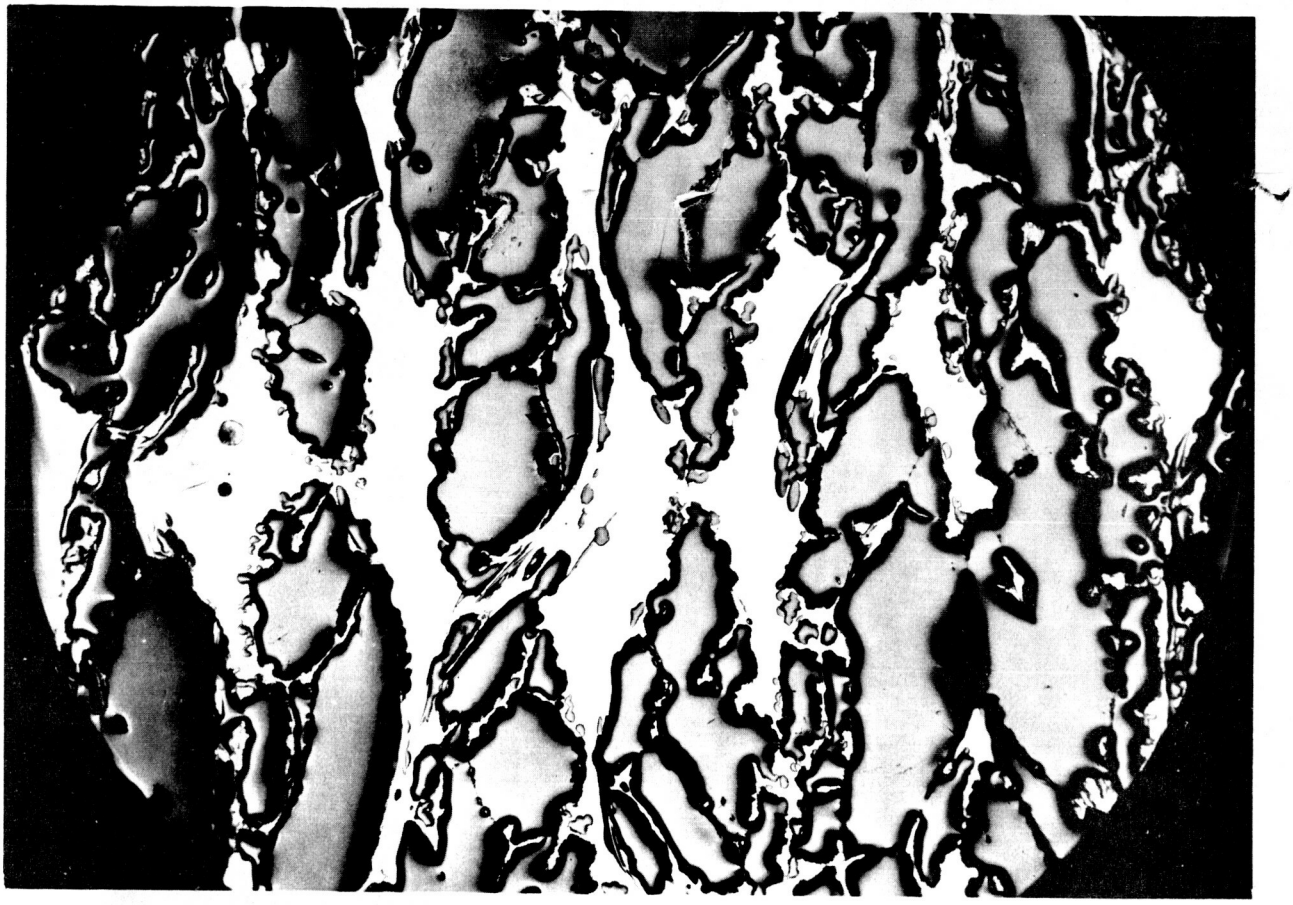

a. M-8841, 50X

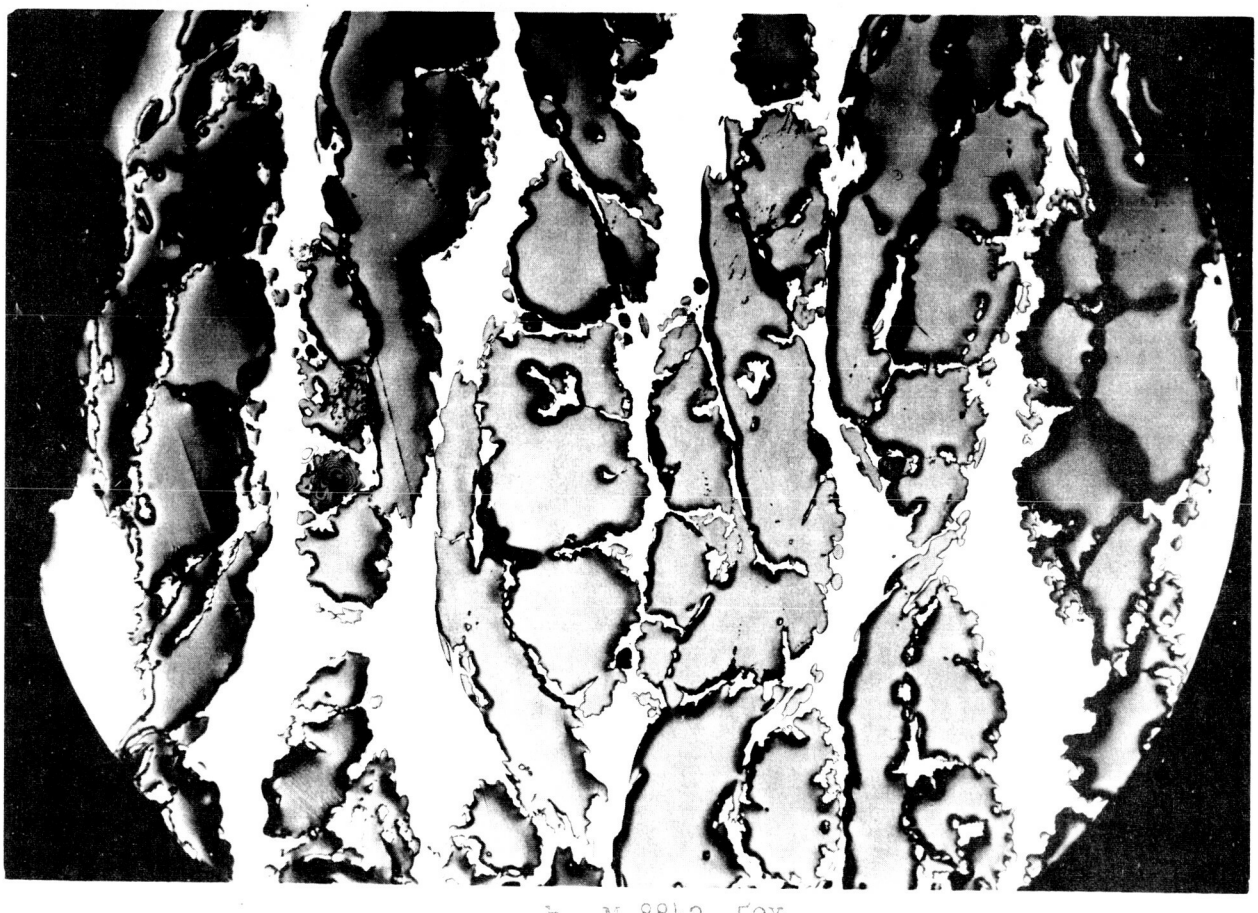

b. M-8842, 50X

Figure I-13 2900°F Rapid-Heat Char Sample 9-15A-3-16

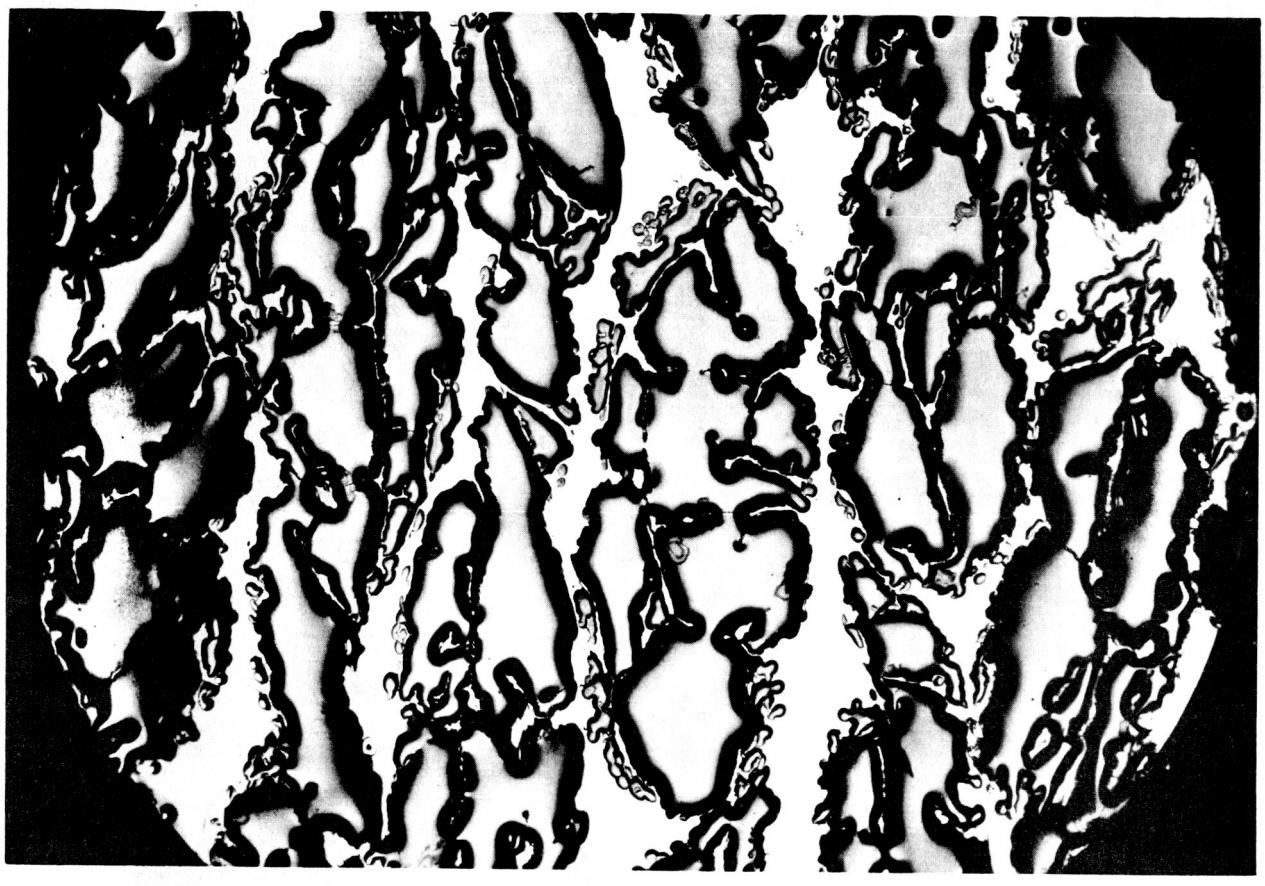

a. M-8831, 50X

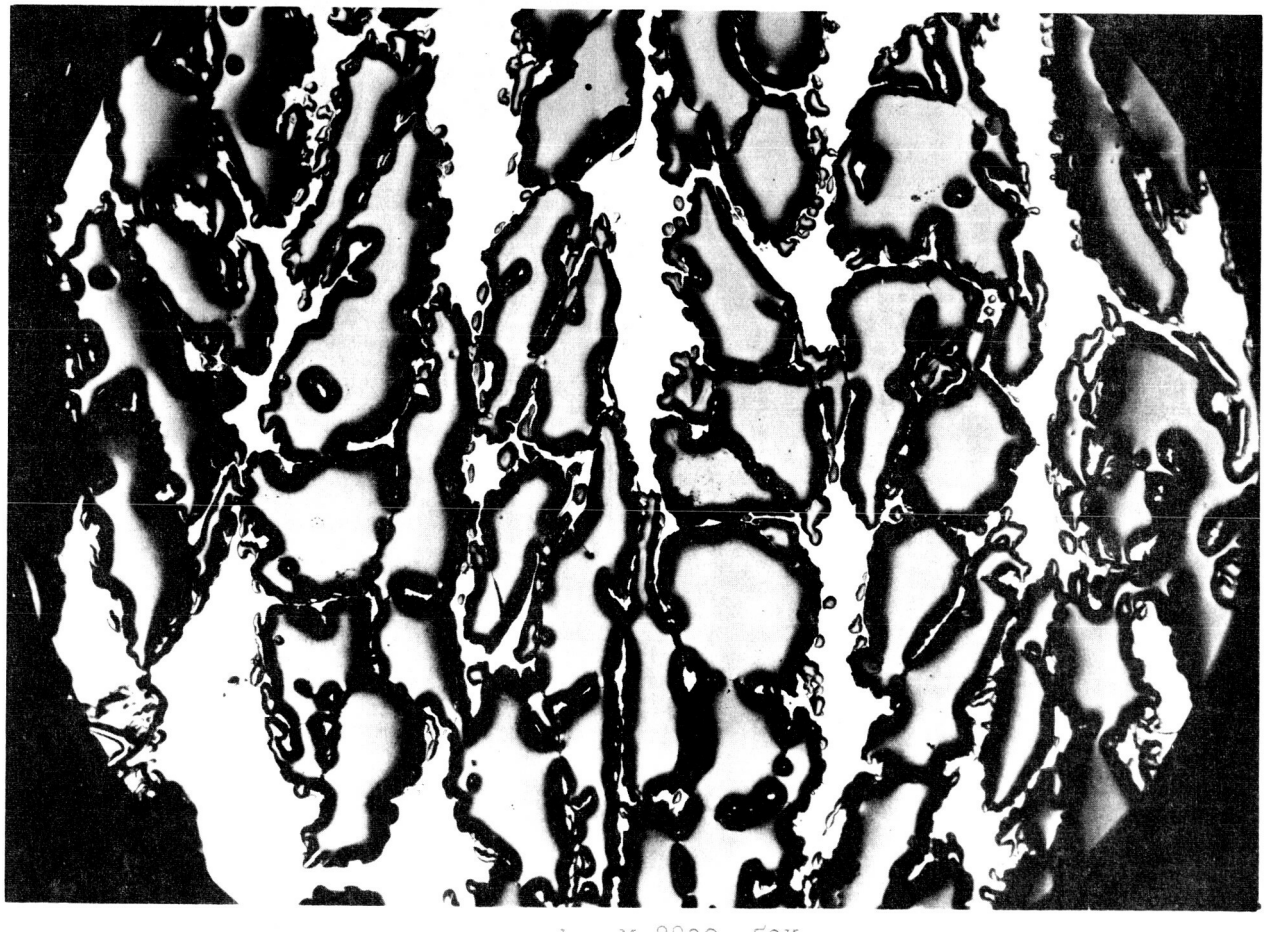

b. M-8832, 50X

Figure I-14 2900°F Rapid-Heat Char Sample 9-15-B-6-16

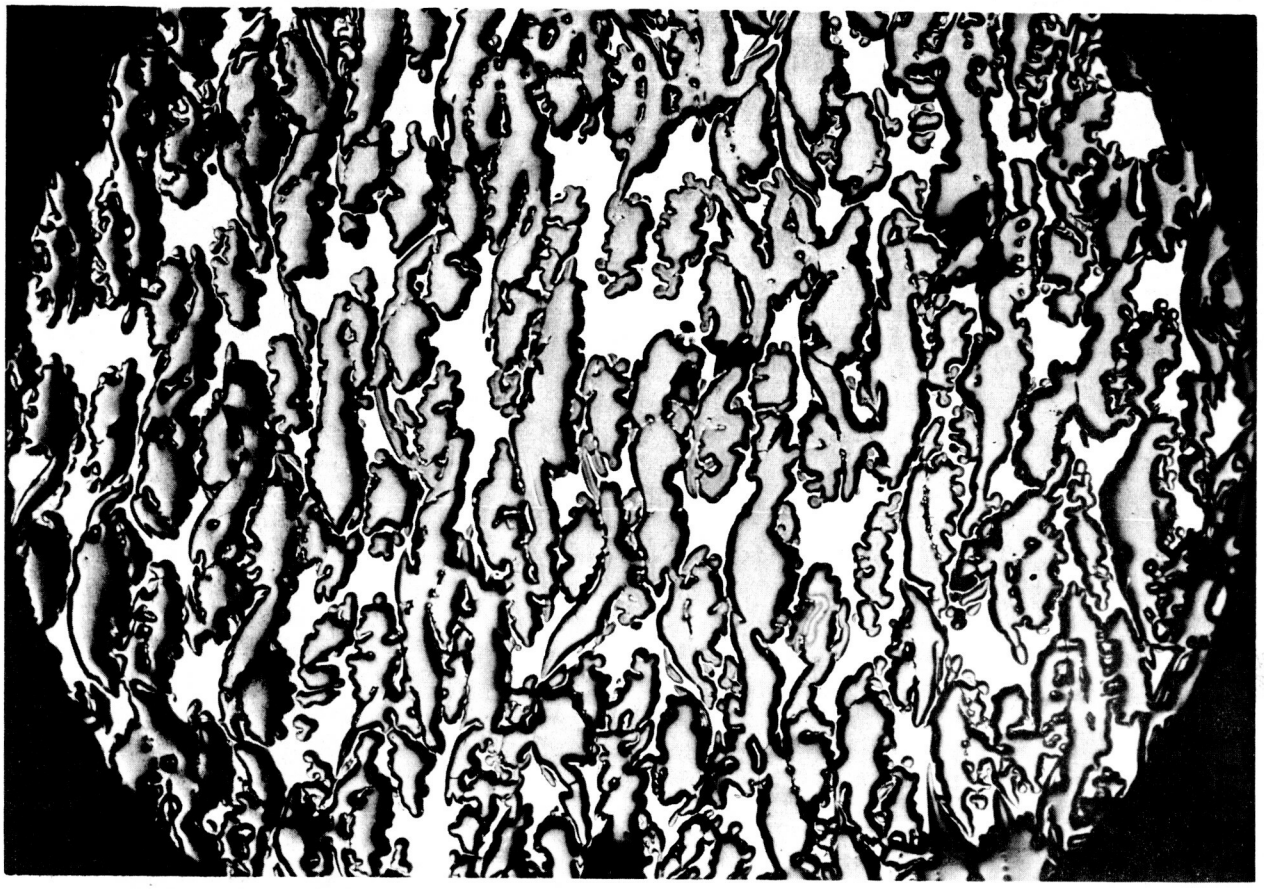

a. M-8833, 50X

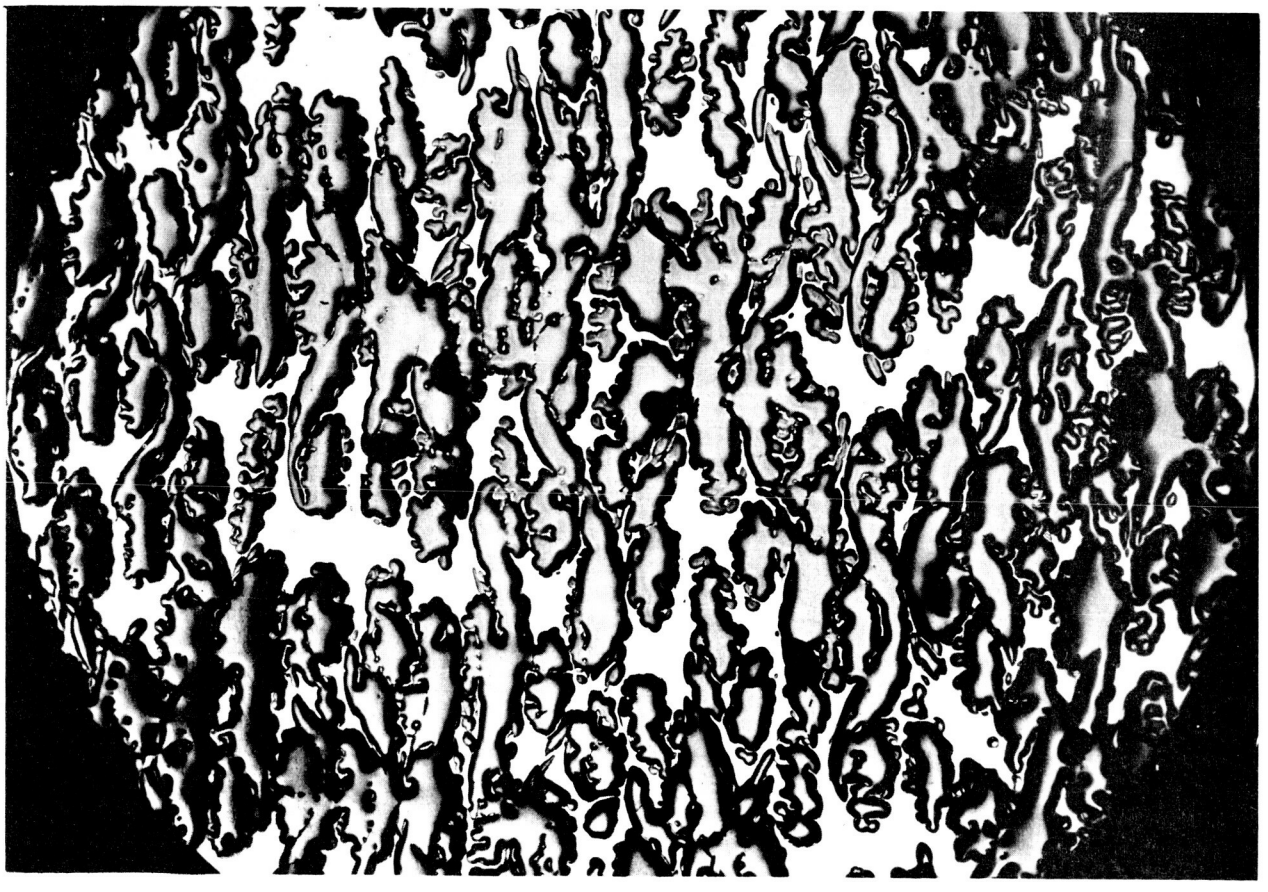

b. M-8834, 50X

Figure I-15 2900°F Rapid-Heat Char Sample 9-15-C-4-16

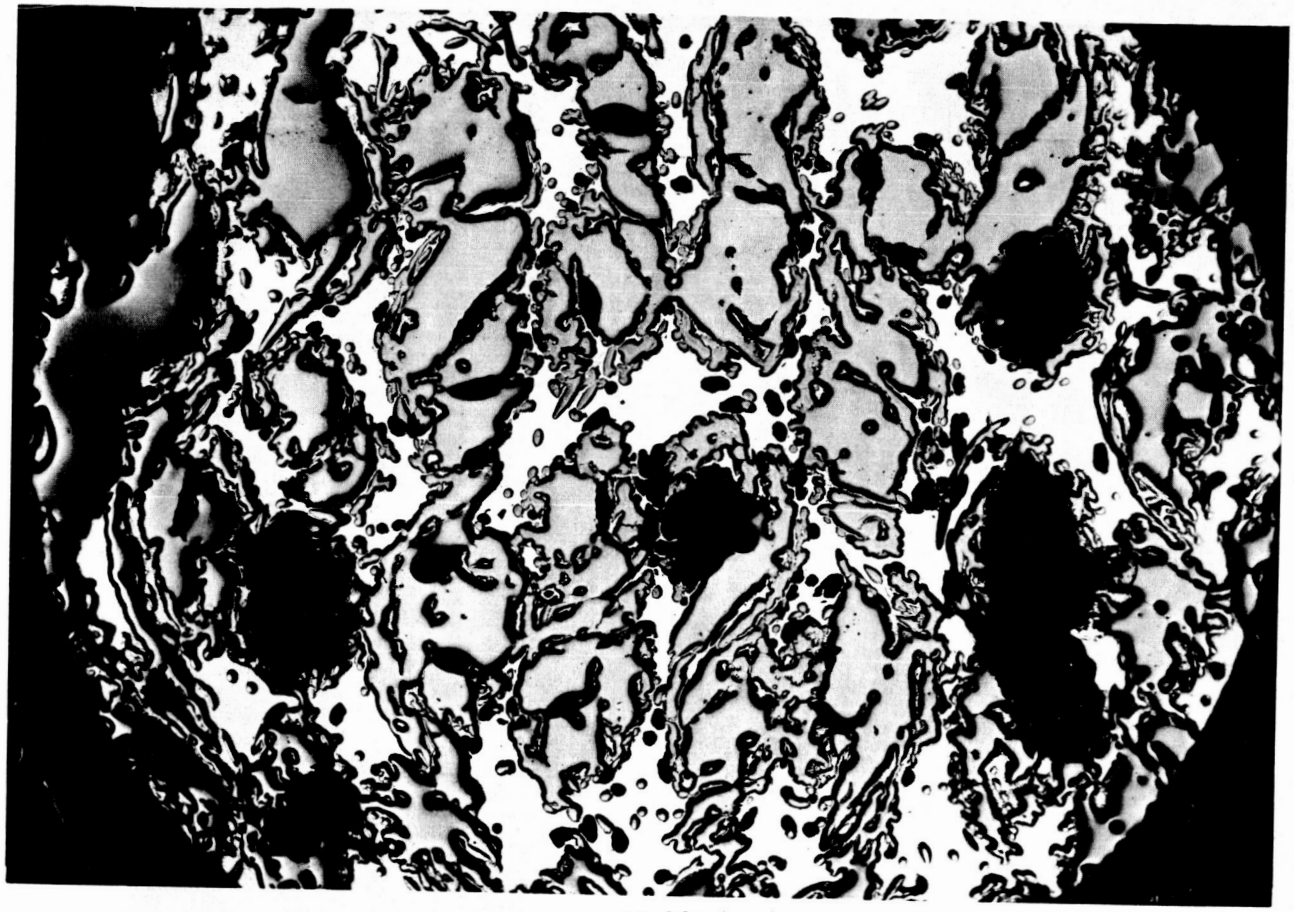

a. M-8835, 50X

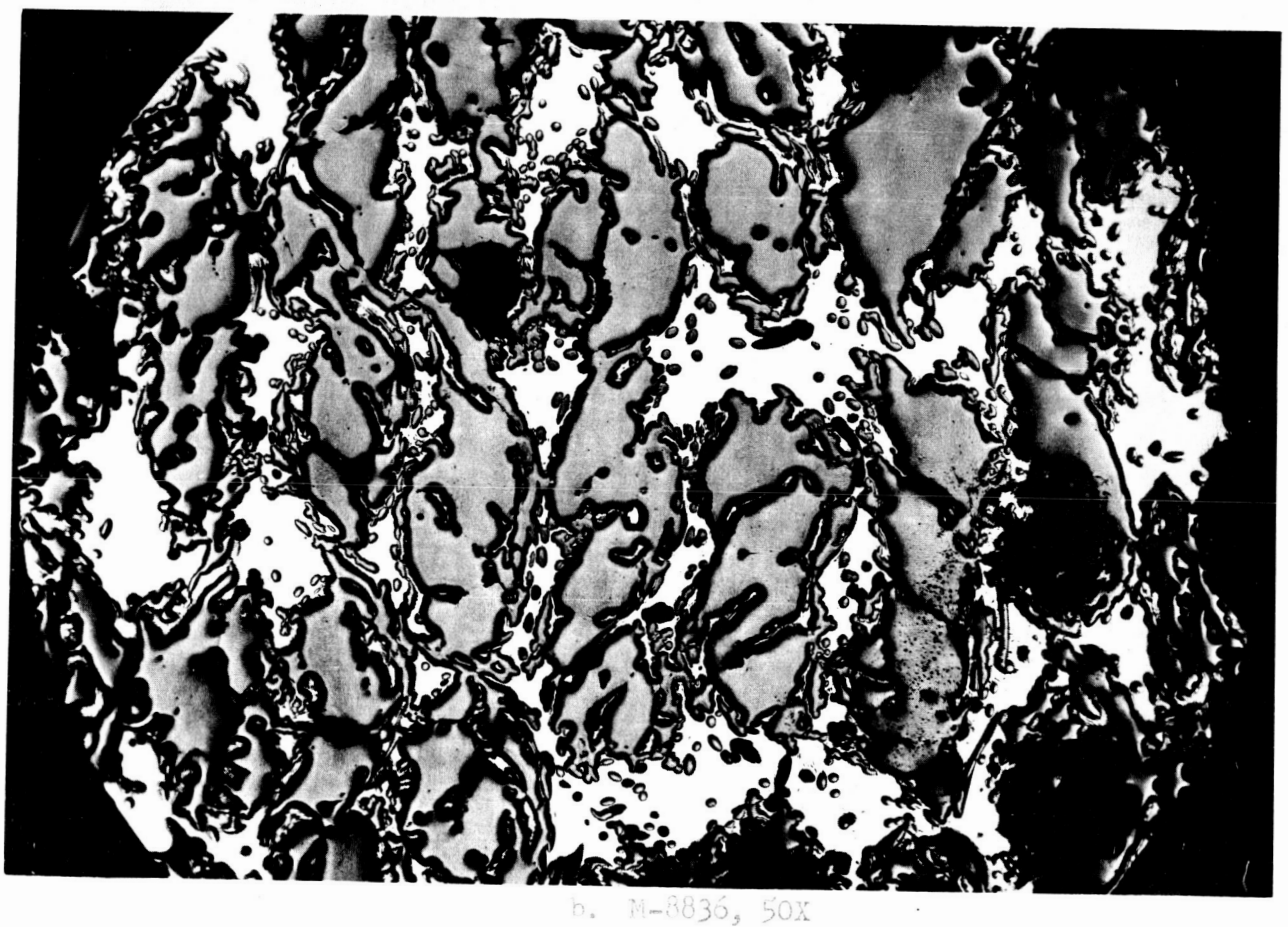

b. M-8836, 50X

Figure I-16 2900°F Rapid-Heat Char Sample 9-15-D-9-16

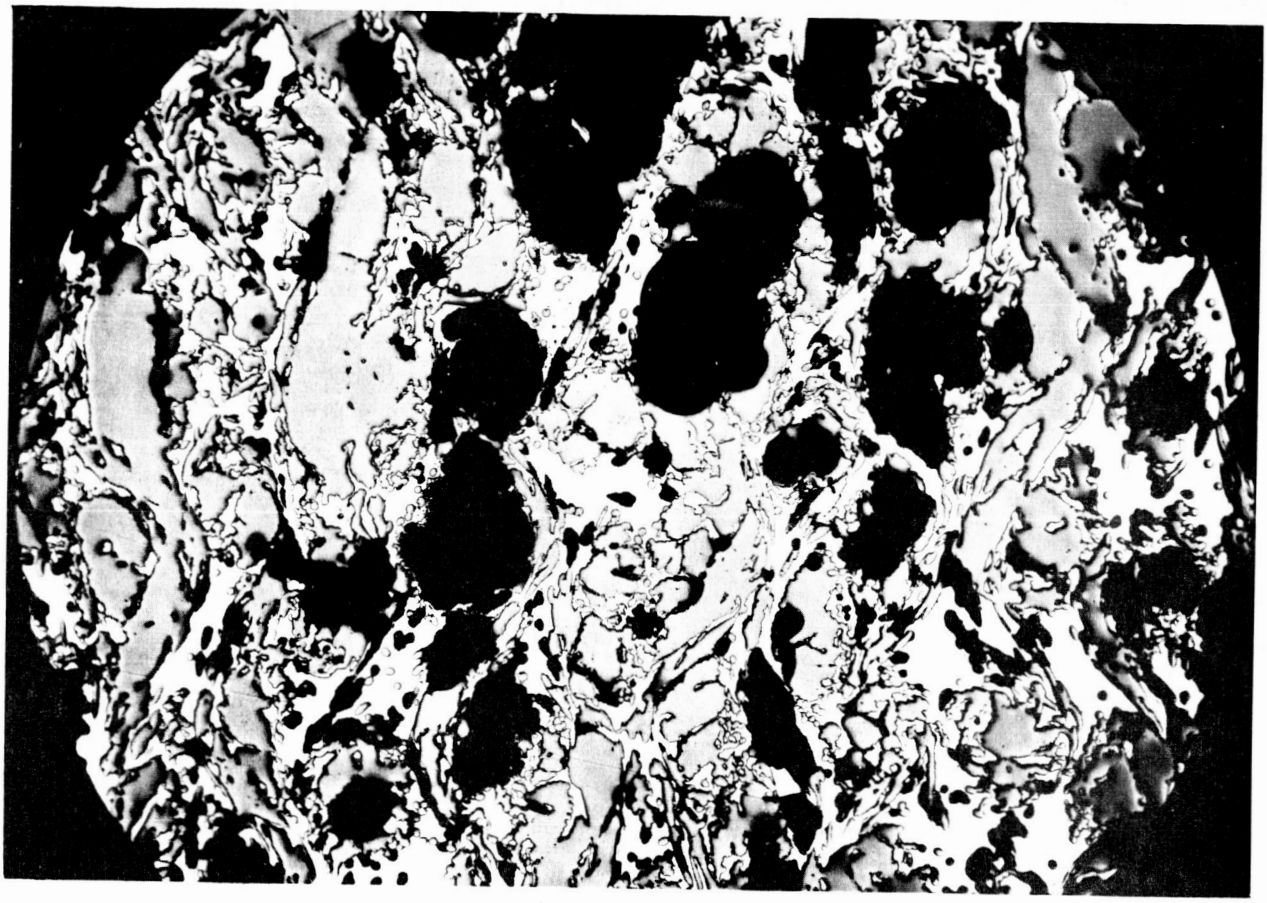

a. M-8837, 50X

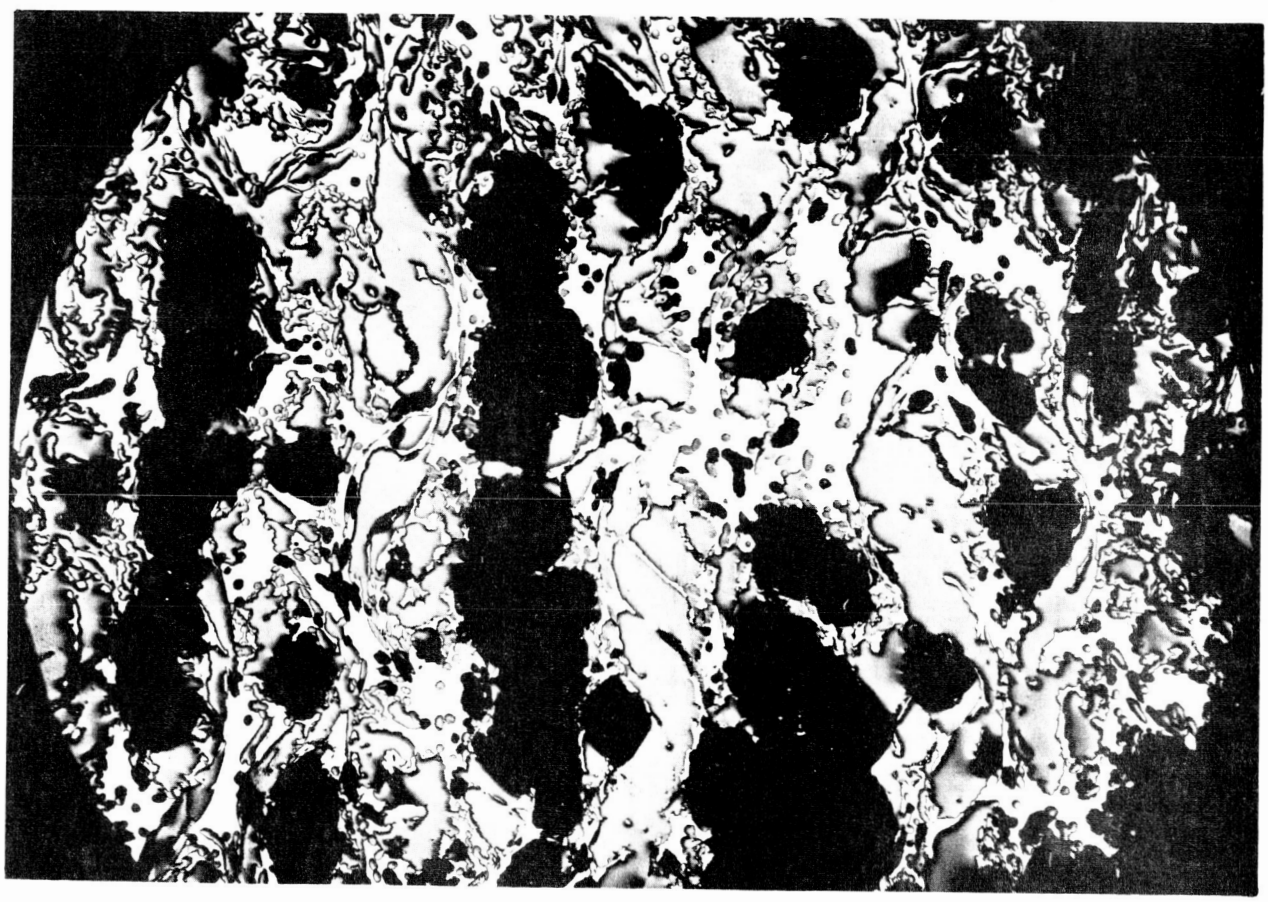

b. M-8838, 50X

Figure I-17 2900°F Rapid-Heat Char Sample 9-15-E-6-16

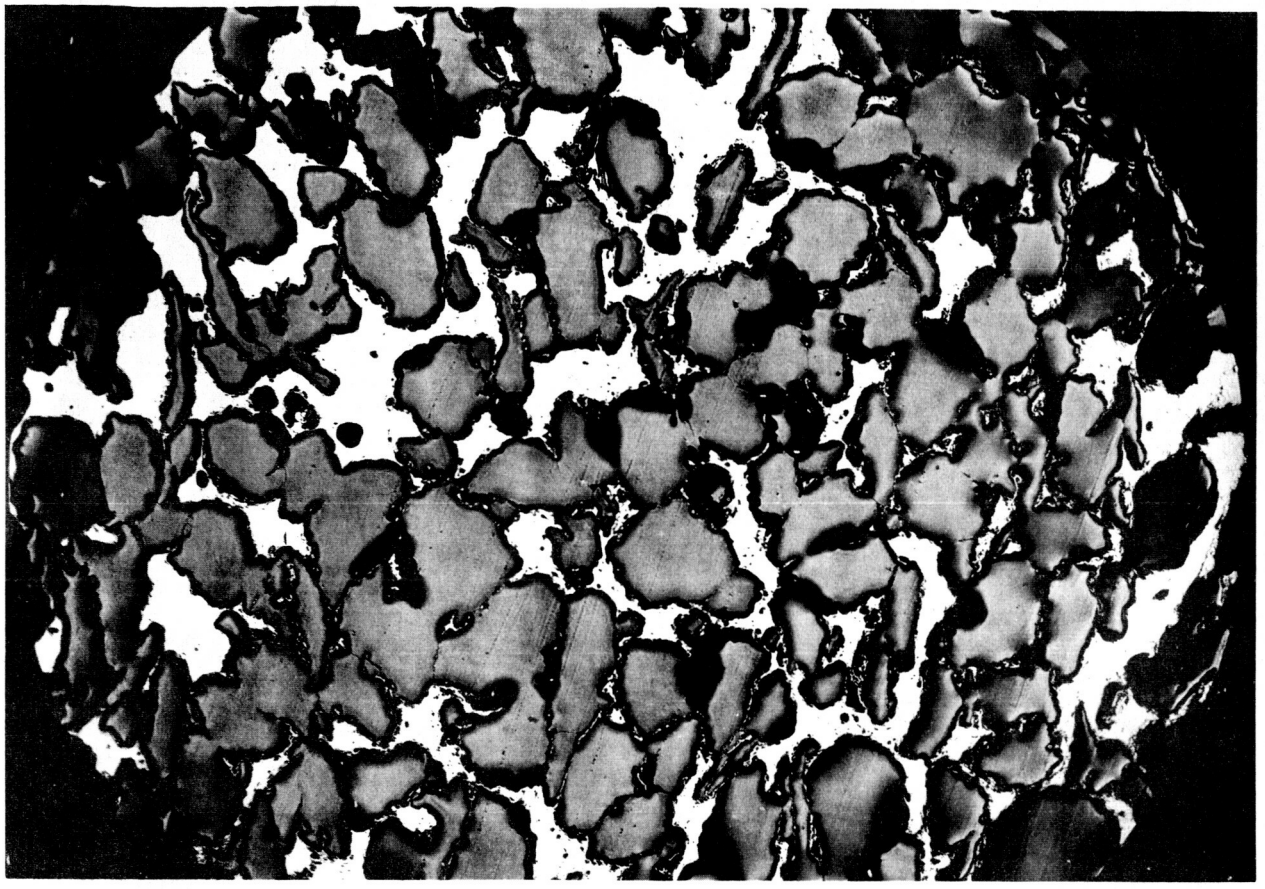

a. M-8839, 50X

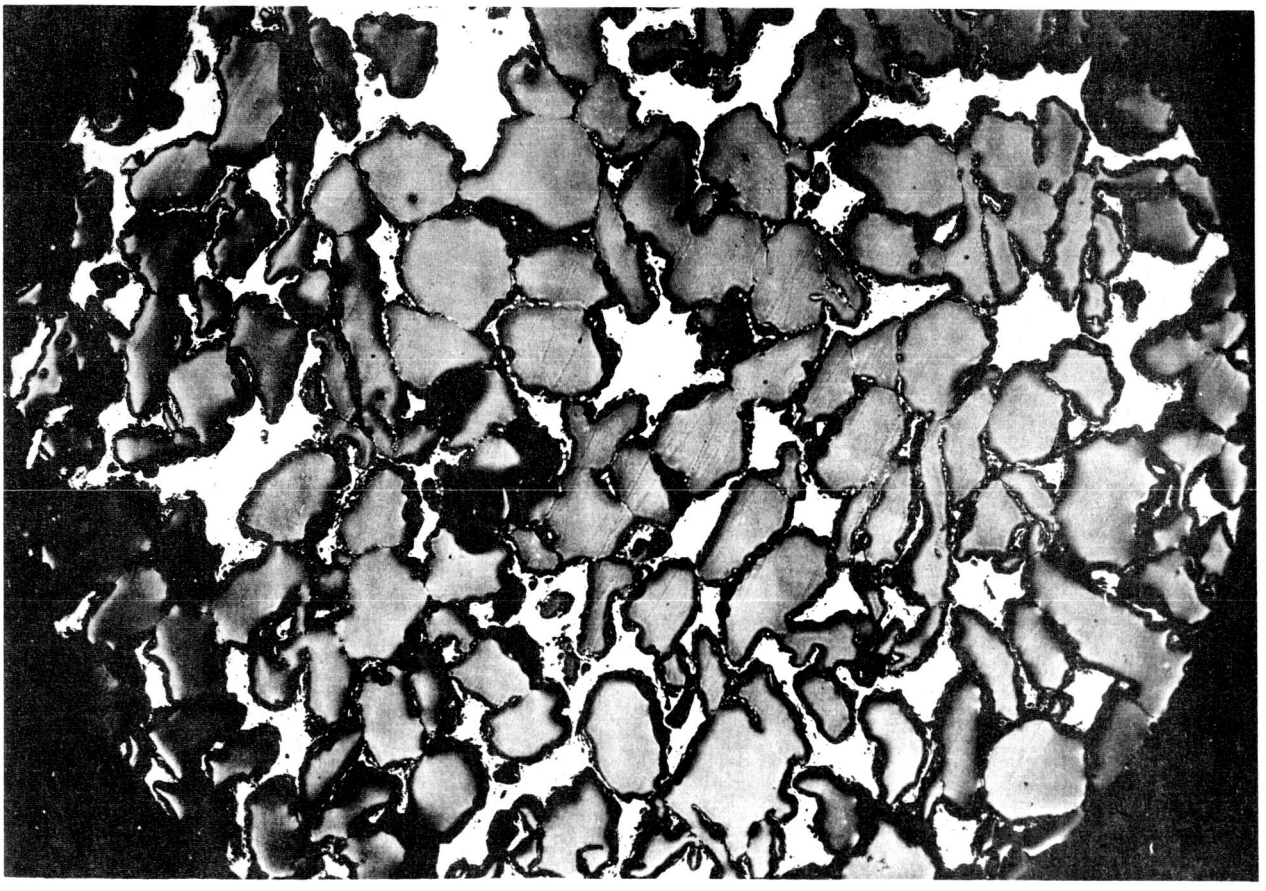

b. M-8840, 50X

Figure I-18 2900°F Rapid-Heat Char Sample Z-1-1-16